CHAPTER X

PION AND KAON INTERACTIONS WITH NUCLEI‡

1. INTRODUCTION

Pion and kaon interactions with nuclei provide a novel set of circumstances not covered in Chapters VII to IX. The pion–nucleon system shows (see Fig. 1.1) a strong resonance called the Δ, of mass 1.232 GeV and width 115 MeV. This is an excited state of the nucleon whose spin J is $\frac{3}{2}$, and whose isospin T is $\frac{3}{2}$. We shall call it a particle despite its short lifetime, given by $\hbar/\Gamma = 1.7\,\text{fm}/c = 0.59 \times 10^{-23}$ s. When a pion, whose energy is near the resonance energy, strikes a nucleus, the formation of the Δ is highly likely, creating thereby a Δ–nucleon hole state in the target nucleus. In this energy domain the Δ–hole state will act as an isolated doorway state [Kisslinger and Wang (73, 76)] through which all pion–nucleus reactions will proceed. We are familiar with such doorway states. Some examples include the isobar analog resonance, the Gamow–Teller resonance, and the electric dipole resonance, which can be described as collective proton particle–neutron hole states and proton particle–proton hole states, respectively. Although the Δ–h configuration is similar in character to these nuclear examples, there is one very significant difference. In the present case, the Δ is itself a resonance in the pion–nucleon system. Many of the pion–nucleon data can be explained if it is assumed that the reaction under study proceeds through the resonance Δ. Thus the theory of pion–nuclear reactions to be developed in this chapter begins with an analysis of the pion–nucleon resonant state. Introducing it into the nucleus permits us to study the impact of the nuclear medium on its properties and thus on the properties of the Δ.

‡Eisenberg and Koltun (80); Ericson and Weise (88); Moniz and Lenz (90).

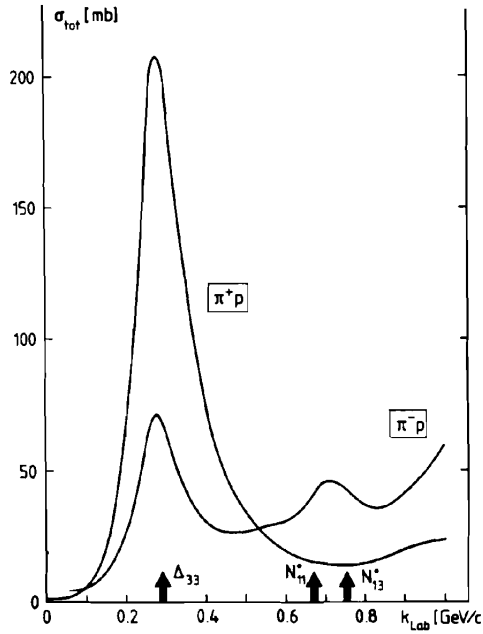

FIG. 1.1. Pion–nucleon total cross sections. [From Ericson and Weise (88).]

This pivotal role is played by the Δ within a restricted energy domain. It is not dominant near threshold nor at high energies. Like other projectiles, discussed in Chapter IX, the pion at high energies can induce inelastic and quasi-elastic scattering. The reaction theory used in these cases is quite straightforward and we shall discuss only inelastic scattering here. We shall, however, discuss charge exchange reactions, which are a special feature of pion reactions. These include the single charge exchange reaction (SCX)

$$\pi^+ + {}_ZA \rightarrow \pi^0 + {}_{(Z+1)}A \tag{1.1}$$

$$\pi^- + {}_ZA \rightarrow \pi^0 + {}_{(Z-1)}A \tag{1.2}$$

and the double charge exchange reaction (DCX)

$$\begin{aligned} \pi^+ + {}_ZA &\rightarrow \pi^- + {}_{(Z+2)}A \\ \pi^- + {}_ZA &\rightarrow \pi^+ + {}_{(Z-2)}A \end{aligned} \tag{1.3}$$

The SCEX reaction has its analog in

$$p + {}_ZA \rightarrow n + {}_{(Z+1)}A \tag{1.4}$$

which might be thought of as a reaction in which a π^+ is transferred to the target nucleus. There is no well-studied corresponding nuclear reaction for the DCEX reaction. The DCEX reaction is of special interest, because it is thought to involve a two-step process involving in each step a change in charge (e.g., $\pi^- \to \pi^0 \to \pi^+$). Such a two-step process is sensitive to correlations in the target nucleus since it involves successive interactions with two nucleons of the target.

The pion is a boson. As a consequence, it can be created or destroyed. The elementary interaction is, for example,

$$p + p \rightleftharpoons \pi^+ + d \tag{1.5}$$

It was by comparing these two reactions and using detailed balance that the intrinsic spin of the pion was found to be zero. These elements, the absorption and production of pions, must of course be taken into account in any theory of pion–nuclear collision.

The strangeness exchange reaction by means of which hypernuclei are formed will be a major focus of the section on kaon–nuclear interactions. In this reaction

$$K^- + A(Z,N) \to {}_{\Lambda}A(Z,N-1) + \pi^- \tag{1.6}$$

a neutron in the target nucleus is converted into Λ via the elementary reaction

$$K^- + n \to \Lambda + \pi^- \tag{1.7}$$

Hypernuclei have also been formed through the inverse reaction:

$$\pi^+ + A(Z,N) \to {}_{\Lambda}A(Z,N-1) + K^+$$

The formation of the Σ hypernucleus through the reactions

$$K^- + A(Z,N) \to {}_{\Sigma}A(Z,N-1) + \pi^- \tag{1.8}$$

and

$$\begin{aligned} K^- + A(Z,N) &\to {}_{\Sigma}A(Z-1,N) + \pi^- \\ &\to {}_{\Sigma}A(Z-1),N) + \pi^+ \end{aligned} \tag{1.9}$$

is more problematic. If it exists, one must understand why the strong interaction transition

$$\Sigma + p \to \Lambda + n \tag{1.10}$$

does not immediately convert it into a Λ hypernucleus if the Λ is captured by the host nucleus or, as is likely, results in the Λ simply leaving the nucleus with no hypernuclear formation.

The Λ hypernucleus has received considerable study, revealing several important aspects of the Λ–nucleon interaction, such as charge symmetry breaking, a weak spin-orbit force as compared to the nucleon–nucleon case, and the need for a three-body (Λnn) repulsive interaction. In addition, in the Λ hypernucleus one can study the weak interaction

$$\Lambda + n \rightarrow n + n \tag{1.11}$$

The free-space decay of the Λ,

$$\Lambda \rightarrow n + \pi \tag{1.12}$$

is reduced, especially in the heavier nuclei, because of the Pauli principle. The energy of the nucleon produced in the decay equation (1.12) is much less than the Fermi energy; most of the kinetic energy is carried by the pion so that there may not be an unoccupied level for the nucleon to occupy.

Investigations of hypernuclei have been hampered by the lack of adequate facilities. This is not the case for pion physics, where the intense beams at Los Alamos (LAMPF) at SIN near Zürich and at TRIUMF at Vancouver have been available since the late 1960s.

2. PION–NUCLEON SYSTEM

A. The Pion

The three pions π^+, π^0, and π^- form an isospin triplet ($T = 1$). They have zero spin and odd parity. The mass of the charged pions is 139.6 MeV. The mass of the neutral pion is 135.0. The lifetime of the charged pions is 2.6×10^{-8} s, that of the π^0 is 8.4×10^{-17} s. The form factor for the charged pion has been determined from the scattering of the high-energy pions by the electron in a hydrogen atom. Its root mean-square charge radius is

$$\langle r_\pi^2 \rangle^{1/2} = (0.66 \pm 0.01)\,\text{fm} \tag{2.1}$$

B. Isospin Symmetry

The pion–nucleon interaction is, except for the Coulomb and mass effects, isospin invariant. This means that the combined system can have an isospin of $\frac{3}{2}$ and $\frac{1}{2}$. Any system composed of a pion and nucleon $|\pi n\rangle$ can be decomposed into states of a definite isospin:

$$|\pi n\rangle = \sum_{T,T_3} |T, T_3\rangle (T T_3 | 1 t_\pi; \tfrac{1}{2} t_n) \tag{2.2}$$

Therefore,

$$
\begin{aligned}
&|\pi^+ p\rangle = |\tfrac{3}{2}, \tfrac{3}{2}\rangle = \Delta^{++} && Q = 2\\
&|\pi^+ n\rangle = \frac{1}{\sqrt{3}}[|\tfrac{3}{2}, \tfrac{1}{2}\rangle + \sqrt{2}|\tfrac{1}{2}, \tfrac{1}{2}\rangle] = \frac{1}{\sqrt{3}}[\Delta^+ + \sqrt{2}|\tfrac{1}{2}, \tfrac{1}{2}\rangle] && Q = 1\\
&|\pi^0 p\rangle = \frac{1}{\sqrt{3}}[\sqrt{2}|\tfrac{3}{2}, \tfrac{1}{2}\rangle - |\tfrac{1}{2}, \tfrac{1}{2}\rangle] = \frac{1}{\sqrt{3}}[\sqrt{2}\Delta^+ - |\tfrac{1}{2}, \tfrac{1}{2}\rangle] && Q = 1\\
&|\pi^0 n\rangle = \frac{1}{\sqrt{3}}[\sqrt{2}|\tfrac{3}{2}, -\tfrac{1}{2}\rangle + |\tfrac{1}{2}, -\tfrac{1}{2}\rangle] = \frac{1}{\sqrt{3}}[\sqrt{2}\Delta^0 + |\tfrac{1}{2}, -\tfrac{1}{2}\rangle] && Q = 0\\
&|\pi^- p\rangle = \frac{1}{\sqrt{3}}[|\tfrac{3}{2}, -\tfrac{1}{2}\rangle - \sqrt{2}|\tfrac{1}{2}, -\tfrac{1}{2}\rangle] = \frac{1}{\sqrt{3}}[\Delta^0 - \sqrt{2}|\tfrac{1}{2}, -\tfrac{1}{2}\rangle] && Q = 0\\
&|\pi^- n\rangle = |\tfrac{3}{2}, -\tfrac{3}{2}\rangle = \Delta^- && Q = -1
\end{aligned}
\tag{2.3}
$$

where Q is the charge of each system.

One can invert these relations and thus express the $T = \frac{3}{2}$ state, the Δ, in terms of the pion–nucleon system. We find that

$$
\begin{aligned}
\Delta^{++} &= |\pi^+ p\rangle && T_3 = \tfrac{3}{2}\\
\Delta^+ &= \frac{1}{\sqrt{3}}[|\pi^+ n\rangle + \sqrt{2}|\pi^0 p\rangle] && T_3 = \tfrac{1}{2}\\
\Delta^0 &= \frac{1}{\sqrt{3}}[\sqrt{2}|\pi^0 n\rangle + |\pi^- p\rangle] && T_3 = -\tfrac{1}{2}\\
\Delta^- &= |\pi^- n\rangle && T_3 = -\tfrac{3}{2}
\end{aligned}
\tag{2.4}
$$

Any isospin invariant operator will be diagonal in isospin space:

$$\langle T T_3 | O | T', T_3' \rangle = O_T \delta(T, T') \delta(T_3, T_3') \tag{2.5}$$

The transition matrix $\mathscr{T}$ is such an operator. Therefore,

$$\langle \pi^+ p | \mathscr{T} | \pi^+ p \rangle = \mathscr{T}_{3/2} \tag{2.6a}$$

$$\langle \pi^- p | \mathscr{T} | \pi^- p \rangle = \tfrac{1}{3}\mathscr{T}_{3/2} + \tfrac{2}{3}\mathscr{T}_{1/2} \tag{2.6b}$$

$$\langle \pi^0 n | \mathscr{T} | \pi^- p \rangle = \frac{\sqrt{2}}{3}(\mathscr{T}_{3/2} - \mathscr{T}_{1/2}) \tag{2.6c}$$

The amplitudes $\mathscr{T}_{3/2}$ and $\mathscr{T}_{1/2}$ are functions of the spin and energy and momentum variables. By comparing the possible reaction cross sections, one can obtain the two amplitudes. Because of the linear relation between the total cross section and the imaginary part of $\mathscr{T}$, we have from (2.6)

$$\begin{aligned} \sigma(\pi^+ p) &= \sigma_{3/2} \\ \sigma(\pi^- p) &= \tfrac{1}{3}\sigma_{3/2} + \tfrac{2}{3}\sigma_{1/2} \end{aligned} \tag{2.7}$$

where the subscripts indicate the isospin channel.

It may be convenient to parametrize the isospin dependence of $\hat{\mathscr{T}}$ by

$$\hat{\mathscr{T}} = a + b\mathbf{t}_n \cdot \mathbf{T}_\pi \tag{2.8}$$

where a and b are functions of spin, energy, and momentum variables. The quantity a is referred to as the *isoscalar* component, b the *isovector*. The vector $\mathbf{t}_n$ is the isospin operator acting on the nucleon

$$\mathbf{t}_n = \tfrac{1}{2}\boldsymbol{\tau}_n \qquad t_n^2 = \tfrac{3}{4} \tag{2.9}$$

The vector $\mathbf{T}$ acts on the pion with the normalization

$$T_\pi^2 = 2 \tag{2.10}$$

since the pion has an isospin, $T = 1$. Since $\mathbf{T} = \mathbf{T}_\pi + \mathbf{t}_n$ is conserved, one can show that

$$\begin{aligned} \mathbf{T}_\pi \cdot \mathbf{t}_n &= \tfrac{1}{2}(\hat{T}^2 - 2 - \tfrac{3}{4}) \\ &= \begin{cases} \tfrac{1}{2} & T = \tfrac{3}{2} \\ -1 & T = \tfrac{1}{2} \end{cases} \end{aligned} \tag{2.11}$$

Parenthetically, one can construct the projection operators on to the $T = \frac{3}{2}$ and $\frac{1}{2}$ states, respectively. They are

$$P_{3/2} = \tfrac{2}{3}(1 + \mathbf{T}_\pi \cdot \mathbf{t}_n) \tag{2.12}$$

$$P_{1/2} = \tfrac{1}{3}(1 - 2\mathbf{T}_\pi \cdot \mathbf{t}_n) \tag{2.13}$$

Using (2.9), one finds from (2.6) that

$$\mathscr{T}_{3/2} = a + \frac{b}{2} \qquad \mathscr{T}_{1/2} = a - b \tag{2.14}$$

The total cross sections for the two most readily available reactions are

$$\sigma(\pi^+ p) = \sigma_{3/2}$$
$$\sigma(\pi^- p) = \tfrac{1}{3}\sigma_{3/2} + \tfrac{2}{3}\sigma_{1/2} \tag{2.15}$$

Coulomb effects modify these results.

C. Pion–Nucleon Scattering

The most striking feature of pion–nucleon scattering is the Δ resonance. This occurs when the momentum of the pion in the center-of-mass system is 230 MeV/c ($k = 1.15\,\text{fm}^{-1}$), corresponding to a mass of 1.232 GeV. The peak cross sections show clearly that the resonant cross sections are for a $T = \frac{3}{2}$ state. Assuming that at the resonance peaks $\sigma_{3/2} \gg \sigma_{1/2}$, one finds from (2.15) and (2.7) that

$$\sigma(\pi^+ p)/\sigma(\pi^- p)/\sigma(\pi^0 n \leftarrow \pi^- p) = (1/\tfrac{1}{3}/\tfrac{2}{9})$$

at resonance. This result is in agreement with experiment (see Fig. 1.1). Second, one can also determine the spin at the resonance. The resonant cross section for $(\pi^+ p)$ scattering, assuming no inelasticity is given by $2\pi/k_{cm}^2(2J+1) = 19\text{fm}^2 = 190\,\text{mb}$ for $J = \frac{3}{2}$, confirming that the Δ^{++} is $J = \frac{3}{2}$ state, and the inelasticity is small. The resonance must occur in the $l = 1$, p-wave channel yielding a unique angular distribution. The amplitude for the scattering of a zero-spin particle by a particle of spin $\frac{1}{2}$ is given for each isospin channel according to (V.2.44) by

$$\hat{f} = A + B\boldsymbol{\sigma}\cdot\mathbf{n} \qquad \mathbf{n} = \frac{\mathbf{k}_i \times \mathbf{k}_f}{|\mathbf{k}_i \times \mathbf{k}_f|} \tag{2.16}$$

where

$$A = \frac{1}{k}\sum_l [(l+1)f_l^{(+)} + l f_l^{(-)}]P_l(\cos\vartheta) \tag{2.17}$$

and

$$B = \frac{i}{k}\sum [f_l^{(+)} - f_l^{(-)}]P_l^{(1)}(\cos\vartheta) \tag{2.18}$$

$$P_l^{(1)}(\cos\vartheta) = \sin\vartheta \frac{d}{d(\cos\vartheta)} P_l(\cos\vartheta)$$

The quantities $f_l^{(+)}$ and $f_l^{(-)}$ are the partial wave amplitudes for the $j = l + \frac{1}{2}$ and $j = l - \frac{1}{2}$ states. In terms of phase shifts, $f_l^{(+)}$ is

$$f_l^{(+)} \equiv \frac{1}{2ik}(e^{2i\delta_l^+} - 1) \tag{2.19}$$

with a similar expression for $f_l^{(-)} \cdot \delta_l^{(+)}$ will be complex if there is any inelasticity. The differential cross section is

$$\frac{d\sigma}{d\Omega} = \frac{1}{k^2}[|A|^2 + |B|^2] \tag{2.20}$$

The total integrated cross section is

$$\sigma = \frac{4\pi}{k^2}\sum[(l+1)|f_l^{(+)}|^2 + l|f_l^{(-)}|^2]$$

The polarization parameters $\mathbf{P}$ and Q are

$$\mathbf{P} = 2\frac{\text{Re}\, AB^*}{|A|^2 + |B|^2}\mathbf{n} \qquad Q = \frac{2\,\text{Im}\, AB^*}{|A|^2 + |B|^2} \tag{2.20'}$$

For the Δ^{++} resonance, $l = \frac{1}{2}$, $J = \frac{3}{2}$, so that

$$\frac{d\sigma}{d\Omega} = \frac{1}{k^2}|f_l^{(+)}|^2(4\cos^2\vartheta + \sin^2\vartheta) \tag{2.21}$$

in agreement with experiment (see Fig. 2.1). At 0°, $d\sigma/d\Omega = 30$ mb at resonance. It will be noted that as the pion energy deviates from resonance, the angular distributions are no longer symmetric about 90°. This is because of the presence of nonresonant amplitudes, for example coming from $\mathscr{T}_{1/2}$. The low-energy behavior of the phase shift is given by the limit

$$\delta_{2T,2J}^{(L)} \to a_{2T,2J}^{(L)} q^{2L+1} \qquad q \to 0 \tag{2.22}$$

For S waves, a is referred to as the scattering length; for P waves a has the dimensions of a volume and therefore could be called the *scattering volume.* The numerical values for a are [Moniz and Lenz (91)]

$$\begin{aligned} a_{3,1}^S &= (-0.092 \pm 0.002)m_\pi^{-1} \\ a_{1,1}^S &= (0.170 \pm 0.004)m_\pi^{-1} \end{aligned} \tag{2.23}$$

and

$$\begin{aligned} a_{3,1}^P &= (-0.043 \pm 0.004)m_\pi^{-3} \\ a_{3,3}^P &= (0.214 \pm 0.004)m_\pi^{-3} \\ a_{1,1}^P &= (-0.082 \pm 0.006)m_\pi^{-3} \\ a_{1,3}^P &= (-0.029 \pm 0.005)m_\pi^{-3} \end{aligned} \tag{2.24}$$

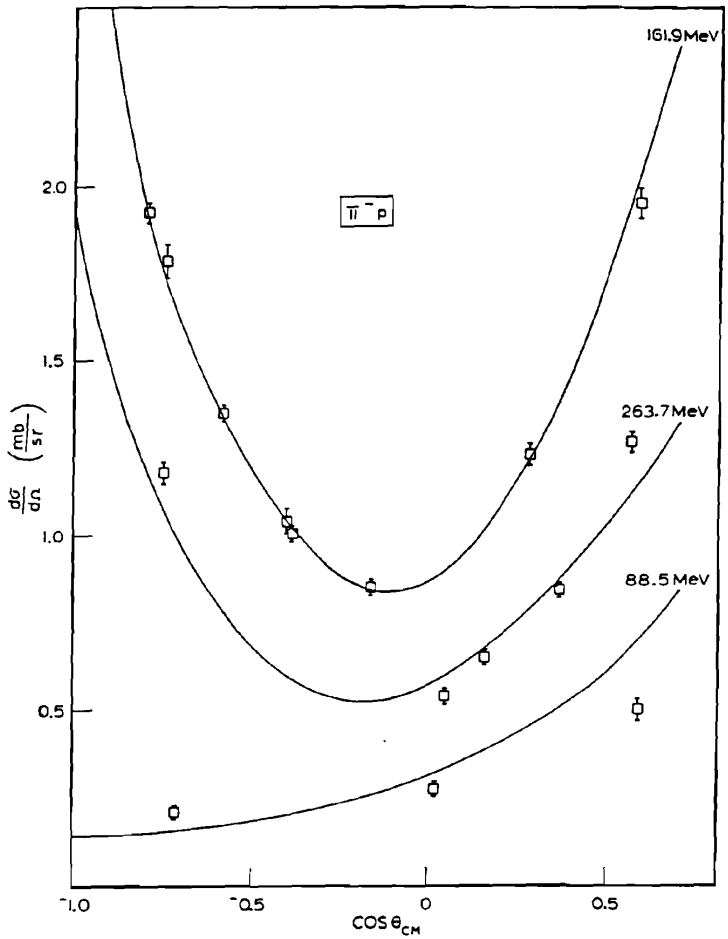

FIG. 2.1. Angular distributions for $\pi^- p$ scattering. [From Rowe, Solomon, and Landau (78).]

We note that the nonresonant P-wave amplitudes are negative, corresponding to a relatively weak repulsion. Moreover, the isoscalar quantity in (2.8) is very small for S waves. Using

$$a_s = \tfrac{2}{3}a^S_{3,1} + \tfrac{1}{3}a^S_{1,1}$$

we obtain $a_s = -0.0046\, m_\pi^{-1}$.

At higher energies, the empirical phase shifts as determined by Rowe, Solomon, and Landau (78) are presented in Figs. 2.2 to 2.4. The curves are labeled by $L_{2T,2S}$. The phase shift $\delta(P_{33})$ rises rapidly from zero through $\pi/2$, the resonance value of δ. The phases $\delta(P_{13})$ and $\delta(P_{31})$ are increasingly negative.

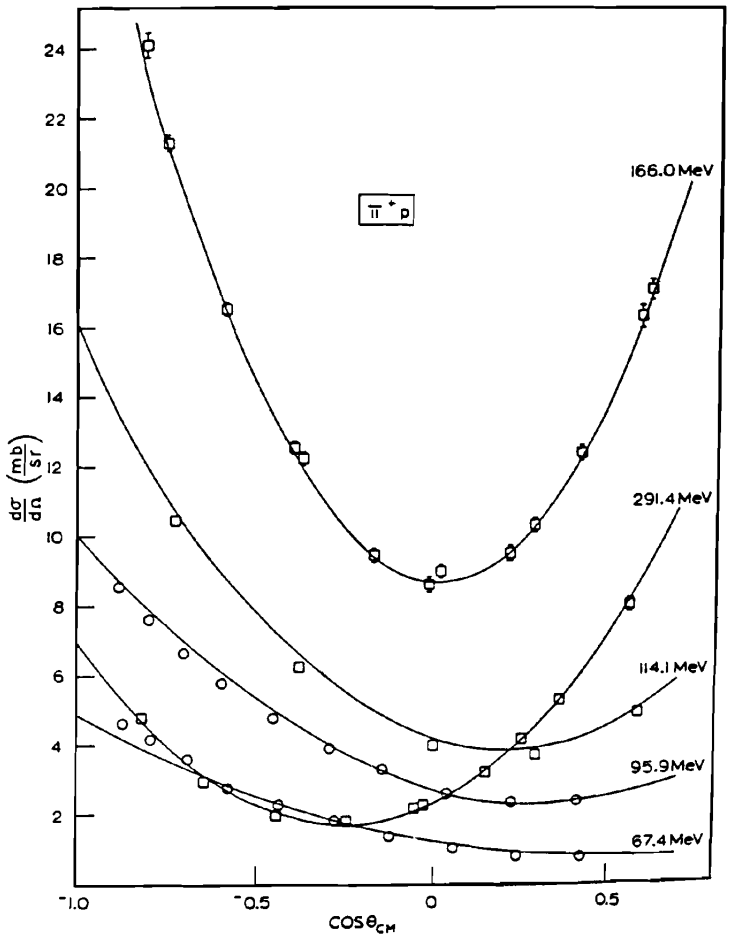

FIG. 2.2. Angular distributions for $\pi^+ p$ scattering. [From Rowe, Solomon, and Landau (78).]

The phase shift $\delta(P_{11})$ $(T = \frac{1}{2}s - \frac{1}{2})$ turns about and crosses the real axis, becoming positive and rising rapidly, indicating the effect of a resonance at a mass of 1.440 GeV with a width of 200 ± 80 MeV.

Rowe, Solomon, and Landau (78) have given a useful parametrizaion of the phase shifts for pion energies less than 400 MeV. It is

$$\tan \delta_l = \left(\frac{k}{m_\pi}\right)^{2l+1}\left[b + c\left(\frac{k}{m_\pi}\right)^2 + d\left(\frac{k}{m_\pi}\right)^4\right] + x\left(\frac{k}{k_0}\right)^{2l+1}\frac{\Gamma_0\sqrt{s_0}}{s_0 - s} \quad (2.25)$$

where k and s are the πn center-of-mass momentum and (energy)^2, respectively.

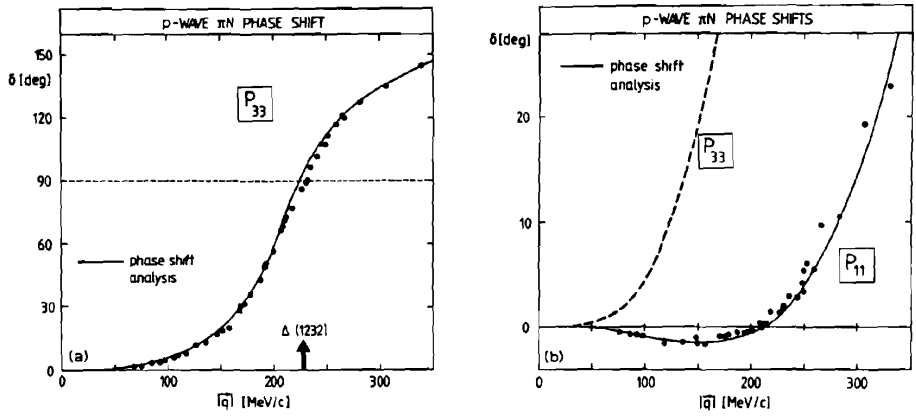

FIG. 2.3. Empirical pion–nucleon p-wave phase shifts versus center-of-mass momentum $|\mathbf{q}|$ Rowe, Solomon, and Landau (78). [From Ericson and Weise (88).]

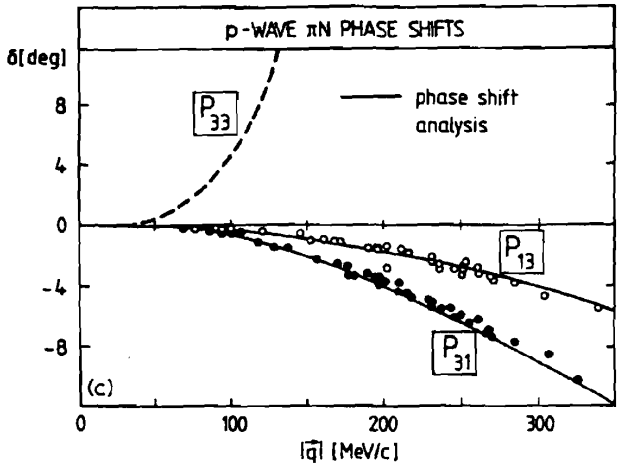

FIG. 2.4. Empirical pion–nucleon p-wave phase shifts versus center-of-mass momentum $|\mathbf{q}|$ [Rowe, Solomon, and Landau (78)]. [From Ericson and Weise (88).]

The resonance form is meaningful only for the P_{33} and P_{11} phases. The values of the parameters are given in Table 2.1.

Principally because of the Coulomb interaction, isospin symmetry is broken. The masses of the Δ's are not all equal, nor are their widths equal. For example, $M(\Delta^0) - M(\Delta^{++}) = 2.7 \pm 0.3$ MeV and $\Gamma(\Delta^0) - \Gamma(\Delta^{++}) = 6.6 \pm 1.0$ MeV [Pedroni, Gabathuler, et al. (78)].

Inelastic pion–nucleon reactions occur when pions are produced. The threshold energy for the $\pi n \to \pi\pi n$ reaction is about 179 MeV in the laboratory

TABLE 2.1 Parameters for (2.26)

	x	$\sqrt{s_0}$ (GeV)	k_0 (GeV/c)	Γ_0 (GeV)	b (10^{-2})	c (10^{-3})	d (10^{-4})
S_{11}	0.44	1.550	0.477	0.105	16.8 ± 0.75	-35.4 ± 5.4	27 ± 11
S_{31}	0.31	1.655	0.550	0.170	-11.2 ± 0.20	-30.7 ± 1.1	21 ± 2
P_{11}	0.61	1.435	0.393	0.230	-5.71 ± 0.54	25.4 ± 2.1	-29 ± 3
P_{13}	0.23	1.815	0.656	0.255	-1.31 ± 0.08	1.22 ± 0.32	-0.4 ± 0.3
P_{31}	0.22	1.850	0.678	0.200	-2.91 ± 0.08	3.45 ± 0.27	-1.5 ± 0.2
P_{33}	0.99	1.233	0.228	0.116	11.4 ± 0.30	-15.4 ± 2.1	7.2 ± 2.1

Source: Rowe, Solomon, and Landau (78).

reference frame. It appears that many of the data for this reaction can be understood under the assumption that the final state is a two-body state, of which one body is an isobar. For example, the two-body state could be a $\pi + \Delta$, or a 2π isobar, such as the spin 1 ρ or the spin 0 σ plus a nucleon. Such a hypothesis can be tested by calculating the ratios of the production of various possible two-pion + nucleon final states, using the isospin properties of the isobars and comparing with experiment. For example, suppose that the reaction is

$$\pi^- + p \rightarrow \begin{cases} \pi^+\pi^- p \\ \pi^0\pi^0 n \\ \pi^-\pi^0 p \end{cases} \tag{2.26}$$

Suppose that the reaction can be described as leading to $\Delta^+\pi^-$, $\Delta^0\pi^0$, and $\Delta^-\pi^+$ states with the subsequent decay of the Δ^+, Δ^-, and Δ^0. Using the isospin Clebsch–Gordan coupling coefficients and for simplicity considering only the $T = \frac{1}{2}$ channel, one finds that

$$|T, T_3\rangle = |\tfrac{1}{2}, -\tfrac{1}{2}\rangle = \sqrt{\tfrac{1}{6}}(\Delta^+\pi^- - \sqrt{2}\Delta^0\pi^0 + \sqrt{3}\Delta^-\pi^+) \tag{2.27}$$

Now using (2.4), which expressed the $\Delta^+, \Delta^0, \Delta^-$ in terms of nucleon + pion amplitudes, one can obtain the branching ratios for the three final states of (2.26), namely,

$$\sigma_{1/2}(\pi^+\pi^- n)/\sigma_{1/2}(\pi^0\pi^- p)/\sigma_{1/2}(\pi^0\pi^0 n) = 5/2/2 \qquad T = \tfrac{1}{2}$$

which can be compared with experiment.

Problem. Consider the $T = \frac{3}{2}$ channel. Show that $|\frac{3}{2}, -\frac{1}{2}\rangle = \sqrt{\frac{1}{15}}[-\sqrt{8}\Delta^+\pi^- + \Delta^0\pi^0 + \sqrt{6}\Delta^-\pi^+]$. Calculate the cross section ratio for the three reactions of (2.26).

D. The Isobar Description of the Δ

We shall not enter into the dynamics underlying the properties of the Δ. Suffice it to say that it is the simplest excitation of the three-quark system, whose ground state is the nucleon. In this excitation the spin of a quark is flipped while the isospin ($d \rightleftharpoons u$ quarks) may also change. Our goal in this section is to obtain a consistent description of the Δ, which will prove to be useful when we consider π-nucleus scattering.

The expression for the $\mathcal{T}$ matrix for resonant scattering for an isolated resonance has been derived in Chapter III [Eq. (III.2.18)]. We recall that one proceeds by dividing the Hilbert space in two through the use of the projection operators P and $Q = 1 - P$, where the space subtended by P contains the incident and exit channels. Then as seen from Chapter III, the $\mathcal{T}$ matrix is given by

$$\mathcal{T} = \mathcal{T}_P + \left\langle \psi_f^{(-)} H_{PQ} \frac{1}{E - H_{QQ} - W_{QQ}} H_{QP} \psi_f^{(+)} \right\rangle \tag{2.28}$$

where $H_{PQ} \equiv PHQ$, and so on, and

$$W_{QQ} = H_{QQ} \frac{1}{E^{(+)} - H_{PP}} H_{PQ} \tag{2.29}$$

$\mathcal{T}_P$ is the nonresonant scattering in P space, that is, a consequence of the Schrödinger equation

$$(E - H_{PP})\psi = 0 \tag{2.30}$$

In the case of a single isolated resonance, one chooses Q to contain only one state—the resonant state Φ. Then

$$\mathcal{T} = \mathcal{T}_P + \mathcal{T}_R = \mathcal{T}_P + \frac{\langle \psi_f^{(-)} H_{PQ} \Phi \rangle \langle \Phi H_{QP} \psi_i^{(+)} \rangle}{E - \langle \Phi H \Phi \rangle - \langle \Phi H_{QP} [1/(E^+ - H_{PP})] H_{PQ} \Phi \rangle} \tag{2.31}$$

In the application to pion–nucleon scattering, we shall limit the discussion to the $\pi^+ + p \to \Delta^{++}$ resonance. The results for other channels can be obtained from isospin invariance. The state vector Φ is $\Delta(\mu_\Delta)$, where μ_Δ is the z component of the Δ spin of $\frac{3}{2}$. The operator H_{QP} couples the Δ to the pion–nucleon states of P space. We take it to be given by

$$H_{QP} = g h(k^2) \mathbf{k} \cdot \mathbf{S}^\dagger \tag{2.32}$$

where g is a coupling constant, $h(k^2)$ is a form factor, $h(0) = 1$, $\mathbf{k}$ is the center of mass relative momentum of the pion–nucleon system, and $\mathbf{S}^\dagger$ is referred to

as the transition spin operator. The form given by (2.32) is determined by angular momentum and parity invariance. One recalls that the pion is a *pseudoscalar* spin-zero particle. Hence the interaction must itself transform like a pseudoscalar. The transition operator $\mathbf{S}^\dagger$ converts a nucleon of spin-$\frac{1}{2}$, z component μ_n into a Δ of spin-$\frac{3}{2}$, z component μ_Δ. It therefore has the matrix elements

$$\langle \tfrac{3}{2}\mu_\Delta|\mathbf{S}^\dagger|\tfrac{1}{2}\mu_n\rangle \equiv \sum_\mu (1\mu\tfrac{1}{2}\mu_n|\tfrac{3}{2}\mu_\Delta)\mathbf{e}_\mu \tag{2.33}$$

where

$$\mathbf{e}_{\pm 1} = \mp \frac{1}{\sqrt{2}}(\hat{\mathbf{a}}_1 \pm \hat{\mathbf{a}}_2) \tag{2.34}$$

$$\mathbf{e}_0 = \hat{\mathbf{a}}_3$$

Here $\hat{\mathbf{a}}_i$ are three perpendicular unit vectors. From this result we have

$$\begin{aligned}\mathbf{S}^\dagger = {} & \mathbf{e}_1[|\tfrac{3}{2}\rangle\langle\alpha + \sqrt{\tfrac{1}{3}}|\tfrac{1}{2}\rangle\langle\beta] + \mathbf{e}_{-1}[\sqrt{\tfrac{1}{3}}|-\tfrac{1}{2}\rangle\langle\alpha + |-\tfrac{3}{2}\rangle\langle\beta] \\ & + \mathbf{e}_0\sqrt{\tfrac{2}{3}}[\tfrac{1}{2}\rangle\langle\alpha + |-\tfrac{1}{2}\rangle\langle\beta]\end{aligned} \tag{2.35}$$

where $|\cdot\rangle$ refers to the state vector $|\frac{3}{2}\mu_\Delta\rangle$. We have tabulated only μ_Δ. The states α and β are the $+\frac{1}{2}$, $-\frac{1}{2}$ spin states of the nucleon, respectively. In component form,

$$\begin{aligned}S_1^\dagger &= -\frac{1}{\sqrt{2}}[|\tfrac{3}{2}\rangle\langle\alpha + \sqrt{\tfrac{1}{3}}|\tfrac{1}{2}\rangle\langle\beta] + \frac{1}{\sqrt{2}}[\sqrt{\tfrac{1}{3}}|-\tfrac{1}{2}\rangle\langle\alpha + |-\tfrac{3}{2}\rangle\langle\beta] \\ S_2^\dagger &= -\frac{i}{\sqrt{2}}[|\tfrac{3}{2}\rangle\langle\alpha + \sqrt{\tfrac{1}{3}}|\tfrac{1}{2}\rangle\langle\beta] - \frac{i}{\sqrt{2}}(\sqrt{\tfrac{1}{3}}|-\tfrac{1}{2}\rangle\langle\alpha + |-\tfrac{3}{2}\rangle\langle\beta] \\ S_3^\dagger &= \sqrt{\tfrac{2}{3}}[|\tfrac{1}{2}\rangle\langle\alpha + |-\tfrac{1}{2}\rangle\langle\beta]\end{aligned} \tag{2.36}$$

We now define the product $S_i S_j^\dagger$ by

$$S_i S_j^\dagger = \sum S_i|\mu_\Delta\rangle\langle\mu_\Delta S_j^\dagger \tag{2.37}$$

This operator acts only on the nucleon spinors. One may show using (2.36) that

$$S_i S_j^\dagger = \tfrac{2}{3}\delta_{ij} - \tfrac{1}{3}\sigma_i\sigma_j$$

and

$$S_i^\dagger S_j = \tfrac{2}{3}\delta_{ij} + \tfrac{1}{3}\sigma_i\sigma_j \tag{2.38}$$

From (2.38) we have the useful result

$$\begin{aligned}\mathbf{A}\cdot\mathbf{S}\mathbf{S}^\dagger\cdot\mathbf{B} &= \tfrac{2}{3}\mathbf{A}\cdot\mathbf{B} - \tfrac{1}{3}(\boldsymbol{\sigma}\cdot\mathbf{A})(\boldsymbol{\sigma}\cdot\mathbf{B}) \\ &= \tfrac{1}{3}\mathbf{A}\cdot\mathbf{B} - \tfrac{1}{3}i\boldsymbol{\sigma}\cdot(\mathbf{A}\times\mathbf{B})\end{aligned} \tag{2.39}$$

Note that a similar development can be made in isospin space where the $T=\frac{1}{2}$ nucleon is transformed to a $T=\frac{3}{2}\Delta$.

We return to the numerator, N, of $\mathscr{T}_R$ in (2.31), which can be written using (2.32) as follows:

$$\hat{N}=g^2\sum_{\mu_\Delta} h(k'^2)(\mathbf{k}'\cdot\mathbf{S})|\Delta(\mu_\Delta)\rangle\langle\Delta(\mu_\Delta)|(\mathbf{k}\cdot\mathbf{S}^\dagger)h(k^2)$$

or

$$\hat{N}=\frac{g^2}{3}h(k^2)h(k'^2)[\mathbf{k}'\cdot\mathbf{k}-i\boldsymbol{\sigma}\cdot(\mathbf{k}'\times\mathbf{k})] \tag{2.40}$$

To complete the calculation of the numerator N, one must take the matrix element of $\hat{N}$ between appropriate initial and final nucleon spinors. The form factor $h(k^2)$ measures the overlap of the incident and final pion–nucleon wave function with the Δ wave function. The resonance denominator D in (2.31) is given by ($E=$ total energy)

$$D(E)=E-\bar{m}_\Delta-\frac{g^2}{3}\int\frac{d\mathbf{k}}{(2\pi)^3}\frac{h^2(k^2)\kappa^2}{E^{(+)}-m-m_\pi-\kappa^2/2\mu}\qquad E^{(+)}=E+i\varepsilon \tag{2.41}$$

where $\bar{m}_\Delta=\langle\Delta|H|\Delta\rangle$, μ is the pion–nucleon reduced mass (units $\hbar=c=1$). The real part of the integral will combine with the parameter $\bar{m}_\Delta$ to yield the Δ mass, m_Δ. The imaginary part of the integral equals twice the width of the Δ resonance. The ratio N/D, given by (2.40) and (2.41), is the Breit–Wigner result, describing the Δ.

The discussion above is nonrelativistic. The relativistic generalization adopted by Hirata, Koch, Lenz, and Moniz (78, 79) and by Horikawa, Thies, and Lenz (80) replaced $D(E)$ by a form obtained from the Blankenbecler–Sugar reduction of the Bethe–Salpeter equation. According to Moniz and Lenz (91), the $D(E)$ of (2.41) should be replaced by

$$D(s)=s-\bar{m}_\Delta^2-\frac{2g^2}{3}\int\frac{d\boldsymbol{\kappa}}{(2\pi)^3}(\omega_\kappa+E_\kappa)\frac{m_\pi m}{\omega_\kappa E_\kappa}\frac{\kappa^2h^2(\kappa^2)}{s^{(+)}-(\omega_\kappa+E_\kappa)^2} \tag{2.42}$$

where

$$\omega_\kappa^2\equiv m_\pi^2+\kappa^2\qquad E_\kappa^2=m^2+\kappa^2$$

and s is the square of the invariant energy. Both expressions for D, (2.41) and (2.42), include only pion–nucleon scattering in the expression for the W_{QQ} term. Other inelastic processes, such as $\pi+n\to\pi+\pi+n$ or $\pi+n=\gamma+n$, can also contribute to the Δ width but are not significant at or near the resonance energy.

Problem. Take the nonrelativistic limit of (2.42) and compared with (2.41)

The width can be obtained from the singularity in (2.42):

$$\text{Im}\, D = \frac{1}{3\pi} g^2 \int d\kappa (\omega_\kappa + E_\kappa) \frac{m_\pi m}{\omega_\kappa E_\kappa} \kappa^4 h^2(\kappa^2) \delta(s - (\omega_\kappa + E_\kappa)^2)$$

The argument of the δ function is zero when κ^2 equals κ_0^2, where

$$\kappa_0^2 = \frac{1}{4s}[s - (m - m_\pi)^2][s - (m + m_\pi)^2] \tag{2.43}$$

Therefore,

$$\text{Im}\, D = \frac{g^2}{3\pi}(\omega_{\kappa_0} + E_{\kappa_0}) \frac{m_\pi m}{\omega_{\kappa_0} E_{\kappa_0}} \frac{\kappa_0^4 h^2(\kappa_0^2) \omega_{\kappa_0} E_{\kappa_0}}{2\kappa_0 (\omega_{\kappa_0} + E_{\kappa_0})^2}$$

or

$$\text{Im}\, D = \frac{1}{6\pi} g^2 \frac{m_\pi m}{\sqrt{s}} \kappa_0^3 h(\kappa_0^2) \tag{2.44}$$

In the laboratory frame, the width and Im D are related by

$$\Gamma = \left(\frac{1}{m}\right) \text{Im}\, D \tag{2.45}$$

A good fit to the resonance phase shifts is obtained, according to Moniz and Lenz (91), with

$$h(k^2) \equiv \frac{1}{1 + k^2/\alpha^2} \tag{2.46}$$

when $\alpha = (0.56\,\text{fm}^{-1})$, $\bar{m}_\Delta = 1384\,\text{MeV}$, and $g = 8.72/m_\pi$.

3. PION–NUCLEUS SCATTERING

The scattering of pions by nuclei involves a number of novel features, compared to reactions induced by projectiles considered so far in this volume. At low energies ($E_\pi < 80\,\text{MeV}$) the pion–nucleon interaction is weak and multiple scattering theory is used to understand the results. The optical model potential contains significant nonlocal contributions in addition to the customary central and spin-orbit potentials. In the kinetic energy range 80 to 400 MeV, Δ resonance formation is the dominant mode and an isobar-doorway state model is appropriate. It is this last feature that is of interest to the theory of reactions, for it provides an observable example of the impact of the nuclear medium on the propagation of a short-lived system through that medium.

A. Low Energy: $E_\pi < 80$ MeV

Multiple scattering theory (see Chapter II) has been used to obtain the form of the pion–nucleon optical potential in this energy range. Since multiple scattering theory is a high-energy approximation, its validity for the scattering of low-energy pions whose wavelength/2π is on the order or larger than the internuclear distance in the nucleus must be justified. The first-order (and higher-order) optical potential

$$V^{(1)} = \frac{A-1}{A} \sum_{i=1}^{A} \langle 0|t_i|0\rangle \tag{3.1}$$

depends directly on the pion–nucleon scattering. To fit the data the parameters describing pion–nucleon scattering must be modified, replaced by effective parameters. These modifications are ascribed to higher-order effects which are said to describe the impact of the medium on the pion–nucleon interaction. It is, however, not correct to employ the multiple scattering second-order potential $V^{(2)}$ to determine those effects. In the derivation, presented in Chapter II, of $V^{(2)}$ the approximation is made in which the nuclear Hamiltonian, H_N, in the propagator is replaced by a constant. This is equivalent to the fixed scatterer approximation (or $m_\pi/m \to 0$), which is not valid at these energies. However, we shall use $V^{(2)}$ to indicate the form of the media modification, adjusting its parameters as well as those of $V^{(1)}$ to obtain a fit for experiment. The results are physically meaningful since these parameters vary slowly with respect to nucleus and energy.

At low energy the scattering amplitude f_i for pion–nucleon scattering in the center-of-mass pion nucleon frame can be parametrized as follows:

$$f_{\pi n}(\mathbf{k}_{cm}, \mathbf{k}'_{cm}) = b'_0 + c'(\mathbf{k}_{cm}\cdot\mathbf{k}'_{cm}) + id'\boldsymbol{\sigma}\cdot(\mathbf{k}_{cm} \times \mathbf{k}'_{cm}) \tag{3.2}$$

where b' depends on isospin

$$b' = b'_0 + b'_1(\mathbf{T}_\pi\cdot\boldsymbol{\tau})$$

and similarly for parameters c' and d'. [Note that $\mathbf{t}$ of (2.8) $= \tau/2$.] The coefficients b', c' d' depend on energy and momentum transfer $\mathbf{q} = (\mathbf{k} - \mathbf{k}')$. At threshold ($E_\pi = 0$) the coefficients have the following values [Ericson and Weise (88)]:

$$\begin{aligned} b'_0 &= -0.010(3)m_\pi^{-1} & b'_1 &= -0.091 m_\pi^{-1} \\ c'_0 &= 0.208(3)m_\pi^{-3} & c'_1 &= 0.175(2)m_\pi^{-3} \\ d'_0 &= -0.190(2)m_\pi^{-3} & d'_1 &= -0.069(2)m_\pi^{-3} \end{aligned} \tag{3.3}$$

The c' term, the p-wave scattering amplitude, is clearly dominant, demonstrating the importance of the Δ resonance even at very low energies. From the results

$(\mathbf{T}_\pi \cdot \tau)|\pi^+ p\rangle = 1$ and $(\mathbf{T}_\pi \cdot \tau)|\pi^+ n\rangle = -1$, we see that the $\pi^+ + p$ scattering spin averaged amplitude is $c'_0 + c'_1 = 0.38 m_\pi^{-3}$, and the $\pi^+ + p$ amplitude is given by $c'_0 - c'_1 = 0.03 m_\pi^{-3}$. We therefore expect that π^+ nuclear scattering will be more sensitive to the proton distribution, while the opposite will be the base for π^- scattering.

We shall need the transition matrix t_i in the pion–nucleon center-of-mass frame, in terms of $f_{\pi n}$ in (3.2). This relation is given by (II.7.16). It is

$$t_{\pi A} = -2\pi \frac{k_L}{k_{\rm cm} E_L} \frac{1 + 2E_L/Am + (m_\pi/Am)^2}{(1 + m_\pi^2/AmE_L)(1 + E_L/Am)} f_{\pi n} \tag{3.4}$$

where k_L is the pion momentum in the laboratory frame, E_L the corresponding energy including its rest mass, and Am the mass of the target nucleus. In addition, it is necessary to transform the momenta $\mathbf{k}_{\rm cm}$ and $\mathbf{k}'_{\rm cm}$ to the pion–nucleon frame momenta, $\mathbf{k}$ and $\mathbf{k}'$.

We consider the transformation from the reference frame in which the incident pion has a momentum of $\mathbf{k}$ and the target nucleon a momentum of $-\mathbf{k}/A$ to the frame in which the pion and nucleon have momenta of $\mathbf{k}_{\rm cm}$ and $-\mathbf{k}_{\rm cm}$, respectively. For all but the lightest nucleus, the pion energy in the first of these frames equals the pion laboratory energy, E_L. The boost in velocity $\mathbf{v}$ in units of c required to transform to the nucleon–pion center-of-mass frame is determined by the Lorentz transformation:

$$k_{\rm cm} = \gamma(k - vE_L) = \gamma\left(\frac{k}{A} + mv\right) \tag{3.5}$$

This yields

$$v = \left(1 - \frac{1}{A}\right)\frac{k}{m + E_L} \tag{3.6}$$

For the maximum pion kinetic energy considered (80 MeV), $v^2 = 0.0245$. Hence in (3.5), one may safely put $\gamma = 1$, so that

$$\mathbf{k}_{\rm cm} = \mathbf{k}\left[1 - \frac{E_L(1 - 1/A)}{m + E_L}\right] = \mathbf{k}\frac{m + E_L/A}{m + E_L} \simeq \mathbf{k}\frac{m}{m + E_L} \tag{3.7}$$

Similarly,

$$\mathbf{k}'_{\rm cm} = \mathbf{k}' - \frac{\mathbf{k}(1 - 1/A)E'_L}{E_L + m} \tag{3.8}$$

We thus obtain

$$\mathbf{k}_{\rm cm} \times \mathbf{k}'_{\rm cm} = \frac{m}{m + E_L}(\mathbf{k} \times \mathbf{k}') \tag{3.9}$$

Evaluating $\mathbf{k}_{cm}\cdot\mathbf{k}'_{cm}$ takes more work but one finds that to $O(k^2/m^2, k'^2/m^2)$,

$$\mathbf{k}'_{cm}\cdot\mathbf{k}_{cm} \simeq \frac{m}{m+E_L}\mathbf{k}\cdot\mathbf{k}' - \frac{k^2 m E_L}{(m+E_L)^2}\left(1-\frac{1}{A}\right)$$

Note that

$$k^2 = \tfrac{1}{2}(\mathbf{k}-\mathbf{k}')^2 + \mathbf{k}\cdot\mathbf{k}' + \tfrac{1}{2}(\mathbf{k}-\mathbf{k}')\cdot\left(\frac{\mathbf{k}+\mathbf{k}'}{2}\right)$$

We drop the last term on the assumption that it will average to zero and/or because it is zero on the energy shell. Inserting the approximate result into the equation for $\mathbf{k}_{cm}\cdot\mathbf{k}'_{cm}$ and using the notation

$$\mathbf{k}-\mathbf{k}' = \mathbf{q}$$

one obtains

$$\mathbf{k}_{cm}\cdot\mathbf{k}'_{cm} = \left(\frac{m}{m+E_L}\right)^2\left[\mathbf{k}\cdot\mathbf{k}' - \frac{E_L}{2m}q^2\right] \tag{3.10}$$

Substituting (3.9) and (3.10) into (3.2) and (3.4) yields

$$t_{\pi A} = b + c\left[(\mathbf{k}\cdot\mathbf{k}') - \frac{E_L}{2m}\left(1-\frac{1}{A}\right)q^2\right] + id\boldsymbol{\sigma}\cdot(\mathbf{k}\times\mathbf{k}') \tag{3.11}$$

where the coefficients b, c, d are proportional to b', c', and d' of (3.2). They are functions of the momentum transfer and the energy.

Inserting (3.11) into (3.1) yields

$$V(\mathbf{r},\mathbf{r}') = \frac{A-1}{(2\pi)^6}\int d\mathbf{k}\int d\mathbf{k}' e^{i\mathbf{k}\cdot\mathbf{r}}\rho(\mathbf{q})t_{\pi A}e^{-i\mathbf{k}'\cdot\mathbf{r}'} \tag{3.12}$$

Assuming that the coefficients b, c, and d vary slowly with q allows us to replace them by their value at $q=0$, $b^{(0)}$, $c^{(0)}$, and $d^{(0)}$. The integration in (3.12) can then be performed easily. For example, consider the $\mathbf{k}\cdot\mathbf{k}'$ term:

$$\begin{aligned} V_p &= c^{(0)}\frac{A-1}{(2\pi)^6}\int d\mathbf{k}'\int d\mathbf{k} e^{i\mathbf{k}\cdot\mathbf{r}}\mathbf{k}\cdot\mathbf{k}'\rho(\mathbf{k}-\mathbf{k}')e^{-i\mathbf{k}'\cdot\mathbf{r}'} \\ &= c^{(0)}\frac{A-1}{(2\pi)^6}\nabla\cdot\nabla'\int d\mathbf{k}\int d\mathbf{k}' e^{i\mathbf{k}\cdot\mathbf{r}}\rho(\mathbf{k}-\mathbf{k}')e^{-i\mathbf{k}'\cdot\mathbf{r}'} \\ &= c^{(0)}(A-1)(\nabla\cdot\nabla')\delta(\mathbf{r}-\mathbf{r}')\rho(\mathbf{r}) \end{aligned} \tag{3.12'}$$

Acting on $\psi(r')$ yields

$$\int V_p(\mathbf{r},\mathbf{r}')\psi(\mathbf{r}')d\mathbf{r}' = -c^{(0)}(A-1)\nabla\cdot\rho\nabla\psi \tag{3.13}$$

Hence the first term in the multiple scattering series is

$$V^{(1)} = (A-1)\left[b^{(0)}\rho - c^{(0)}\nabla\cdot\rho\nabla - c^{(0)}\frac{E_L}{2m}(\nabla^2\rho) + d^{(0)}\boldsymbol{\sigma}\cdot\mathbf{l}\frac{1}{r}\frac{\partial\rho}{\partial r}\right] \tag{3.14}$$

where in the last term ρ has been assumed to be spherical, a function of r only. Potential $V^{(1)}$ is known as the *Kisslinger potential.*

It was pointed out in the preceding section that the form we have used in developing $V^{(1)}$, (3.2), should be modified as follows [see (2.32)]:

$$c' \to c'h(k)h(k'), \qquad \text{where } h(k_{\text{cm}}) = \frac{1}{1+k_{\text{cm}}^2/\alpha^2} \qquad \alpha = 0.56\,\text{fm}^{-1} \tag{3.15}$$

Using this form, it is possible, with some approximation, to carry through the calculation leading to (3.12′). One obtains

$$V'_p = c^{(0)}(A-1)\nabla\cdot\nabla'\left(\rho\left(\frac{\mathbf{r}+\mathbf{r}'}{2}\right)\frac{\alpha^3}{8\pi}e^{-\alpha|\mathbf{r}-\mathbf{r}'|}\right)$$

so that

$$\int V'_p(\mathbf{r},\mathbf{r}')\psi(\mathbf{r}')\mathrm{d}\mathbf{r}' = -c^{(0)}(A-1)\nabla\cdot\int\rho\left(\frac{\mathbf{r}+\mathbf{r}'}{2}\right)\frac{(\alpha')^3}{8\pi}e^{-\alpha'|\mathbf{r}-\mathbf{r}'|}\nabla'\psi(\mathbf{r}')d\mathbf{r}' \tag{3.16}$$

where

$$\alpha' = \alpha\cdot\frac{m+E_L}{m}$$

The quantity $(\alpha'^3/8\pi)e^{-\alpha'|\mathbf{r}-\mathbf{r}'|}$ is a spread-out delta function becoming a delta function as $\alpha' \to \infty$. To obtain some feeling as to when the introduction of the form factor $h(k)$ is important, replace $\psi(\mathbf{r}')$ by $e^{i\mathbf{k}\cdot\mathbf{r}'}$, ρ by a constant ρ_0. The integral in (3.16) then equals

$$i\mathbf{k}e^{i\mathbf{k}\cdot\mathbf{r}}\frac{\rho_0}{(1+k^2/\alpha'^2)^2} \tag{3.17}$$

which is to be compared with $i\mathbf{k}\rho_0$ obtained from (3.13). Using the value of $\alpha' = 0.69\,\text{fm}^{-1}$, (3.16), one sees that the factor $1/[(1+k^2/\alpha'^2)]^2$ becomes important at relatively low energies.

The Lorentz–Lorenz Effect. The Kisslinger potential, (3.14), is the first-order term in the multiple scattering series for the optical potential. We shall now consider higher-order terms, or more physically the effects of correlations. Following Eisenberg and Koltun (80), the second-order term involving pair correlations will be considered first. We have remarked earlier on the approximations involved, but the result will provide us with a form that will be useful in obtaining the semiempirical optical potential.‡ We shall use (II.4.43) at zero energy. One further approximation will be made, namely $V^{(1)}$ and $\bar{\varepsilon}$, in (II.4.27) for the inverse of the propagator will dropped. With these modification one obtains

$$\tilde{V}^{(2)}_{\text{opt}}(\mathbf{k},\mathbf{k}') = (A-1)^2 \int \frac{d\mathbf{k}''}{(2\pi)^3} \tilde{t}(\mathbf{k},\mathbf{k}'') \frac{1}{-(1/2\mu)k''^2 + i\varepsilon} t(\mathbf{k}'',\mathbf{k}') \tilde{C}(\mathbf{k}''-\mathbf{k},\mathbf{k}'-\mathbf{k}'') \tag{3.18}$$

where $\mu = E_L m/(m+E_L)$. We consider only the effect of the P-wave term, so that (3.18) becomes

$$\tilde{V}^{(2)}_{\text{opt}}(\mathbf{k},\mathbf{k}') = -2\mu c^2 (A-1)^2 \int \frac{d\mathbf{k}''}{(2\pi)^3} (\mathbf{k}\cdot\mathbf{k}'')(\mathbf{k}''\cdot\mathbf{k}') \frac{1}{(k''^2/2\mu) - i\varepsilon} \tilde{C}(\mathbf{k}''-\mathbf{k},\mathbf{k}'-\mathbf{k}'')$$

One can decompose the numerator into a "monopole" and a "quadrupole" term:

$$(\mathbf{k}\cdot\mathbf{k}'')(\mathbf{k}''\cdot\mathbf{k}') = \tfrac{1}{3}\mathbf{k}\cdot\mathbf{k}'(k'')^2 + [(\mathbf{k}\cdot\mathbf{k}'')(\mathbf{k}''\cdot\mathbf{k}') - \tfrac{1}{3}(\mathbf{k}\cdot\mathbf{k}')(k'')^2] \tag{3.19}$$

Dropping the quadrupole term [see Warszawski, Gal, and Eisenberg (78)], $\tilde{V}^{(2)}$ becomes

$$\tilde{V}^{(2)}(\mathbf{k},\mathbf{k}') = -\tfrac{1}{3}(2\mu)(A-1)^2 c^2 (\mathbf{k}\cdot\mathbf{k}') \int \frac{d\mathbf{k}''}{(2\pi)^3} \tilde{C}(\mathbf{k}''-\mathbf{k},\mathbf{k}'-\mathbf{k}'') \tag{3.20}$$

Introducing the Fourier transform of $\tilde{C}$ yields

$$\begin{aligned}\tilde{V}^{(2)}(\mathbf{k},\mathbf{k}') &= -\tfrac{1}{3}(2\mu)(A-1)^2 c^2 (\mathbf{k}\cdot\mathbf{k}') \int d\mathbf{r}_1 e^{i(\mathbf{k}'-\mathbf{k})\cdot\mathbf{r}_1} C(\mathbf{r}_1,\mathbf{r}_1) \\ &= \tfrac{1}{3}2\mu(A-1)^2 c^2 (\mathbf{k}\cdot\mathbf{k}') \int \rho^2(\mathbf{r}_1) e^{i(\mathbf{k}'-\mathbf{k})\cdot\mathbf{r}_1} d\mathbf{r}_1 \end{aligned} \tag{3.21}$$

‡An optical analogy makes use of the fact that long-wavelength electromagnetic interactions with matter are, as in the case of the $\mathbf{k}\cdot\mathbf{k}'$ term of (3.11), dipole in nature. Therefore, there should be a term in the optical potential that is similar to the Clausius–Massotti term in the index of refraction for electromagnetic waves. This analogy has been exploited particularly by Madga and Torlief Ericson (66). [See also the most recent discussions by Ericson and Weise (88).] For a more extensive bibliography on the derivation of the Lorentz–Lorentz and other density-dependent effects, such as that induced by ρ-meson excitation [Baym and Brown (75)], see Eisenberg and Koltun (80).

Transforming to coordinate space and including the first-order P-wave contribution, one obtains

$$V_p(\mathbf{r}) = -(A-1)c_0\nabla\cdot[\rho - \tfrac{1}{3}(A-1)2\mu c_0\rho^2]\nabla \tag{3.22}$$

Eisenberg and Koltun (80) calculate the next-order term, making it plausible that

$$V_p(\mathbf{r}) = -(A-1)c_0\nabla\cdot\frac{\rho}{1+\tfrac{1}{3}2\mu(A-1)c_0\rho}\nabla \tag{3.23}$$

This should replace the $c^{(0)}$ term in (3.14). One should bear in mind that the form factors $h(k)$ have not been inserted and that only a subset of the higher-order terms has been summed. The cross-terms with the nonresonant components of $V^{(1)}$ have not been included, for example. Finally, (3.14) suitably modified by (3.23) does not contain absorption effects. The constants b, c, and so on, are nearly real in this energy range, indicating, as expected, that the inelastic and quasi-elastic cross sections are small. The Pauli principle plays an important role here.

The significant absorption reaction is the $\pi(2n)\to 2n$. Of course, there is the single-step process $\pi + n \to n$, but this involves a large momentum mismatch; that is, the energy of the final nucleon yields a larger momentum than that provided by the incident pion and the Fermi motion of the target nucleon. A more likely process is thought to be absorption of the pion by two nucleons which would go off in opposite directions with equal momenta (or nearly equal if the incident pion has some kinetic energy). The probability of this process is proportional to the (density)^2, since two nucleons are involved. These terms are introduced phenomenologically, so that $V^{(1)}$ reads

$$V = (A-1)\left\{b^{(0)}\rho + B^{(0)}\rho^2 - \nabla\cdot\frac{c^{(0)}\rho + AC^{(0)}\rho^2}{1+\xi(2\mu)(A-1)[c^{(0)}\rho + AC^{(0)}\rho^2]}\nabla - \tfrac{1}{2}\nabla^2\left[\frac{E_L}{m}c^{(0)}\rho + \frac{E_L}{2m}AC^{(0)}\rho^2\right]\right\} \tag{3.24}$$

where the spin-orbit terms have been omitted. The empirical parameter ξ replaces the factor of $\frac{1}{3}$ in (3.23). $B^{(0)}$ and $C^{(0)}$ are complex. Thus even when $b^{(0)}$, $c^{(0)}$, and $d^{(0)}$ are taken from pion–nucleon scattering, we are left with five empirical parameters whose values are obtained by fitting the experimental data.

The factors $b^{(0)}$ and $c^{(0)}$ parametrize the pion–nucleon t matrix. To obtain these in terms of the pion–nucleon scattering amplitude $f_{\pi n}$, we make use of (3.4). Dropping the recoil terms, (3.4) becomes

$$t_{\pi A} = -2\pi\frac{k_L}{k_{\mathrm{cm}}E_L}f_{\pi n} = -\frac{2\pi}{E_L}\left(1+\frac{E_L}{m}\right)f_{\pi n} \tag{3.25}$$

Each of the quantities in (3.3) must therefore be multiplied by $-2\pi/E_L(1+E_L/m)$. However, the parameter $B^{(0)}$ should contain the factor $(1+E_L/2m)$ since the interaction is with two nucleons. According to (3.10), the parameter c' of (3.2) should be multiplied by $(m/m+E_L)^2$ upon transforming to the laboratory reference frame. putting all these factors together yields

$$V = -\frac{2\pi}{E_L}\left\{\left(1+\frac{E_L}{m}\right)b'\rho + \left(1+\frac{E_L}{2m}\right)B'\rho^2 - \nabla\cdot\frac{\dfrac{1}{1+E_L/m}c' + \dfrac{A}{1+E_L/2m}C'}{1+4\pi\xi(A-1)\left[\dfrac{c'}{1+E_L/m}+\dfrac{AC'}{1+E_L/2M}\right]} - \frac{1}{2}\frac{E_L}{m}\nabla^2\left(\frac{c'}{1+E_L/m}+\frac{1}{2}\frac{AC'}{1+E_L/2m}\right)\right\} \tag{3.26}$$

The effect of the form factors $h(k^2)$ has not been included in (3.26). This potential is then inserted into the Klein–Gordon equation,

$$[\nabla^2 + (E_L - V_C)^2 - 2E_L V - m_\pi^2]\vartheta = 0$$

where V_C is the Coulomb potential and terms proportional to $(V)^2$ have been dropped. The results of Ericson and Weise (88) for the parameters b'_0, b'_1, c'_0, c'_1, and so on, are presented in Table 3.1.

The quantity $(b'_0)_{\text{eff}}$ is $b_0 - (1-m_\pi/m)[b_0^2 + 2b_1^2]\langle 1/r\rangle$, with $\langle 1/r\rangle$ taken to be $0.91\,m_\pi$. The term subtracted from b_0 is a second-order multiple scattering correction. These results should be compared with the values given in (3.3). The agreement with experiment is illustrated in Fig. 3.1. The predicted reaction cross sections are shown in Fig. 3.2.

TABLE 3.1 Low-Energy Optical Model Parameters

	π Atom	$T_\pi = 50$ MeV	Units
$(b'_0)_{\text{eff}}$	-0.03	$-0.04+0.004i$	m_π^{-1}
b'_1	-0.09	-0.09	m_π^{-1}
c'_0	0.23	$0.25+0.01i$	m_π^{-3}
c'_1	0.15	$0.16+0.005i$	m_π^{-3}
ξ	0.47	0.47	
B'	$0.002+0.05i$	$-0.005+0.03i$	m_π^{-4}
AC'	$0.04+0.12i$	$0.05+0.07i$	m_π^{-6}

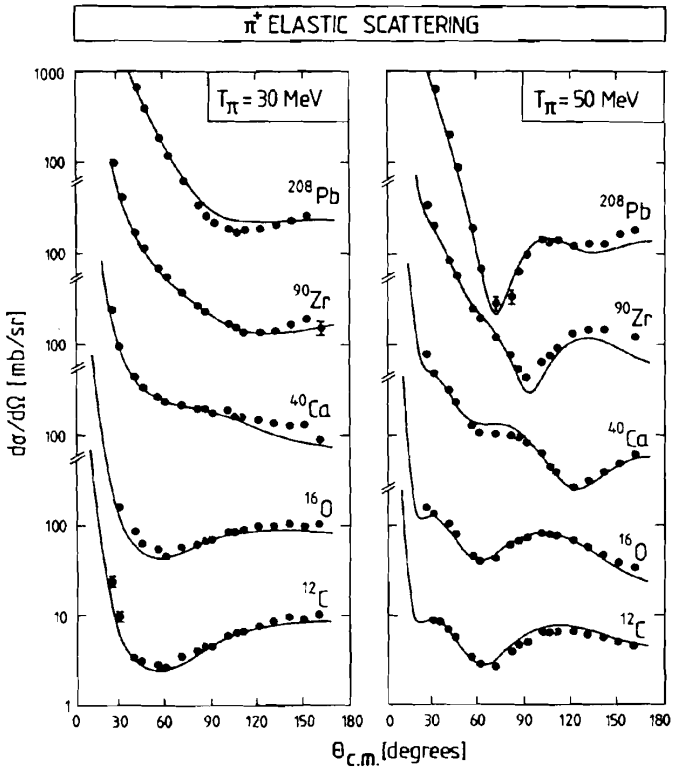

FIG. 3.1. Angular distributions for π^+ elastic scattering on various nuclei at $T_\pi = 30$ and 50 MeV [Carr, McManus, and Strickler (82)]. [From Ericson and Weise (88).]

B. Pion Energy 80–400 MeV; The Resonance Region

The dominant physical process in this energy range is the absorption of the incident pion by one of the nucleons in the target nucleus, forming a Δ. The Δ propagates through the nucleus, colliding with other nucleons. The Δ eventually decays into a nucleon + pion, leaving the nucleus in the ground state (elastic scattering) or excited (inelastic scattering). In an equivalent description the pion is absorbed by the target nucleus, forming a Δ–hole state, that is, a system consisting of $A - 1$ nucleons plus a Δ. This state acts as a doorway to more complex states, such as the $\Delta - n - 2$ hole state, and generally to Δ–hole plus multiparticle–hole states.

These two descriptions are equally valid. However, the first suggests a multiple scattering description, while the second suggests a doorway state description. In this volume we describe the latter, first proposed by Kisslinger and Wang (73, 76) and further exploited by Hirata, Koch, Lenz, and Moniz (78, 79) and Horikawa, Thies, and Lenz (80). A critical review of this area, including an

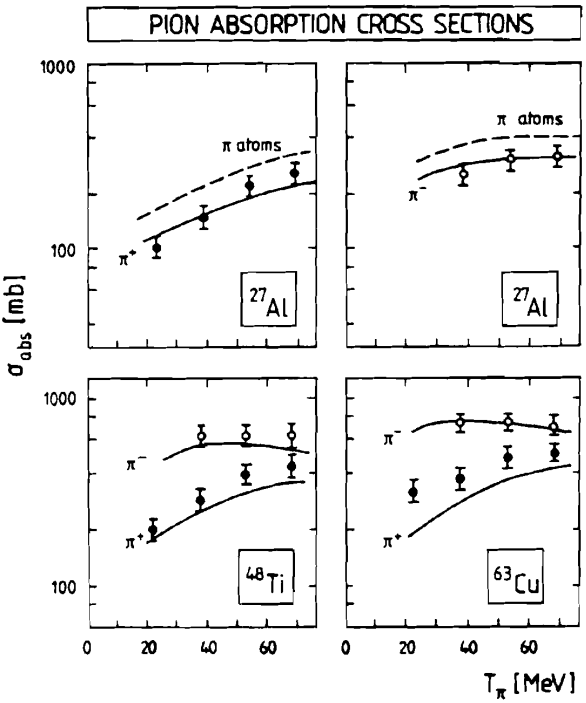

FIG. 3.2. Pion absorption cross sections for various nuclei as a function of energy [Carr, McManus, and Strickler (82)]. [From Ericson and Weise (88).]

analysis of both approaches, is being prepared by Lenz and Moniz (91). The reader is referred to this article for a discussion of the multiple scattering description together with an extensive list of references.

In the language of Chapter III, P space contains the states of A baryons, containing a maximum of one Δ and at least one but no more than one pion. As usual, the other degrees of freedom are contained in Q space. Perhaps the most important term in Q space is the two-pion + baryon system, which is generated by the reaction $(\pi n \to \pi\pi n)$. The Hamitonian H_{PP} we shall use is

$$H = \tilde{H}_A + h_\pi^0 + H' \tag{3.27}$$

where

$$\tilde{H}_A = H_n^0 + H_\Delta^0 + V_A(n) + V_A(\Delta) + H(n\Delta \to nn) + H(\pi n \to \Delta) + \text{hermitian conjugates of the last two terms} \tag{3.28}$$

The quantities h_π^0, H_n^0, and H_Δ^0 contain the mass and kinetic energy operators. The single-particle potentials $V_A(n)$ and $V_A(\Delta)$ approximate in shell model fashion the potential in which a nucleon or the Δ move. The term $H(n\Delta \to nn) + H(nn \to n\Delta)$

describes a Δ–nucleon collision in which the Δ is deexcited to a nucleon, and vice versa, a process that in nucleon–nucleon scattering leads to the production of a Δ. The last term $H(\pi n \to \Delta)$ describes the formation of a Δ by absorption of the pion by a nucleon, or vice versa, the decay of the Δ into a pion + nucleon.

We define a set of mutually orthogonal projection operators P_π, P_A, and P_Δ. The first of these, P_π, projects onto the space, consisting of the states of A nucleons and one pion. Thus

$$P_\pi H P_\pi = h_\pi^0 + H_A \equiv H_\pi \tag{3.29}$$

where

$$H_A = \sum_i (T_i + U_i) \qquad \Sigma U_i = V_A(n) \tag{3.30}$$

and

$$h_\pi^0 = T_\pi + m_\pi \tag{3.31}$$

The operator P_A projects onto a space containing only nucleons, so that

$$P_A H P_A = H_A \tag{3.32}$$

Finally, the operator P_Δ projects onto a space containing one Δ and $(A-1)$ nucleons:

$$P_\Delta H P_\Delta = \Delta m + \sum_i (H_i^{A-1} + T_{\Delta,i} + V_{\Delta,i}) \equiv H_\Delta \tag{3.33}$$

where $\Delta m = m_\Delta - m_n$, and the subscript i in the sum denotes the nucleon, which has been converted into a Δ. The sum $\sum V_{\Delta,i} = V_A(\Delta)$. The nondiagonal terms are

$$P_\Delta H P_\pi = H(\pi n \to \Delta) = \sum_i \hat{g}_i \equiv H_{\Delta\pi} \tag{3.34}$$

and

$$P_\Delta H P_A = H(\Delta n \to nn) = \sum_{i<j} v_{\Delta n}(i,j) \equiv H_{\Delta A} \tag{3.35}$$

The operator $H_{\Delta\pi}$ describes the absorption of a pion to form a delta. The operator $\hat{g}_i$ is given by (2.32):

$$\hat{g}_i \equiv g h(k^2) \mathbf{k} \cdot \mathbf{S}_i^\dagger \tag{3.36}$$

Finally, $H_{\Delta A}$ is $H(n\Delta \to nn)$. The corresponding wave functions

$$P_\pi \Psi = \psi_\pi \qquad P_A \Psi = \psi_A \qquad P_\Delta \Psi = \psi_\Delta \tag{3.37}$$

satisfy the Schrödinger equations (Ψ is the exact state vector)

$$(E - H_\pi)\psi_\pi = H_{\pi\Delta}\psi_\Delta \tag{3.38a}$$

$$(E - H_A)\psi_A = H_{A\Delta}\psi_\Delta \tag{3.38b}$$

$$(E - H_\Delta)\psi_\Delta = H_{\Delta A}\psi_A + H_{\Delta\pi}\psi_\pi + H_{\Delta Q}\psi_Q \tag{3.38c}$$

$$(E - H_Q)\psi_Q = H_{Q\Delta}\psi_\Delta \tag{3.38d}$$

where $Q\Psi \equiv \psi_Q$ contains all the channels, such as the Δ–hole, many p–h states not subtended by $P_\pi + P_A + P_\Delta$ (i.e., $Q = 1 - P_\pi - P_A - P_\Delta$). We have made the strong doorway state hypothesis, that only ψ_Δ connects to Q space. By the process of elimination one can obtain the transition matrix of various reactions. First, let us obtain a description of ψ_Δ. We "solve" (3.38a):

$$\psi_\pi = \phi_\pi^{(+)} + \frac{1}{E^+ - H_\pi} H_{\pi\Delta}\psi_\Delta$$

where $\phi_\pi^{(+)}$ is the incident pion–nuclear wave function. Second, from (3.38b) we find that

$$\psi_A = \frac{1}{E^+ - H_A} H_{A\Delta}\psi_\Delta$$

Hence

$$\left(E - H_\Delta - H_{\Delta A}\frac{1}{E^+ - H_A}H_{A\Delta} - H_{\Delta\pi}\frac{1}{E^+ - H_\pi}H_{\pi\Delta} - H_{\Delta Q}\frac{1}{E^+ - H_Q}H_{Q\Delta}\right)\psi_\Delta = H_{\Delta\pi}\phi_\pi^{(+)} \tag{3.39}$$

To simplify the appearance of these equations, introduce the definitions

$$H_{\Delta A}\frac{1}{E - H_A}H_{A\Delta} \equiv W_\Delta^{(A)} \tag{3.40a}$$

$$H_{\Delta\pi}\frac{1}{E - H_\pi}H_{\pi\Delta} \equiv W_\Delta^{(\pi)} \tag{3.40b}$$

and

$$H_{\Delta Q}\frac{1}{E - H_Q}H_{Q\Delta} \equiv W_\Delta^{(Q)} \tag{3.40c}$$

Equation (3.39) becomes

$$(E - H_\Delta - W_\Delta)\psi_\Delta = H_{\Delta\pi}\phi_\pi^{(+)} \tag{3.41}$$

where

$$W_\Delta = W_\Delta^{(A)} + W_\Delta^{(\pi)} + W_\Delta^{(Q)} \tag{3.42}$$

Inserting (3.41) into (3.38) yields expressions for the ψ_π and ψ_A. From ψ_π one can obtain the $\mathcal{T}$ matrix for π-nucleus scattering

$$\mathcal{T}_{\pi\pi} = \mathcal{T}_{\pi\pi}^{P} + \left\langle \phi_\pi^{(-)} H_{\pi\Delta} \frac{1}{E^{(+)} - H_\Delta - W_\Delta} H_{\Delta\pi} \phi_\pi^{(+)} \right\rangle \tag{3.43}$$

where $\mathcal{T}_{\pi\pi}^{P}$ is the amplitude for nonresonant reactions, One can also obtain the amplitude for π absorption, assuming the absence of nonresonant terms:

$$\mathcal{T}_{\mathrm{ab}} = \left\langle \psi_A^{(-)} H_{A\Delta} \frac{1}{E^{(+)} - H_\Delta - W_\Delta} H_{\Delta\pi} \phi_\pi^{(+)} \right\rangle \tag{3.44}$$

where $\psi_A^{(-)}$ is an excited state of the target nucleus in the continuum, usually a $2p$–$2h$ state.

Each of the components of W_Δ corresponds to a physical process. The operator $W_\Delta^{(A)}$ describes a process in which the Δ is converted into a nucleon, thereby forming the target nucleus again. This is followed by propagation and recovery of the Δ. We shall refer to it as *absorption*. The operator $W_\Delta^{(\pi)}$ describes the decay of the Δ into a π + nucleon, forming the target nucleus plus a pion. This is followed by propagation and reabsorption of the pion to form the Δ.

To evaluate $\mathcal{T}_{\pi\pi}$ or $\mathcal{T}_{\mathrm{ab}}$, it is necessary to determine the states of the operator $H_\Delta + W_\Delta$. Not all the states, of course: rather, that state which is most strongly excited by the incident pion. The principal component is presumed to be a Δ–hole state. We shall therefore look for that linear combination of Δ–hole states which diagonalize (approximately, of course) $H_\Delta + W_\Delta$. This is the doorway state. Toward that end we shall examine and approximate W_Δ.

Consider first $W_\Delta^{(\pi)'}$, where the prime indicates that we have removed the incident channel; that is, the intermediate states will only be those in which the target nucleus is excited. If P_0 is the projection operator for the nuclear ground state and $Q_0 = 1 - P_0$ is its complement, then

$$W_\Delta^{(\pi)'} = H_{\Delta\pi} Q_0 \frac{1}{E - H_\pi} H_{\pi\Delta} \tag{3.45}$$

Inserting (3.34), we have

$$W_\Delta^{(\pi)'} = \sum_{i,j} \hat{g}_i^\dagger Q_0 \frac{1}{E - H_\pi} \hat{g}_j \tag{3.46}$$

where i and j indicate the nucleon which is converted into a Δ (and vice versa).

We separate the diagonal and nondiagonal contributions:

$$W_{\Delta}^{(\pi)'} \equiv W_{D}^{(\pi)} + W_{ND}^{(\pi)} \tag{3.47}$$

where

$$W_{D}^{(\pi)} = \sum \hat{g}_i^{\dagger} Q_0 \frac{1}{E - H_{\pi}} \hat{g}_i \tag{3.48}$$

This term corresponds to the case where the system returns to a Δ–hole configuration while W_{ND} involves a final system consisting of a Δ–p–$2h$ configuration. The latter, W_{ND}, is referred to as the *rescattering* term.

Similarly, $W_{\Delta}^{(A)}$ can be broken up into a term in which the Δ–h configuration is preserved and a term in which the final system involves the Δ–p–$2h$ configuration, so that

$$W_{\Delta}^{(A)} = W_{D}^{(A)} + W_{ND}^{(A)} \tag{3.49}$$

Hence the denominator in (3.43) can be rewritten

$$E^{(+)} - H_{\Delta} - W_{\Delta} = E^{(+)} - H_{\Delta} - W'_{D} - W^{(Q)} \tag{3.50}$$

where

$$W'_{D} = W_{D}^{(\pi)} + W_{D}^{(A)} \tag{3.51}$$

and

$$W^{(Q)} = W_{\Delta}^{(Q)} + W_{ND}^{(\pi)} + W_{ND}^{(A)} \tag{3.52}$$

The decomposition could have been introduced at an earlier stage [Eq. (3.38)] by the addition of suitable projection operators or through use of the multistep theory of Chapter VII. Physically, one should note that the Δ–p–$2h$ state can be generated either through the rescattering term or through $W_{ND}^{(A)}$. Both mechanisms must be considered when the generation of a Δ–p–$2h$ configuration is important, as it is in the case of double charge exchange ($\pi^- \to \pi^+$).

To make the Pauli-blocking effect explicit, we replace Q_0 in (3.48) by $1 - P_0$, where P_0 is the projection onto occupied levels. Thus

$$W_{D}^{(\pi)} = \sum \hat{g}_i^{\dagger} \frac{1}{E - H_{\pi}} \hat{g}_i + W_{PB}^{(\pi)} \tag{3.53}$$

where

$$W_{PB}^{(\pi)} \equiv -\sum \hat{g}_i \frac{P_0}{E - H_{\pi}} \hat{g}_i \tag{3.54}$$

Equation (3.50) is therefore

$$E^{(+)} - H_{\Delta} - W_{\Delta} = E^{(+)} - H_{\Delta} - w_{\Delta} - W_{PB}^{\pi} - w_{gs} - W^{(Q)} \tag{3.55}$$

where

$$w_\Delta = \sum g_i^\dagger \frac{1}{E - H_\pi} g_i + W_\Delta^{(A)} \tag{3.56}$$

and

$$w_{gs} = H_{\Delta\pi} P_0 \frac{1}{E - H_\pi} H_{\pi\Delta} \tag{3.57}$$

But

$$\begin{aligned} H_\pi &= T_\pi + m_\pi + H_A \\ &= T_\pi + m_\pi + T_i + U_i + H_{A-1} \\ &\simeq T_\Delta + U + H_{A-1} + m_\pi \end{aligned} \tag{3.58}$$

In the last equation the pion–nucleon center-of-mass kinetic energy has been replaced by the Δ kinetic energy T_Δ and U is now the average Δ–nucleus potential. Because the nuclear wavefunctions are antisymmetrized, the sum in (3.56) can be replaced by a single term. This is identical with the similar term appearing in the denominator of (2.31) except that H_{PP} is now given by H_π as approximated by (3.58). Therefore,

$$\sum_i \hat{g}_i^\dagger \frac{1}{E - H_\pi} \hat{g}_i = \Sigma(E - T_\Delta - U - H_{A-1} - m_\pi) \tag{3.59}$$

where Σ is defined by

$$\Sigma(E) \equiv H_{QP} \frac{1}{E^+ - H_{PP}} H_{PQ}$$

from (2.31).

The denominator of (3.43) becomes

$$\begin{aligned} E^{(+)} - H_\Delta - W_\Delta = E^{(+)} &- H_\Delta - W_D^{(A)} \\ &- \Sigma(E - T_\Delta - U - H_{A-1}) - W_{PB}^{(\pi)} - W^{(Q)} - w_{gs} \end{aligned}$$

To make further progress, we linearize Σ by expanding $E - \Sigma$ about its zero, $E - E_R + i\Gamma/2$. We obtain

$$\begin{aligned} E^{(+)} - H_\Delta - W_\Delta = E - E_R(E) + \frac{i\Gamma(E)}{2} \\ - \gamma(E - T_\Delta - U - H_{A-1}) - W_{PB}^{(\pi)} - W^{(Q)} - w_{gs} \end{aligned} \tag{3.60}$$

where

$$\gamma = 1 + \left(\frac{\partial \Sigma}{\partial E}\right)_{E = E - E_R + i\Gamma/2} \tag{3.61}$$

and

$$\mathcal{U} = U + \frac{1}{\gamma} W_D^{(A)}$$

The expression

$$\mathcal{H} = \gamma(T_\Delta + \mathcal{U} + H_{A-1}) + W_{PB}^{(\pi)} + W^{(Q)} \tag{3.62}$$

is the Δ–nucleus interaction. Medium modifications are given by γ and $W_{PB}^{(A)} + W^{(Q)}$. In the notation of Feshbach (82),

$$W^Q \equiv \hat{W}^\downarrow \tag{3.63}$$

and

$$w_{gs} \equiv \hat{W}^\uparrow \tag{3.64}$$

where $\hat{W}^\downarrow$ is the spreading operator and $\hat{W}^\uparrow$ the escape operator.

Expression (3.66) is now in a form that makes a phenomenological approach possible. One adopts the optical model strategy by replacing $\hat{W}^\downarrow$ with a spreading potential composed of central and spin-orbit terms:

$$\hat{W}^\downarrow = W_0 \rho(r) + 2\mathbf{L}_\Delta \cdot \boldsymbol{\Sigma}_\Delta V_{LS}^{(0)} \mu r^2 e^{-\mu r^2} \tag{3.65}$$

where $\boldsymbol{\Sigma}_\Delta$ is the spin-$\frac{3}{2}$ operator for the Δ. The matrix elements of other terms $\hat{W}^\uparrow$ and $W_{PB}^{(\pi)}$ can be evaluated in the Δ–hole basis. For details, see Hirata, Koch, Lenz, and Moniz (79).

Doorway States. We now turn to the problem of obtaining the eigenstates of

$$\mathcal{H} \equiv H_\Delta + W_\Delta = \gamma(T_\Delta + \mathcal{U} + H_{A-1}) + W_{PB}^{(\pi)} + \hat{W}^\downarrow \tag{3.66}$$

as given in (3.62). The potential $\mathcal{U}$ is taken by Hirata, Koch, Lenz, and Moniz (79) to be proportional to the nucleon density with a depth of 55 MeV. The remaining parameters are W_0, $V_{LS}^{(0)}$, and μ. The method used by these authors and Horikawa, Thies, and Lenz (80) was suggested by the results they obtained when the eigenfunctions of $\mathcal{H}$ were determined using harmonic oscillator wave functions. It was found that the contribution of one particular eigenfunction dominated the $\mathcal{T}$ matrix for elastic scattering. Moreover, the overlap of this wave function, D, with the state developed by the first interaction was large; that is,‡

$$\frac{|\langle \tilde{D}|\hat{g}\psi_\pi^{(+)}\rangle|^2}{|\langle \psi_\pi^{(+)}|\hat{g}^\dagger \hat{g}\psi_\pi^{(+)}\rangle|^2} = 0.9 \tag{3.67}$$

‡In the notation of Chapter III this ratio is

$$\frac{|\langle \Phi_d H_{dp}\psi^{(+)}\rangle|^2}{|\langle \psi^{(+)}|H_{pd}H_{dp}|\psi^{(+)}\rangle|^2}$$

Here $\tilde{D}$ is the adjoint to the D used because $\mathscr{H}$ is complex and $\psi^{(+)}$ is the scattering solution of (3.38*a*). This result suggested the use of the Lanczos method [Morse and Feshbach (53, p. 1155); see also Whitehead, Watt, Cole, and Morrison (77)]. Let

$$D_0 = \hat{g}\psi_\pi^{(+)}\rangle \tag{3.68}$$

Then D_1 is generated by

$$D_1 = \mathscr{H}D_0 - \frac{\langle \tilde{D}_0 \mathscr{H} D_0 \rangle}{\langle \tilde{D}_0 D_0 \rangle} D_0 \tag{3.69}$$

Note the orthogonality:

$$\langle \tilde{D}_0 D_1 \rangle = 0$$

State D_2 is obtained by operating on D_1 and orthogonalizing with respect to D_0 and D_1:

$$D_2 = \mathscr{H}D_1 - \frac{\langle \tilde{D}_1 \mathscr{H} D_1 \rangle}{\langle \tilde{D}_1 D_1 \rangle} D_1 - \frac{\langle \tilde{D}_0 \mathscr{H} D_1 \rangle}{\langle \tilde{D}_0 D_0 \rangle} D_0 \tag{3.70}$$

$$\langle \tilde{D}_0 D_2 \rangle = \langle \tilde{D}_1 D_2 \rangle = 0 \tag{3.71}$$

One continues this process obtaining the general expression for the nth iterate D_n:

$$D_n = \mathscr{H}D_{n-1} - \frac{\langle \tilde{D}_{n-1} \mathscr{H} D_{n-1} \rangle}{\langle \tilde{D}_{n-1} D_{n-1} \rangle} D_{n-1} - \frac{\langle \tilde{D}_{n-2} \mathscr{H} D_{n-1} \rangle}{\langle \tilde{D}_{n-2} D_{n-2} \rangle} D_{n-2} \tag{3.72}$$

D_n is not only orthogonal to D_{n-1} and D_{n-2} but to D_{n-3}, $D_{n-\alpha}$ as well. One can show (this is left as an exercise) that

$$\langle \tilde{D}_\beta \mathscr{H} D_\alpha \rangle = 0 \qquad \text{unless } \beta = \alpha, \quad \alpha \pm 1 \tag{3.73}$$

The three-term recurrence formula (3.72) thus generates an orthogonal set. To obtain the eigenvalue of $\mathscr{H}$, one expands the eigenfunction ψ_Δ in terms of the iterates D_n:

$$\psi = \Sigma a_n D_n \tag{3.74}$$

Operating with $\mathscr{H}$ on ψ, we find that

$$\mathscr{H}\psi = \Sigma a_n \mathscr{H} D_n = \left[a_{n-1} + \frac{\langle \tilde{D}_n \mathscr{H} D_n \rangle}{\langle \tilde{D}_n D_n \rangle} a_n + \frac{\langle \tilde{D}_n \mathscr{H} D_{n+1} \rangle}{\langle \tilde{D}_n D_n \rangle} a_{n+1} \right] D_n \qquad n > 0 \tag{3.75}$$

and

$$\mathscr{H}\psi = \left[\frac{\langle \tilde{D}_0 \mathscr{H} D_0\rangle}{\langle \tilde{D}_0 D_0\rangle} a_0 + \frac{\langle \tilde{D}_0 \mathscr{H} D_1\rangle}{\langle \tilde{D}_0 D_0\rangle} a_1\right] D_0 \qquad n=0 \tag{3.76}$$

The eigenvalue problem $\mathscr{H}\psi = \varepsilon\psi$ yields

$$a_{n-1} + \left[\frac{\langle \tilde{D}_n \mathscr{H} D_n\rangle}{\langle \tilde{D}_n D_n\rangle} - \varepsilon\right] a_n + \frac{\langle \tilde{D}_n \mathscr{H} D_{n+1}\rangle}{\langle \tilde{D}_n D_n\rangle} a_{n+1} = 0 \qquad n>0 \tag{3.77}$$

To "solve," let

$$R_n \equiv \frac{a_{n-1}}{a_n}$$

Then (3.77) becomes

$$R_n = \left[\varepsilon - \frac{\langle \tilde{D}_n \mathscr{H} D_n\rangle}{\langle \tilde{D}_n D_n\rangle}\right]^{-1} - \frac{\langle \tilde{D}_n \mathscr{H} D_{n+1}\rangle}{\langle \tilde{D}_n D_n\rangle} \frac{1}{R_{n+1}} \tag{3.78}$$

The solution of the equation for R_1 is the continued fraction:

$$R_1 = \varepsilon - \frac{\langle \tilde{D}_1 \mathscr{H} D_1\rangle}{\langle \tilde{D}_1 D_1\rangle} - \frac{\langle \tilde{D}_1 \mathscr{H} D_2\rangle}{\langle \tilde{D}_1 D_1\rangle} \times \frac{1}{\left[\varepsilon_1 - \dfrac{\langle \tilde{D}_2 \mathscr{H} D_2\rangle}{\langle \tilde{D}_2 D_2\rangle}\right] - \dfrac{\langle \tilde{D}_2 \mathscr{H} D_3\rangle}{\langle \tilde{D}_3 D_3\rangle} \dfrac{1}{[\varepsilon - \langle \tilde{D}_3 \mathscr{H} D_3\rangle / \langle \tilde{D}_3 D_3\rangle] - \cdots}} \tag{3.79}$$

One can also obtain an expression for R_1 from (3.76):

$$R_1 = \frac{\langle \tilde{D}_0 \mathscr{H} D_1\rangle / \langle \tilde{D}_0 D_0\rangle}{\varepsilon - \langle \tilde{D}_0 \mathscr{H} D_0\rangle / \langle \tilde{D}_0 D_0\rangle} \tag{3.80}$$

Equating (3.80) with (3.79) yields an equation for ε. There are many solutions for ε, each corresponding to an eigenstate of $\mathscr{H}$. To obtain the wave function corresponding to each ε, we need the expansion coefficients a_n. These are given by

$$\frac{a_n}{a_0} = \frac{1}{R_n} \cdot \frac{1}{R_{n-1}} \cdots \frac{1}{R_1}$$

One can also obtain a continued fraction expression for the $\mathscr{T}$ matrix for elastic scattering. From (3.43) and (3.68) we have

$$\mathscr{T}_{\pi\pi} = \langle \tilde{D}_0 G D_0 \rangle \tag{3.81}$$

where

$$G = \frac{1}{\mathscr{E} - \mathscr{H}} \tag{3.82}$$

The complex energy $\mathscr{E} = E - E_R(E) + i\Gamma(E)/2$. Define the matrix element

$$G_{n0} \equiv \langle \tilde{D}_n G D_0 \rangle \tag{3.83}$$

so that $G_{00} = \mathscr{T}_{\pi\pi}$. We can therefore rewrite (3.82) as follows:

$$\mathscr{E} G_{n0} - \Sigma \langle \tilde{D}_n \mathscr{H} D_\nu \rangle G_{\nu 0} = \delta_{n0}$$

Because of (3.73) this becomes

$$[\mathscr{E} - \langle \tilde{D}_n \mathscr{H} D_n \rangle] G_{n0} = \langle \tilde{D}_n \mathscr{H} D_{n-1} \rangle G_{n-1,0} + \langle \tilde{D}_n \mathscr{H} D_{n-1} \rangle G_{n+1,0} + \delta_{n0} \tag{3.84}$$

The solution of this set of equations has been obtained earlier in this volume. Let

$$\mathscr{H}_{nm} \equiv \langle \tilde{D}_n \mathscr{H} D_m \rangle$$

Then

$$G_{00} = \cfrac{1}{\mathscr{E} - \mathscr{H}_{00} - \cfrac{\mathscr{H}_{01}\mathscr{H}_{10}}{\mathscr{E} - \mathscr{H}_{11} - \cfrac{\mathscr{H}_{12}\mathscr{H}_{21}}{\mathscr{E} - \mathscr{H}_{12} - \cfrac{\mathscr{H}_{23}\mathscr{H}_{32}}{\mathscr{E} - \mathscr{H}_{33} - \cdots}}}} \tag{3.85}$$

This is an exact solution of the elastic scattering problem.

It is also possible to obtain an expression for a reaction. Let us consider as an example the case of inelastic scattering to a state $\phi_{\pi,\alpha}$. The $\mathscr{T}$ matrix is then

$$\mathscr{T}_{\alpha 0}^{\text{inel}} = \langle \phi_{\pi\alpha}^{(-)} \hat{g}^\dagger G D_0 \rangle \tag{3.86}$$

Expanding GD_0 in terms of D_n yields

$$\mathscr{T}_{\alpha 0}^{\text{inel}} = \sum_n \frac{\langle \phi_{\pi\alpha}^{(-)} \hat{g}^\dagger D_n \rangle}{\langle \tilde{D}_n D_n \rangle} G_{n0} \tag{3.87}$$

From (3.84)

$$G_{n0} = \cfrac{1}{\mathscr{E} - \mathscr{H}_{nn} - \cfrac{\mathscr{H}_{n,n+1}\mathscr{H}_{n+1,n}}{\mathscr{E} - \mathscr{H}_{n+1,n+1} - \cfrac{\mathscr{H}_{n+1,n+2}\mathscr{H}_{n+2,n+1}}{\mathscr{E} - \mathscr{H}_{n+2,n+2} - \cdots}}} \tag{3.88}$$

This expression can be inserted into (3.87) to obtain the inelastic transition amplitude. As one can see from (3.87), $\mathscr{T}^{\text{inel}}$ will be especially large if $\hat{g}\phi_{\pi\alpha}$ has a strong overlap with the incident doorway sate.

The convergence of the continued fractions has been studied by Lenz, Moniz, and Yazaki (80). They consider a number of model scattering problems. The convergence to the exact partial wave amplitude and the forward scattering amplitude is determined by the parameter $\mu = (k - \kappa)R$, where $k - \kappa$ is the momentum difference outside and inside the interaction region and R is the radius of that region. Iterations up to a number equal to $|\mu|$ leads to high accuracy. This number is $\leqslant 5$ for pion–nucleon scattering in both the high- and low-energy limits. For light nuclei $|\mu| \sim 1$, which is a great simplification. The convergence of the nonforward amplitude involves a second parameter $\xi = qR$, where q is the momentum transfer. If $\xi \leqslant |\mu|$, then $|\mu|$ determines the number of iterations. If $\xi > |\mu|$, more iterations are needed. One word of caution: These criteria are generalizations obtained from the study of specific models, the square well, and the Woods–Saxon potential and may not be valid for other situations.

An illustrative example is provided by the potential suggested by pion–nucleus scattering in the resonance region:

$$V(r) = \frac{4\pi\rho_0}{R}\frac{\Gamma/2}{E - E_R + i\Gamma/2} f(r)$$

where $f(r)$ is either a square well of radius R or a Woods–Saxon well:

$$f(r) = \frac{1}{1 + e^{(r-R)/a}}$$

Lenz, Moniz, and Yazaki (80) take $R = 1.12A^{1/3}$, $\rho_0 = 0.17\,\text{fm}^{-3}$, $\Gamma = 110\,\text{MeV}$, $E_R = 190\,\text{MeV}$, $A = 16$, k the pion–nucleus relative momentum in units of $\hbar$, $1.5\,\text{fm}^{-1}$, and $a = 0.53\,\text{fm}$. Table 3.2 shows the rate of convergence for these two types of wells for the $L = 0$ wave. N is the iterate number.

The wave function also converges rapidly, as is demonstrated by Fig. 3.3. Another example is given by Hirata, Koch, Lenz, and Moniz (79) for $E_{\pi+} = 163\,\text{MeV}$, $\pi^{-}{}^{16}\text{O}$ scattering. $\hat{W}^{\downarrow}$ is given by the first term in (3.65). The mean potential, $\mathscr{U}$, is taken to be proportional to $\rho(r)$ with a depth of 55 MeV. The results are shown in Table 3.3. The exact result was obtained by a straightforward diagonalization of $\mathscr{H}$ using harmonic oscillator wave functions. We see that

TABLE 3.2 $\mathscr{T}_{L=0}$

N	Square Well	Woods–Saxon
0	$-0.0031 + 0.5461i$	$0.0322 + 0.4961i$
1	$-0.0441 + 0.4172i$	$0.0120 + 0.4256i$
2	$-0.0410 + 0.4172i$	$0.0144 + 0.4298i$
3	$-0.0410 + 0.4172i$	$0.0144 + 0.4298i$

TABLE 3.3

N	$\mathscr{T}_{L=0}$	ε	$\mathscr{T}_{L=4}$	ε
0	$0.155 + 0.490i$	$-53.1 - 154.5i$	$0.060 + 0.280i$	$13.9 - 14.4i$
1	$0.159 + 0.372i$	$-68.7 - 138.5i$	$0.062 + 0.246i$	$-2.7 - 17.7i$
2	$0.154 + 0.381i$	$-68.7 - 138.0i$	$0.059 + 0.251i$	$-3.4 - 22.7i$
"Exact"	$0.154 + 0.381i$	$-68.7 - 138.0i$	$0.059 + 0.250i$	$-3.5 - 23.1i$

convergence for $\mathscr{T}_L$ is very good in both cases. Accurate values of ε are obtained for $L = 0$ after two iterates. Three iterates are needed for ε when $L = 4$, as the value with one iterate is nowhere near the exact answer.

The contribution of the various components of $\mathrm{Im}\,\varepsilon$ are shown in Fig. 3.4. (The qualitative results are not changed by the inclusion of the spin-orbit term in Eq. (3.65) [see Horikawa, Thies, and Lenz (80).] We see that the escape width, $\mathrm{Im}\,W^{\uparrow}$, also referred to as the rescattering term, dominates. The Pauli blocking term does reduce the width substantially, but this is more than made up by $\mathrm{Im}(W^{\uparrow} + W^{\downarrow})$.

This theory has been applied to a number of reactions for which the Δ resonance is important. Background terms that do not involve the Δ must be added. The elastic scattering of π^- by ^{16}O at 114 and 240 MeV is shown in Fig. 3.5. The agreement is good and the need for the spin-orbit term is quite clearly demonstrated. The agreement is not quite as good for ^{12}C, where substantial deviations at back angles are recorded. Comparison has also been made with ^{4}He data [Horikawa, Thies, and Lenz (80)] and with Pb data [Karaoglu and Moniz (86)]. The empirical values of the parameters of the spreading potential W_0, $V_{LS}^{(0)}$, and μ, (3.65), are given in Fig. 3.6 and Table 3.4.

TABLE 3.4 Parameters $V_{LS}^{(0)}$ and μ for the Spin-Orbit Potential

	$\mu\,(\mathrm{fm}^{-2})$	$V_{LS}^{(0)}\,(\mathrm{MeV})$
$\pi^+ + {}^4\mathrm{He}$	0.25	$-4.6 - 1.8i$
$\pi^- + {}^{12}\mathrm{C}$	0.35	$-10 - 4i$
$\pi^- + {}^{16}\mathrm{O}$	0.3	$-10 - 4i$

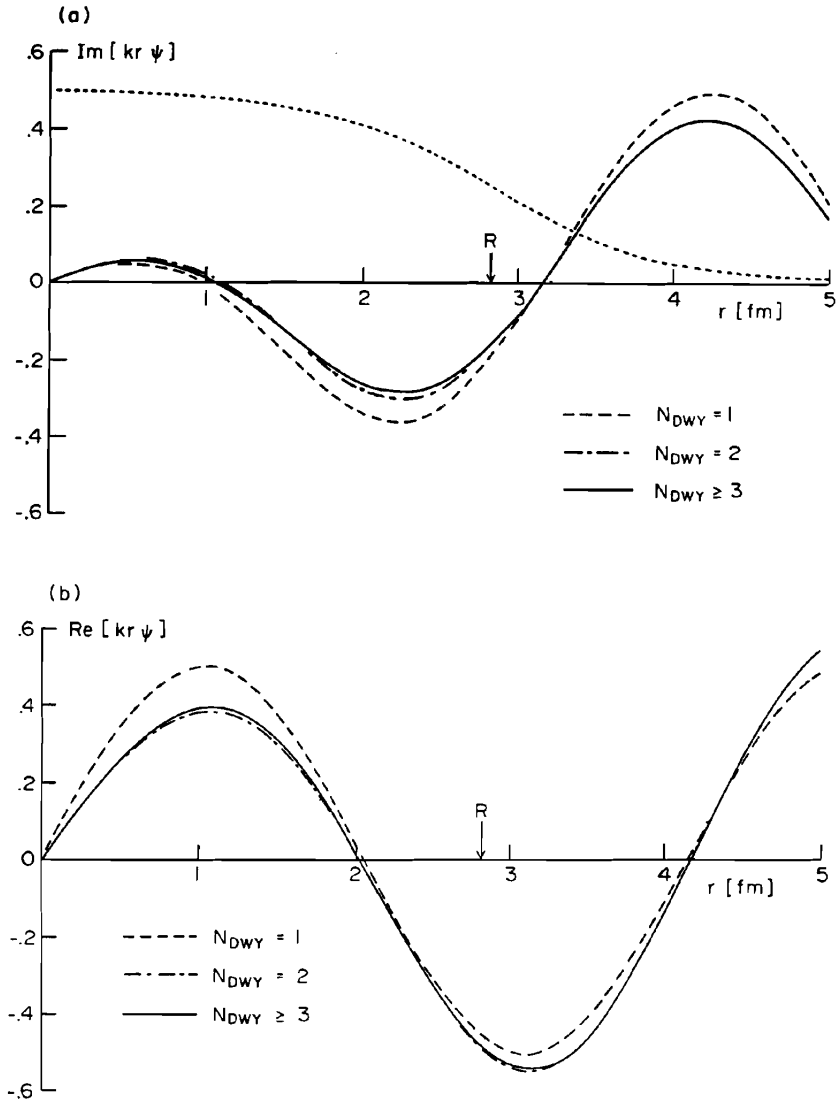

FIG. 3.3. *S*-wave scattering wave function for a Woods–Saxon potential with strength appropriate to intermediate energy pion–nucleus scattering. The (*a*) imaginary and (*b*) real parts of the wave function are shown for different numbers of doorway states. The dotted line in (*a*) shows the shape of the Woods–Saxon potential. [From Lenz, Moniz, and Yazaki (80).]

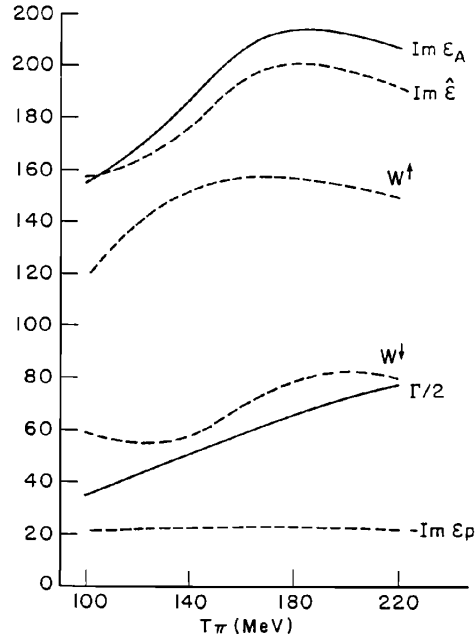

FIG. 3.4. Decomposition of the imaginary part of the doorway expectation value of the isobar-hole Hamiltonian. The eigenvalue of the leading eigenstate is denoted by $\hat{\varepsilon}$, and Γ is the free-space isobar width.

The isobar-doorway model has been applied to inelastic scattering [Lenz, Thies, and Horikawa (82); Takaki (86)] and to nuclear photoabsorption and Compton scattering [Koch, Moniz, and Ohtsuka (84)]. Inelastic scattering and charge exchange scattering are discussed in the following sections. These provide tests of the isobar-doorway model which differ from those made by elastic scattering. The model has been successful, although some puzzles do remain, particularly at back angles. The overall result is that medium effects are very important. As a consequence, the DWA method is not successful in describing reactions in this energy range.

Reviews of the isobar-doorway model have been published by Moniz (78a, b). A review is now being prepared by Lenz and Moniz (91) which will contain a critical analysis of the various methods that have been used. Another approach to the isobar-doorway model is given by Oset with Weise (79). Other procedures are used by Wilkin (79), Lee and Ohta (82), Lee and Kurath (80), Johnson (86), and Liu and Shakin (77, 79).

Inelastic Scattering [Lenz, Thies, and Horikawa (82); Hirata, Lenz, and Thies (83); Takaki (86)]. The excitation of a nucleus by a pion whose energy is in the

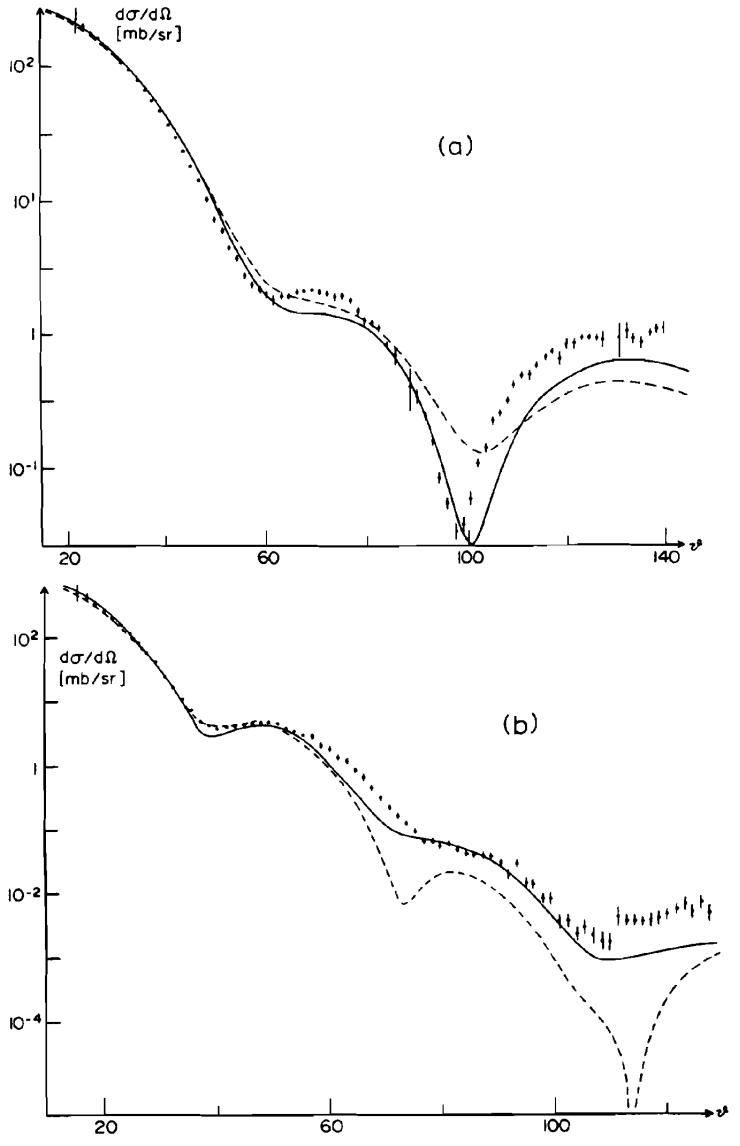

FIG. 3.5. π^{-16}O scattering at 114 and 240 MeV, solid lines, spin-orbit term included (see Fig. 3.6 and Table 3.4 for the strength of central and spin-orbit term); dashed line, without spin-orbit potential ($W_0 = 2 - i55$ at 114 MeV and $W_0 = -12 - i35$ at 240 MeV, $V_{LS} = 0$). [From Horikawa, Thies, and Lenz (80).]

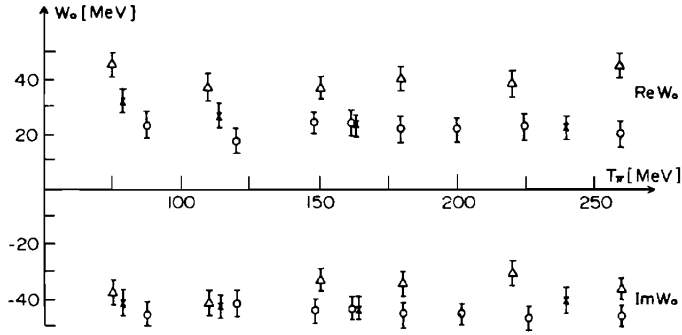

FIG. 3.6. Strength of central part of the spreading potential π–^{4}He (triangles), π–^{12}C (circles) and π–^{16}O (crosses). [From Horikawa, Thies, and Lenz (80).]

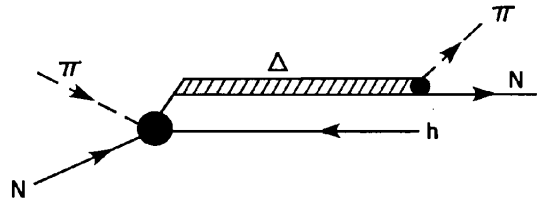

FIG. 3.7. Pion particle–hole excitation.

resonance region is the subject of this section. We consider only those contributions made when the intermediate state involves the Δ. As mentioned earlier, there may be contributions from the nonresonant components of the π–N reaction. The obvious first-order contribution involves the formation of the Δ–hole state. The Δ decays back into a pion plus nucleon so that the residual nucleus has a p–hole (p = particle) excitation. This is illustrated by Fig. 3.7. The amplitude for this process is

$$\mathscr{T}_{fi} = \left\langle \psi_{\pi f}^{(-)} H_{A\Delta} \frac{1}{E - \mathscr{H}_{\Delta}} H_{\Delta A} \psi_{\pi i}^{(+)} \right\rangle \tag{3.89}$$

The DWIA approximation [Lenz, Thies, and Horikawa (82)] consists in using the Δ–hole Hamiltonian for $\mathscr{H}_{\Delta}$ and the elastic scattering wave functions as modified by the Δ resonance described in the preceding section. The quantity $H_{\Delta A}$ is defined by (3.36) and $\mathscr{H}_{\Delta}$ is defined by (3.62). The amplitude equation (3.89) in the DWIA approximation has been studied thoroughly by Lenz, Thies, and Horikawa (82). We are able here to point out a few salient features of their analysis of inelastic π scattering. *Incidentally, most of these remarks apply equally well to elastic scattering.*

We first note that for p–h excitations,

$$H_{A\Delta}H_{\Delta A} = g^2 h(k)\left[\sum_{i<j} \mathbf{S}_i\cdot\mathbf{k}S_j^\dagger\cdot\mathbf{k}'\right]h(k')$$
$$= g^2 h(k)\left[\sum_{i} \mathbf{S}_i\cdot\mathbf{k}S_i^\dagger\cdot\mathbf{k}'\right]h(k') \tag{3.90}$$

In this expression, $\mathbf{k}$ is the center-of-mass momentum/$\hbar$ for the system consisting of a pion and a target nucleon. In the laboratory frame, $\mathbf{k}$ in (3.90) must be replaced by

$$\mathbf{k} \to \mathbf{k} - \alpha\mathbf{K} \tag{3.91}$$

and similarly for $\mathbf{k}'$. The vector $\mathbf{K}$ is the momentum of the nucleon/$\hbar$, while α is E/mc^2, where E is the total energy of the pion in the laboratory frame and m is the nucleon mass. The term proportional to α is referred to as the "recoil" term. The "static" limit is obtained by placing $\alpha = 0$. Equation (3.90) becomes approximately

$$H_{A\Delta}H_{\Delta A} = g^2 h(k)h(k')\sum_i \mathbf{S}_i\cdot(\mathbf{k}-\alpha\mathbf{K})\mathbf{S}_i^\dagger\cdot(\mathbf{k}'-\alpha\mathbf{K}') \tag{3.92}$$

Using (2.39), that is,

$$\mathbf{A}\cdot\mathbf{S}\mathbf{S}^\dagger\cdot\mathbf{B} = \tfrac{1}{3}\mathbf{A}\cdot\mathbf{B} - \tfrac{1}{3}i\boldsymbol{\sigma}\cdot(\mathbf{A}\times\mathbf{B})$$

one obtains

$$H_{A\Delta}H_{\Delta A} = \tfrac{1}{3}g^2 h(k)h(k')\sum_i\{(\mathbf{k}-\alpha\mathbf{K})\cdot(\mathbf{k}'-\alpha\mathbf{K}') - i\boldsymbol{\sigma}_i\cdot[(\mathbf{k}-\alpha\mathbf{K})\times(\mathbf{k}'-\alpha\mathbf{K}')]\} \tag{3.92'}$$

The initial wave function can be factored as follows:

$$\psi_{\pi i}^{(+)} = \chi_i^{(+)}\Psi_i \tag{3.93}$$

where Ψ_i is the wave describing the target nucleus depending only on the internal coordinates. The function $\chi_i^{(+)}$ is the pion–nucleon elastic scattering wave function. Similarly,

$$\psi_{\pi f}^{(-)} = \chi_f^{(-)}\Psi_f$$

Therefore,

$$\mathcal{T}_{fi} = \langle\chi_f^{(-)}t_{fi}\chi_i^{(+)}\rangle \tag{3.94}$$

where

$$t_{fi} = \left\langle \Psi_f H_{A\Delta} \frac{1}{E^* - \mathscr{H}_\Delta} \mathscr{H}_{\Delta A} \Psi_i \right\rangle \tag{3.95}$$

and $E^* = E - E_r + i\Gamma/2$.

Neglecting for the moment the nonlocality indicated by the propagator, we see from (3.92) that t_{fi} will involve the longitudinal density matrix,

$$\rho_{fi} = \left\langle \Psi_f \left| \sum_{\kappa=1}^{A} \delta(\mathbf{r} - \mathbf{r}_\kappa)(1 + \tfrac{1}{2}\tau_z(\kappa)) \right| \Psi_i \right\rangle = \tfrac{3}{2}\rho^p_{fi} + \tfrac{1}{2}\rho^n_{fi} \tag{3.96}$$

and the spin density,

$$\mathbf{S}_{fi} = \left\langle \Psi_f \left| \sum_{\kappa=1}^{A} \delta(\mathbf{r} - \mathbf{r}_\kappa)\boldsymbol{\sigma}(\kappa)(1 + \tfrac{1}{2}\tau_z(\kappa)) \right| \Psi_i \right\rangle \tag{3.97}$$

The factor $(1 + \frac{1}{2}\tau_z)$ gives the 3:1 ratio between the $T = \frac{3}{2}$ isospin total cross sections for $(\pi^+ p)$ and $(\pi^+ n)$. In (3.96) ρ^p_{fi} and ρ^n_{fi} are the proton and neutron density matrices.

Introducing the nonlocality by a first-order expansion of the orbital particle–hole wave functions introduces another set of nuclear operators. These include the convection current

$$\mathbf{j}_{fi}(\mathbf{r}) = \frac{1}{2m} \left\langle \Psi_f \left| \sum_{\kappa=1}^{A} (1 + \tfrac{1}{2}\tau_z(\kappa))[\mathbf{p}(\kappa)\delta(\mathbf{r} - \mathbf{r}_\kappa) + \delta(\mathbf{r} - \mathbf{r}_\kappa)\mathbf{p}(\kappa)) \right| \Psi_i \right\rangle \tag{3.98}$$

and a dyadic

$$\overleftrightarrow{U}_{fi}(\mathbf{r}) = \frac{1}{2m} \left\langle \Psi_f \left| \sum_{\kappa=1}^{A} (1 + \tfrac{1}{2}\tau_z(\kappa))[\mathbf{p}(\kappa)\boldsymbol{\sigma}(\kappa)\delta(\mathbf{r} - \mathbf{r}_\kappa) + \delta(\mathbf{r} - \mathbf{r}_\kappa)\mathbf{p}(\kappa)\boldsymbol{\sigma}(\kappa)] \right| \Psi_i \right\rangle \tag{3.99}$$

These quantities ρ_{fi}, $\mathbf{S}_{fi}$, $\mathbf{j}_{fi}$ and $\overleftrightarrow{U}_{fi}$ are probed by inelastic pion scattering. Combined with electron scattering, they will yield the neutron particle density, spin density, and current density matrices as well as the spin flux tensor $\overleftrightarrow{U}$. Note that the vectors $\mathbf{k}(\kappa)$ are momentum operators acting on the nucleon wave functions.

The modifications because of nonlocality and recoil (whose neglect through closure for the propagator and putting $\alpha = 0$ leads to the "static" solution) are substantial. The calculations involve (1) distorted wave functions for the pions as obtained by the methods discussed earlier, and (2) nucleon and hole orbital wave functions. They are required to yield the transition and spin density matrices as determined from electron scattering. In Fig. 3.8*a* we show the cross

sections for excitation of the 2^+ state (4.44 MeV) in ^{12}C by ρ_{fi} (longitudinal excitation) under various approximations. We see the large differences between the closure and full Δ–h calculations. In Fig. 3.8*b* a similar comparison is made for the 3^- state at 9.64 MeV. The match of the full calculation (the longitudinal excitation dominates) is not quantitatively satisfactory, although qualitative aspects are reproduced. We show just the case of the 2^+ excitation in Fig. 3.8*c*. In the resonance region the calculations do agree reasonably well up to the region of the second maximum. Large discrepancies are found for large momentum transfers. This is possibly not surprising since a similar difficulty exists for elastic scattering. Lenz, Thies, and Horikawa (82) believe that the cause of the discrepancy lies in the Δ–nucleus interaction as described by the spreading potential.

Hirata, Lenz, and Thies (83) point out that the mean field description of the Δ–h spreading potential may be an oversimplification. They propose a model in which the Δ interacts with the nuclear nucleons via a two-body interaction. This interaction can excite one of the nucleons, so that a possible intermediate state consists of a Δ–h plus a p–h state. This is illustrated in Fig. 3.9. Of course, higher-order multistep intermediate states Δ–h, $\nu(p-h)$, where ν is an integer are possible.

The amplitudes corresponding to Figs. 3.7 and 3.9 add up to give the $\mathscr{T}$ matrix:

$$\mathscr{T} = \left\langle \psi_{\pi f}^{(-)} \middle| H_{A\Delta} \frac{1}{E^* - \mathscr{H}_\Delta} H_{\Delta\Delta} \middle| \psi_{\pi i}^{(+)} \right\rangle + \left\langle \psi_{\pi f}^{(-)} \middle| H_{A\Delta} \frac{1}{E^* - \tilde{\mathscr{H}}_\Delta} \tilde{t}_{\Delta N} \frac{1}{E - \mathscr{H}_\Delta} H_{\Delta A} \middle| \psi_{\pi i}^{(+)} \right\rangle \tag{3.100}$$

where $\tilde{t}_{\Delta N}$ is the component of the Δ–N interaction, which results in further nuclear excitation. The quantity $(1/E^* - \tilde{\mathscr{H}}_\Delta)$ is the propagator for the Δ–h, p–h system, and $E^* = E - E_R + i\Gamma/2$.

Equation (3.100) is an example of the amplitude for the multistep direct process described in Chapter VI. The higher-order multistep components are not included. An estimate of their importance using the statistical approach of Chapter VI has not been made.

The Hamiltonian in (8.39) is given by [see (3.53) and (2.60)]

$$H_\Delta = \gamma(T_\Delta + \mathscr{U} + H_{A-1}) + W_{PB}^{(\pi)} + W^{(Q)} \tag{3.101}$$

Hirata, Lenz, and Thies (83) and Takaki (86) replace the spreading potential $W^{(Q)} + \gamma\mathscr{U}$ by a sum of two-body potentials instead of using the mean field as given in (3.65); that is,

$$W^{(Q)} + \gamma\mathscr{U} = \sum \tau(\Delta, i) \equiv t_{\Delta N} = \tilde{t}_{\Delta N} + W_D^{(\pi)} \tag{3.102}$$

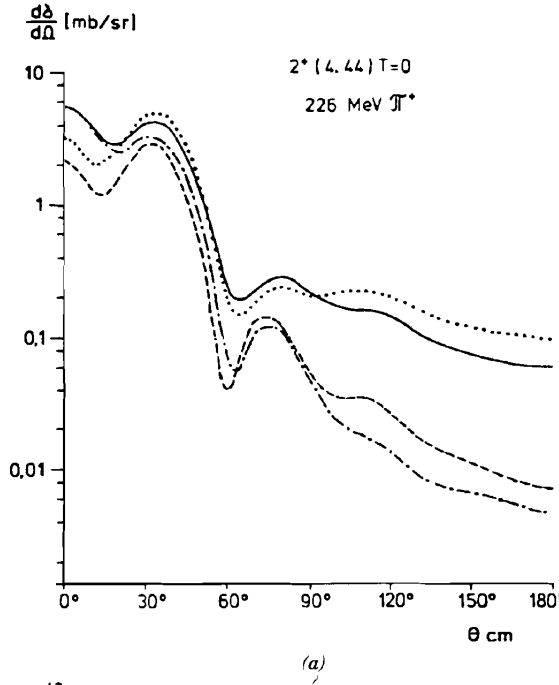

(a)

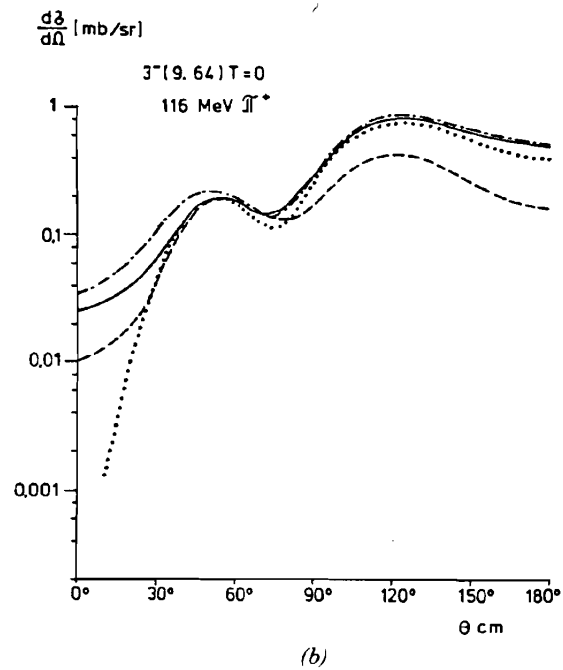

(b)

FIG. 3.8. (*a*) Comparison of various approximations to the Δ Green's function in the transition operator for excitation of the 2^+ (4.44 MeV) $T = 0$ state by 226 MeV π^+ (pure longitudinal parameterization). Dotted curve; closure approximation; solid curve, free

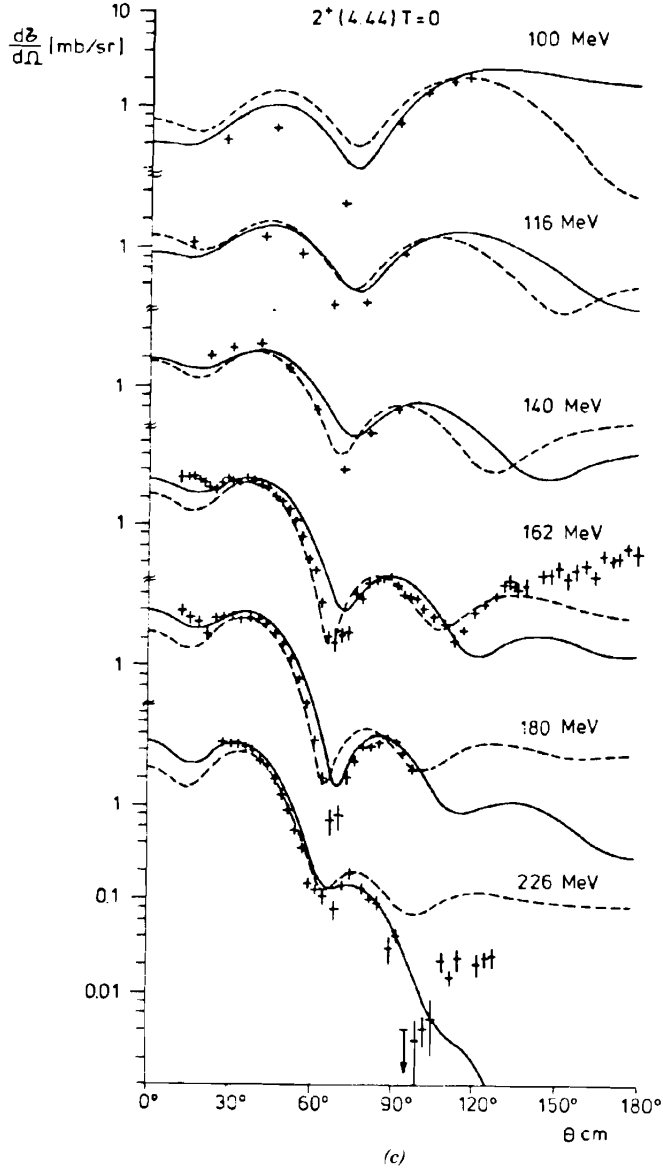

(c)

Δ (kinetic energy only); dashed curve, including central Δ-nucleus potential; dashed–dotted curve, full Δ–h calculation, including Pauli terms and spin-orbit potential. The distorted π wave functions always correspond to the full Δ–h calculation. (*b*) Like (*a*), but 3^- (9.64 MeV) $T = 0$ state, pure longitudinal parameterization, 116-MeV π^+. (*c*) Differential cross sections for the 2^+ (4.44 MeV) $T = 0$ excitation for various pion energies. Solid curves: Δ–h calculations, dashed curves: closure approximation. [From Lenz, Thies, and Horikawa (82).]

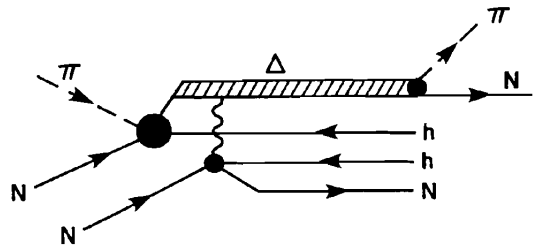

FIG. 3.9. Pion two-particle/two-hole excitation.

The potential $t_{\Delta N}$ contains the diagonal rescattering term [see (3.48)], which does not contribute to the production of the more complex nuclear states. The remainder $\tilde{t}_{\Delta N}$ is the interaction that appears in (3.100). Takaki (86) parametrizes $\tilde{t}_{\Delta N}$ as follows:

$$\tilde{t}_{\Delta N} = \sum_{i,S_\Delta,T_\Delta} C(S_\Delta, T_\Delta)\delta(\mathbf{r}_\Delta - \mathbf{r}_i)P(S_\Delta)P(T_\Delta) \tag{3.103}$$

where S_Δ and T_Δ are the spin and isospin of the interacting Δ–p pair, while $P(S_\Delta)$ and $P(T_\Delta)$ are the corresponding projection operators. Since the Δ spin is $\frac{3}{2}$ and the nucleon spin is $\frac{1}{2}$, S_Δ can be either 2 or 1. The same holds for T_Δ, so that (3.103) contains four complex parameters, $C(11)$, $C(12)$, $C(21)$, and $C(22)$. One relation exists among them: namely, that the mean field that follows from (3.102) agrees with the empirical mean field, $W^{\downarrow}$ [Eq. (3.65)]. The comparison is obtained by taking the diagonal value of $t_{\Delta N}$ in the single-doorway-state approximation. This result, together with fit of the inelastic data for the $(\pi^+, {}^{12}\mathrm{C})$ reaction, permits the determination of the values of $C(S_\Delta, T_\Delta)$. Finally, Takaki approximates $\tilde{\mathscr{H}}_\Delta$ by $\mathscr{H}_\Delta$. Results for the excitation of the 1^+, $T=0$ (12.72 MeV) and the 1^+, $T=1$ (15.11 MeV) levels in ^{12}C are shown in Fig. 3.10 and for the 2^+, $T=0$ (4.4 MeV) level and the 3^-, $T=0$ (9.6 MeV) levels in Fig. 3.11. The values of $C(S_\Delta, T_\Delta)$ obtained from fitting 1^+ excitations are used in the calculation of the 2^+ and 3^- excitations. Qualitative agreement is good, especially at small angles, but there are strong differences from experiment at the back angles at 162 and 266 MeV. At 100 MeV, the full calculations are in good agreement with experiment. One also sees that by taking into account the more complex excitation, Δ–h, p–h, it becomes possible to fit the ratio $\sigma(T=0)/\sigma(T=1)$ as a function of the energy. The disagreement with the data is significant since this model correctly predicts the elastic and total cross sections. We speculate that full agreement with the data will not be attained until more complex excitations are included in the calculation.

Single (SCX) and Double (DCX) Charge Exchange Scattering. An example of an SCX reaction is

$$\pi^+ + {}_Z A \rightarrow {}_{Z+1} A + \pi^0 \tag{3.104}$$

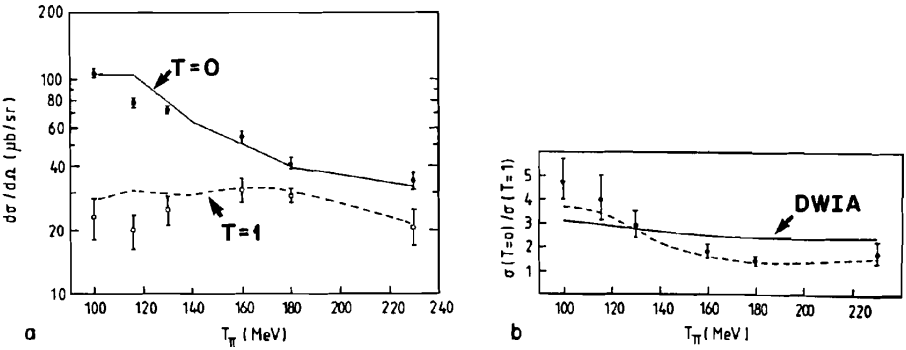

FIG. 3.10. Excitation functions for the 1^+ $T=0$ (12.71 MeV) and $T=1$ (15.11 MeV) excitations. Solid and dashed lines correspond to the full calculations for $T=0$ and $T=1$, respectively. [From Takaki (86).]

It is closely related to the (p,n) reaction as the residual nucleus is identical for both. In the latter case, a most salient feature is the formation of the isobar analog of the target nucleus. We may expect that the reaction (3.104) will also excite the isobar analog states. This is illustrated by Fig. 3.12. With DCX, other giant resonances, such as the electric dipole and double isobar analog states, can also be excited (see Fig. 3.13). Thus once the dynamics of SCX reaction is understood, one should be able to gain further understanding of these resonances. Similarly, the (π^-,π^0) reaction is the image of the (n,p) reaction and would be useful in the study of the nucleus $(Z-1,\ N+1)$.

The isobar analog resonance can be discussed pehnomenologically by using the Lane equation (Chapter V). A similar procedure can be followed here where following the papers of M. Johnson, E. R. Siciliano, and their colleagues [Siciliano, Cooper, Johnson, and Leitch (86), for example], one writes for the potential

$$V = V_0 + V_1(\mathbf{T}_\pi \cdot \mathbf{T}_A) + V_2(\mathbf{T}_\pi \cdot \mathbf{T}_A)^2 \tag{3.105}$$

where V_0, V_1, and V_2 are referred to as the scalar, vector, and tensor potentials. $\mathbf{T}_\pi$ and $\mathbf{T}_A$ are the isospin operators for the pions and nucleus, respectively. Equation (3.105) is the extension, to charge exchange reactions, of the pion optical potential described earlier [see (3.26)]. This potential was used to describe the elastic and total cross sections and involves terms quadratic in ρ (the density) which are a consequence of medium effects. Once one distinguishes between the neutron and proton components of ρ, these quadratic terms lead directly to a tensor contribution to V. It should also be noted that (3.105) contains the most complicated dependence on $\mathbf{T}_\pi$. To confirm this, we need only to recall‡ that

$$(T_{\pi i})^3 = T_{\pi i}$$

‡More completely, $[T_{\pi i}, T_{\pi j}] = iT_{\pi k}$; i,j,k cyclical and $T_{\pi i}T_{\pi j}T_{\pi k} + T_{\pi k}T_{\pi j}T_{\pi i} = \delta_{ij}T_{\pi k} + \delta_{kj}T_{\pi i}$

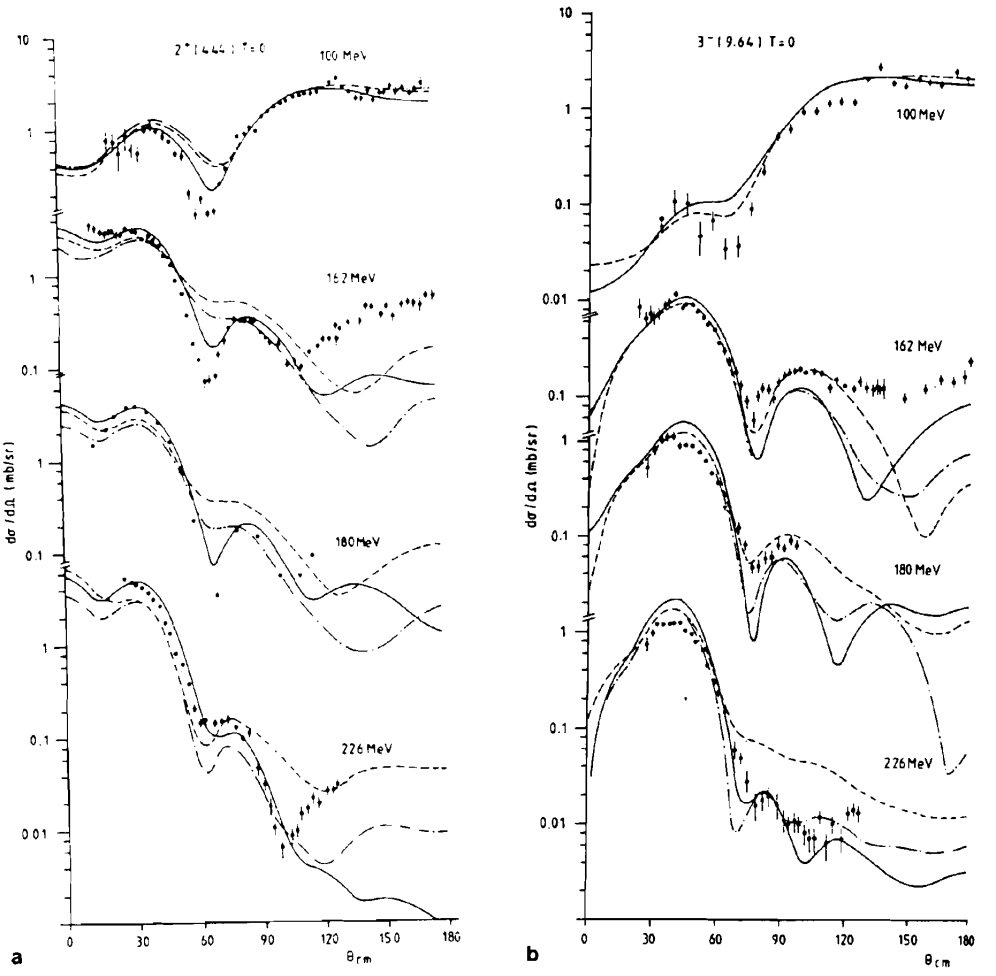

FIG. 3.11. Differential cross sections for (*a*) the 2^+ $T = 0$ (4.4 MeV) and (*b*) the 3^- $T = 0$ (9.6 MeV) excitations for various pion energies. Solid lines correspond to the DWIA calculation, and dashed lines to the full calculation. [From Takaki (86).]

where $T_{\pi i}$ is the ith component of **T**. We emphasize that the tensor term is present as a consequence of the effect of the medium on pion–nucleon interaction. An analysis of the origin of this term will show that it depends on nuclear structure, on Pauli and on both short-range and long-range pair and higher-order correlations.

The solution of the Klein–Gordon equation with the V of (3.105) is relatively straightforward. One can determine the uncoupled equations for each of the

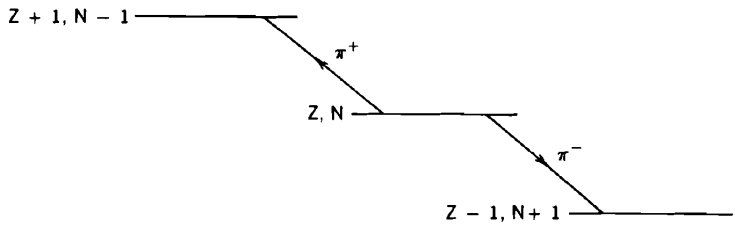

FIG. 3.12. Charge exchange reactions.

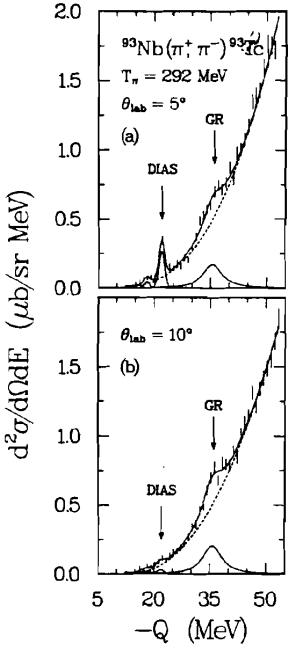

FIG. 3.13. Double-differential cross section spectrum for (π^+, π^-) reaction on a ^{93}Nb target at $T_\pi = 292$ MeV: (*a*) $\theta_{lab} = 5°$; (*b*) $\theta_{lab} = 10°$. The arrows indicate the fitted location of the DIAS and the giant resonance (GR). Short vertical lines represent statistical uncertainty of the data. The dashed line is the fitted background. DIAS, double isobar analog resonance. [From Mordechai, Auerbach, et al. (89).]

three possible isospins of the system $T = T_A \pm 1$ and $T = T_A$. Since

$$\mathbf{T} = \mathbf{T}_\pi + \mathbf{T}_A$$

one can immediately obtain the values of $\mathbf{T}_A \cdot \mathbf{T}_\pi$ that appear in (3.105). One obtains

$$\mathbf{T}_\pi \cdot \mathbf{T}_A = \tfrac{1}{2}[T(T+1) - T_\pi(T_\pi+1) - T_A(T_A+1)] \tag{3.106}$$

Recall that $T_\pi = 1$ and $T_A = \frac{1}{2}(N - Z)$. From the solutions $\psi(T_A + 1)$, $\psi(T_A)$, and $\psi(T_A - 1)$, one can obtain the amplitudes for SCX and DCX. The wave function for the π^+ nucleus system, $\psi_+(T_\pi, T_{\pi z}; T_A, T_{Az})$, is given in terms of the three

solutions $\psi(T_A+1)$, $\psi(T_A)$, and $\psi(T_A-1)$ by

$$\begin{aligned}\psi_+(1,1;T_A,-T_A) = {} & (1;1;T_A,-T_A|T_A+1,1-T_A)\psi(T_A+1)\\ & +(1,1;T_A,-T_A|T_A,1-T_A)\psi(T_A)\\ & +(1,1;T_A,-T_A|T_A-1,1-T_A)\psi(T_A-1)\end{aligned}$$

or

$$\begin{aligned}\psi_+(1,1;T_A,-T_A) = {} & \sqrt{\frac{1}{(2T_A+1)(T_A+1)}}\psi(T_A+1)\\ & +\sqrt{\frac{1}{T_A+1}}\psi(T_A)+\sqrt{\frac{2T_A-1}{2T_A+1}}\psi(T_A-1)\end{aligned} \tag{3.107}$$

The states $\psi(T_A+1)$, and so on, must be chosen so that ψ_+ asymptotically consists of an incident plus outgoing wave. The outgoing wave will contain π^+, π^0, and π^- components corresponding to elastic (or inelastic) SCX and DCX scattering. To obtain the DCX, one needs the wave function for π^0 plus the residual nucleus with isospin T_R, z component T_z. This wave function is

$$\begin{aligned}\psi_0(1,0;T_R,T_z) = {} & (1,0;T_R,T_z|T_A+1,T_z)\psi(T_A+1)+(1,0;T_R,T_z|T_A,T_z)\psi(T_A)\\ & +(1,0;T_R,T_z|T_A-1,T_R)\psi(T_A-1)\end{aligned} \tag{3.108}$$

In the case of "elastic" scattering,

$$\begin{aligned}\psi_0(1,0;T_A,1-T_A) = {} & 2\sqrt{\frac{T_A}{(2T_A+1)(T_A+1)}}\psi(T_A+1)\\ & +\frac{T_A-1}{\sqrt{T_A(T_A+1)}}\psi(T_A)-\sqrt{\frac{2T_A-1}{T_A(2T_A+1)}}\psi(T_A-1)\end{aligned} \tag{3.109}$$

Experimentally, *elastic* scattering to the nucleus $(T_A, 1-T_A)$ does not occur because of the presence of the isobar symmetry breaking Coulomb interaction. The residual nucleus in state ψ_0 is the isobar analog state of the target nucleus. The double isobar analog state is generated by the (π^+,π^-) reaction. It is the residual nucleus in state ψ_-:

$$\begin{aligned}\psi_-(1,-1;T_A,2-T_A) = {} & \sqrt{\frac{T_A(2T_A-1)}{(T_A+1)(2T_A+1)}}\psi(T_A+1)\\ & -\sqrt{\frac{2T_A-1}{T_A(T_A+1)}}\psi(T_A)+\sqrt{\frac{1}{T_A(2T_A+1)}}\psi(T_A-1)\end{aligned} \tag{3.110}$$

Returning to (3.108), the asymptotic boundary condition for ψ_0 is that it contains only an outgoing wave. The same boundary condition applies to the π^- + residual nucleus wave function, ψ_-, generated by the DCX reaction. These boundary conditions together with the boundary conditions for ψ_+ determine the amplitudes of $\psi(T_A+1), \psi(T_A)$, and $\psi(T_a-1)$ and thus the reaction amplitudes.

In the absence of the Coulomb interaction, the transition matrix $\mathcal{T}$ can also be written in the same form given in (3.105),

$$\mathcal{T} = t_0 + t_1(\mathbf{T}_\pi \cdot \mathbf{T}_A) + t_2(\mathbf{T}_\pi \cdot \mathbf{T}_A)^2 \tag{3.111}$$

For "elastic" scattering this equation yields the relationships [Koltun and Singham (89)]

$$\begin{aligned} \mathcal{T}_{11} &= t_0 - T_A t_1 + T_A(T_A+1)t_2 && \pi^+ \to \pi^+ \\ \mathcal{T}_{01} &= \sqrt{T_A}(t_1 - T_A t_2) && \pi^+ \to \pi^0 \\ \mathcal{T}_{-11} &= \sqrt{T_A(2T_A-1)}\,t_2 && \pi^+ \to \pi^- \end{aligned} \tag{3.112}$$

Equation (3.110) implies a connection between π^+- and π^-- or π^0-induced reactions. For example,

$$\mathcal{T}_{-1,-1} = t_0 + T_A t_1 + T_A^2 t_2 \qquad \pi^- \to \pi^- \tag{3.113}$$

These relations will be valid for high energies and light nuclei, where the isospin symmetry-breaking Coulomb interaction is least important. They should fail substantially for low-energy incident pions and heavy target nuclei.

In the high-energy limit, one can establish the relation between V_0, V_1, and V_2 of (3.105) and t_0, t_1, and t_2 of (3.110) by using the eikonal approximation. From (II.5.11) we have

$$\mathcal{T}_{el} = \frac{2\pi i\hbar^2 k}{\mu} \int_0^\infty b\, db\, J_0(2kb \sin \tfrac{1}{2}\vartheta)(e^{i\chi} - 1) \tag{3.114}$$

where

$$\chi = v_0 + v_1(\mathbf{T}_\pi \cdot \mathbf{T}_A) + v_2(\mathbf{T}_\pi \cdot \mathbf{T}_A)^2 \tag{3.115}$$

and

$$v_i(b) = -\frac{\mu}{\hbar^2 k} \int_{-\infty}^{\infty} V_i(\mathbf{b}, z)\, dz$$

These nonrelativistic results can be modified to satisfy relativistic kinematics by using the Klein–Gordon equation [see (II.7.2)]. One can evaluate $e^{i\chi}$ through

use of the recurrence relations [Siciliano, Cooper, Johnson, and Leitch (86)]

$$(\mathbf{T}_\pi \cdot \mathbf{T}_\pi)^3 = -2(\mathbf{T}_\pi \cdot \mathbf{T}_A)^2 + (\mathbf{T}_\pi \cdot \mathbf{T}_A)(\mathbf{T}_A^2 - 1) + \tfrac{1}{2}\mathbf{T}_\pi^2 \mathbf{T}_A^2 \tag{3.116}$$

and

$$(\mathbf{T}_\pi \cdot \mathbf{T}_A)^4 = (\mathbf{T}_\pi \cdot \mathbf{T}_A)^2(\mathbf{T}_A^2 + 3) + \mathbf{T}_\pi \cdot \mathbf{T}_A[2 + \mathbf{T}_A^2(\tfrac{1}{2}\mathbf{T}_\pi^2 - 2)] - \mathbf{T}_\pi^2 \mathbf{T}_A^2 \tag{3.117}$$

Note that $\mathbf{T}_\pi^2 = T_\pi(T_\pi + 1) = 2$ and $\mathbf{T}_A^2 = T_A(T_A + 1)$. One finds that

$$e^{iv_1(\mathbf{T}_\pi \cdot \mathbf{T}_A)} = Ae^{-iv_1} + Be^{iv_1 T_A} + Ce^{-iv_1(T_A + 1)} \tag{3.118}$$

where

$$C = \frac{\mathbf{T}_A \cdot \mathbf{T}_\pi}{T_A(2T_A + 1)}[\mathbf{T}_A \cdot \mathbf{T}_\pi - T_A] \tag{3.119a}$$

$$B = \frac{\mathbf{T}_A \cdot \mathbf{T}_\pi}{(T_A + 1)(2T_A + 1)}[\mathbf{T}_A \cdot \mathbf{T}_\pi(T_A + 1)] \tag{3.119b}$$

and

$$A = 1 - B - C = 1 - \frac{(\mathbf{T}_A \cdot \mathbf{T}_\pi)^2}{T_A(T_A + 1)} \tag{3.119c}$$

For the v_2 term one obtains

$$e^{iv_2(\mathbf{T}_\pi \cdot \mathbf{T}_A)} = ae^{iv_2} + be^{iv_2 T_A^2} + ce^{iv_2(T_A + 1)^2} \tag{3.120}$$

where

$$c = \frac{(1 + \mathbf{T}_A \cdot \mathbf{T}_\pi)(\mathbf{T}_A \cdot \mathbf{T}_\pi - \mathbf{T}_A)}{(2T_A + 1)T_A} \tag{3.120a}$$

$$b = \frac{(1 + \mathbf{T}_A \cdot \mathbf{T}_\pi)(\mathbf{T}_A \cdot \mathbf{T}_\pi + T_A + 1)}{(2T_A + 1)(T_A + 1)} \tag{3.120b}$$

$$a = 1 - \frac{(2T_A + 1)(\mathbf{T}_\pi \cdot \mathbf{T}_A)^2 + 3(\mathbf{T}_\pi \cdot \mathbf{T}_A)}{T_A(2T_A + 1)(T_A + 1)} \tag{3.120c}$$

The quantity $e^{i\chi}$ is

$$e^{i\chi} = e^{iv_0} \cdot e^{iv_1(\mathbf{T}_\pi \cdot \mathbf{T}_A)} \cdot e^{iv_2(\mathbf{T}_\pi \cdot \mathbf{T}_A)^2}$$

We note that the second factor contains both absorptive and regenerative terms. It is necessary, to conserve unitarity, that the net be absorptive, which condition limits the values of v_1 and therefore of V_1. We shall not continue

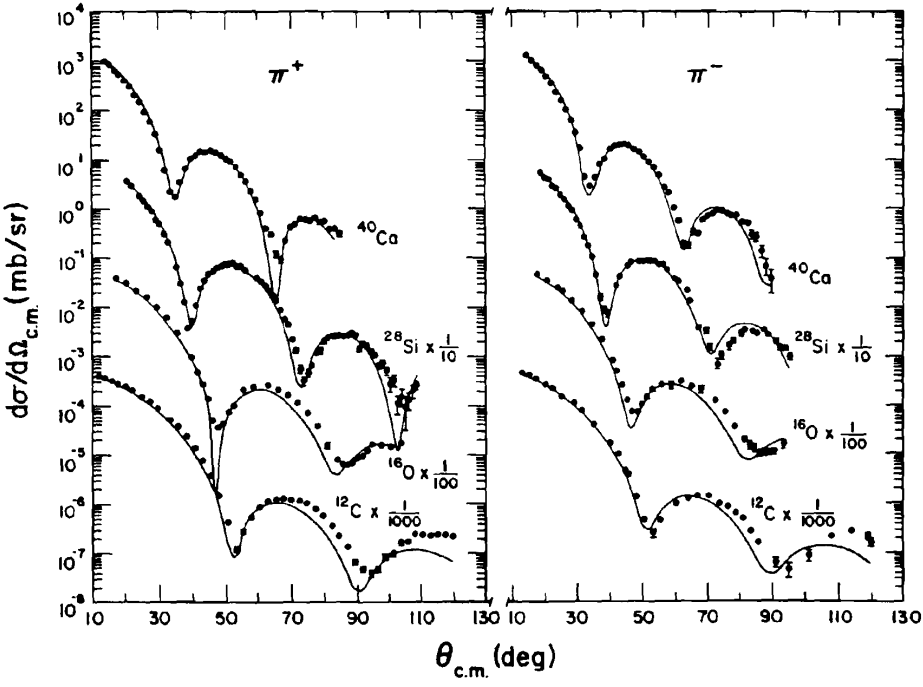

FIG. 3.14. Comparison of theoretical π^+ and π^- elastic scattering cross sections to data at $T_\pi = 164$ MeV for ^{16}O, ^{28}Si, ^{40}Ca, and ^{12}C. [From Greene, Harvey, et al. (84).]

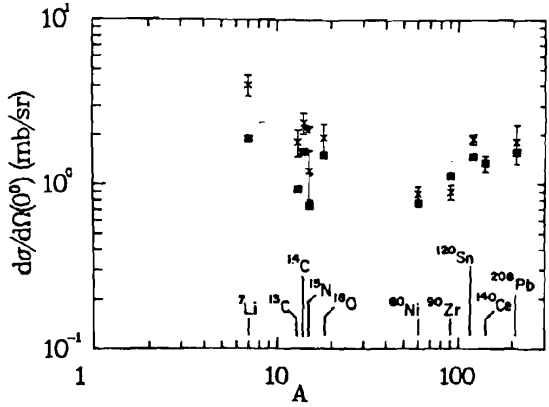

FIG. 3.15. Comparison of theoretical single charge exchange $d\sigma/d\Omega(0^\circ)$ to data at $T_\pi = 165$ MeV. The × represent data and the ■ represent theoretical result. [From Greene, Harvey, et al. (84).]

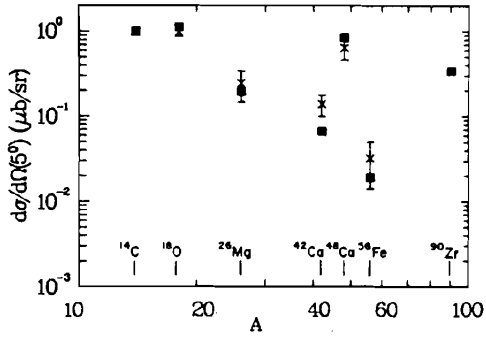

FIG. 3.16. Comparison of theoretical double charge exchange $d\sigma/d\Omega(5^\circ)$ to data at $T_\pi = 164$ MeV. The × represent data and the ■ represent theoretical results. [From Greene, Harvey, et al. (84).]

with development, as exploration of these results has not been made. They do demonstrate the possible importance of the vector and tensor components of V.

The phenomenological theory using potential equation (3.105) has been used by Greene, Harvey, et al. (84) to analyze pion single and double charge exchange scattering to isobaric analog states, and elastic scattering in the resonance region ($E_\pi = 164$ MeV). Suffice it to say that agreement with experiment is obtained as illustrated by Fig. 3.14 for elastic scattering, Figs. 3.15 and 3.16 for SCX and DCX. The DCX angular distribution obtained for ^{18}O and ^{26}Mg and when

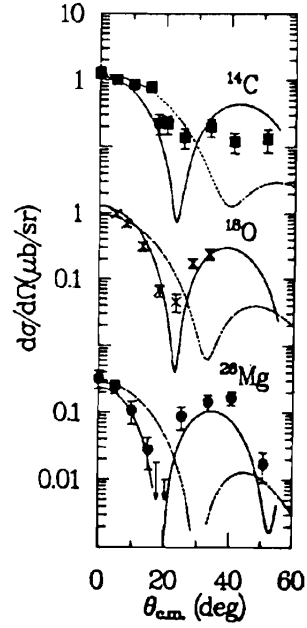

FIG. 3.17. Comparison of theoretical double charge exchange angular distributions to data at $T_- = 164$ MeV. The dashed curves are the lowest-order result. [From Greene, Harvey, et al. (84).]

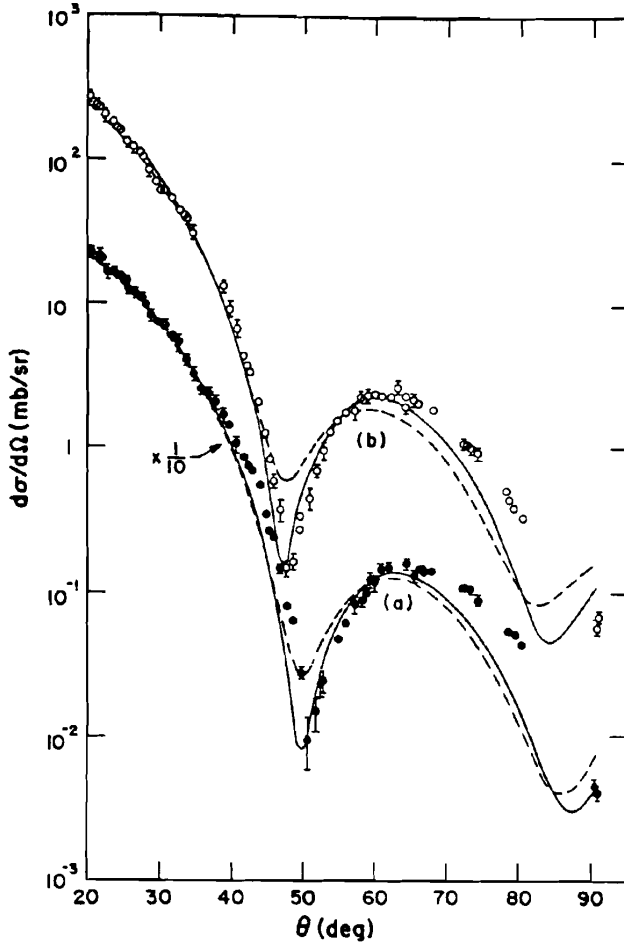

FIG. 3.18. Comparison of theoretical π^+ (*a*) and π^- (*b*) elastic scattering cross section from ^{14}C to data at $T_\pi = 164$ MeV. The solid and dashed curves are, respectively, results with and without the isospin-dependent terms in $U^{(2)}$. [From Greene, Harvey, et al. (84).]

the target nucleus is ^{14}C is shown in Figs. 3.17 and 3.18. This illustrates the importance of the tensor term, V_2, in (3.105). One technical result of importance is the finding of Siciliano, Cooper, Johnson, and Leitch (86) that the plane wave approximation for the pion wave functions is inadequate.

The DCX reaction proceeds along two possible paths. In one a π^+, for example, scatters from a nucleon becoming a π^0. The π^0 then scatters a second time, becoming a π^-. This process is referred to as *sequential*. In the Δ–N interaction, the π^+ is absorbed by a target nucleon, forming a Δ^+. The Δ^+ interacts with the nucleus via $t_{\Delta N}$ [see (3.102)], becoming a Δ^0, which then decays into a π^- and a proton. Calculations of the DCX reaction at low pion

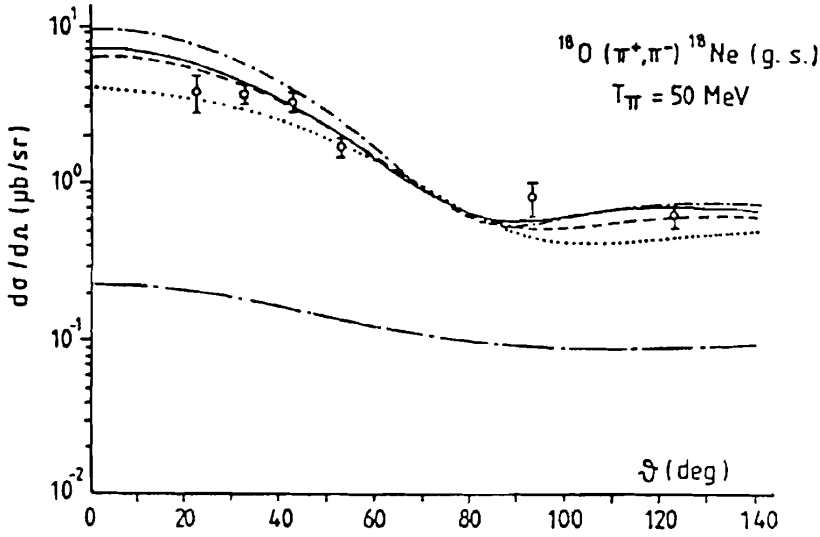

FIG. 3.19. $^{18}O(\pi^+,\pi^-)^{18}Ne$(g.s.) differential cross section: *full sequential* (solid curve), sequential, but keeping only the $J=0$ intermediate nuclear state (dotted-long-dashed curve), with Δ–N *interaction* of strength $\delta v = 0.5 - 1.0i$, $0.2 - 2.8i$, $1.0 + 0.4i$ fm^2 (dashed, dotted, and dotted–dashed curves, respectively). [From Karapiperis (89).]

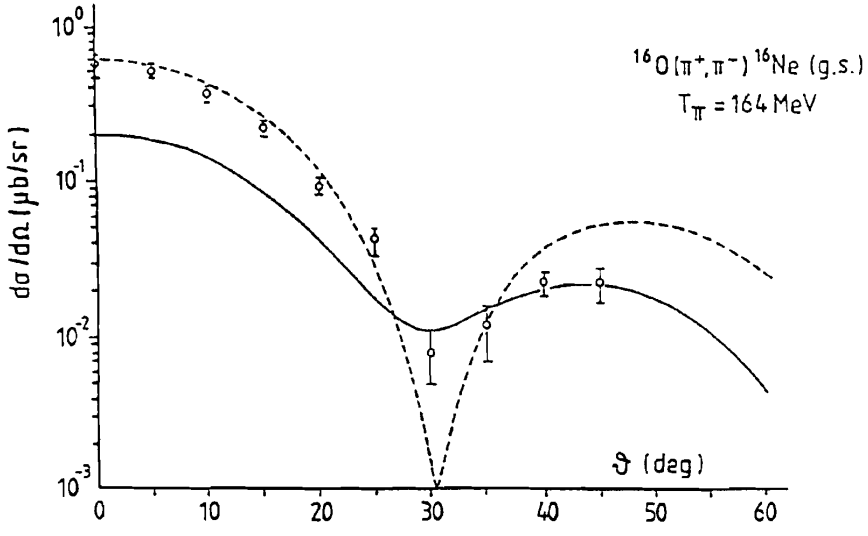

FIG. 3.20. Same as in Fig. 3.19 but for the reaction $^{16}O(\pi^+,\pi^-)^{16}Ne$(g.s.). [From Karapiperis (89).]

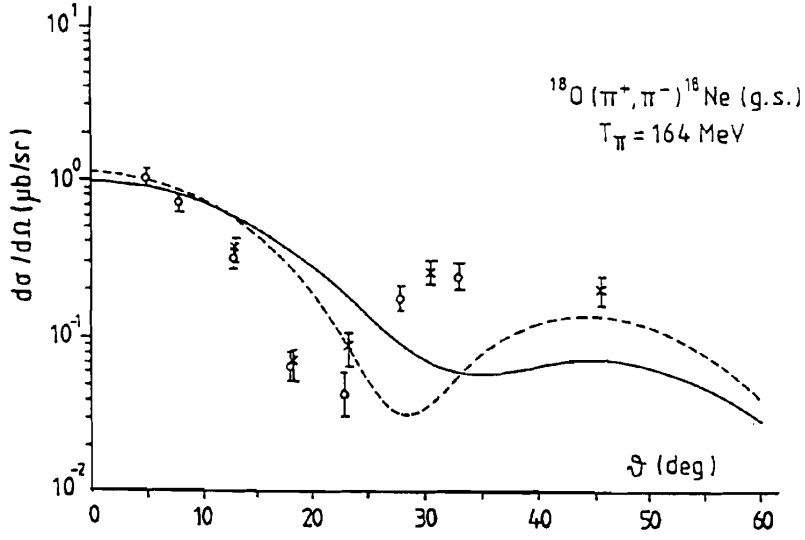

FIG. 3.21. $^{18}O(\pi^+,\pi^-)^{18}Ne$(g.s.) differential cross section: sequential (solid curve) and with Δ–N interaction of strength $\delta v = 2.0 - 0.4i\,\text{fm}^2$ (dashed curve). [From Karapiperis (89).]

energies where the sequential process dominates (~ 50 MeV) have been successful. But calculations in the resonance region in the isobar hole model are not. For an analysis, see Karapiperis and Kobayashi (87) and Karapiperis (89). For an analysis from another point of view, see Siciliano, Johnson, and Sarafian (90). The isobar–hole model uses the analysis described earlier for elastic and inelastic scattering. The results for 50-MeV $^{18}O(\pi^+,\pi^-)^{18}Ne$(g.s.) are satisfactory. See Fig. 3.19. We see that the Δ–N process is relatively unimportant. Distortion effects are very important. At the higher energies good agreement is obtained for the $^{16}O(\pi^+,\pi^-)^{16}Ne$(g.s.). See Fig. 3.20. However, there is strong disagreement with the angular distribution in the reaction $^{18}O(\pi^+,\pi^-)^{18}Ne$ (Fig. 3.21), which is as yet unresolved. Disagreement with the $^{14}C(\pi^+,\pi^-)^{14}O$(g.s.) is also present. Reasons for these disagreements include possibly inadequate nuclear wave functions and the oversimplified form of $t_{\Delta,N}$, (3.105). The importance of nuclear structure has been emphasized by Auerbach, Gibbs, and Piasetsky (87) and Auerbach, Gibbs, Ginocckio, and Kaufmann (88).

4. KAON–NUCLEUS INTERACTION

The kaon is a pseudoscalar (odd parity, spin zero) boson. There are four varieties, the K^+, K^0, K^-, and $\bar{K}_0$. The antiparticle of the K^+ is K^-, and of the K^0, $\bar{K}^0$. This differs from the photon and π^0, which are identical with their antiparticles. The mass of the K^+ and K^0 are, respectively, 493.71 MeV and 497.70 MeV. The

K^0 and K^+ (and the K^-, $\bar{K}^0$) form an isospin-$\frac{1}{2}$ system. The kaon is a "strange" particle in that it has an additional internal quantum number of *strangeness S*. We shall use *hypercharge Y* rather than *S*, where

$$Y = B + S \tag{4.1}$$

and *B* is the baryon number. This permits a symmetrical classification of the bosons and fermions as illustrated by Fig. 4.1. The axes are the value of the *z* component of the isospin, T_3, and *Y*. One observes that the fermion analog of the (K^0, K^+) isodoublet is the nucleon isodoublet; that of the pion isospin one system is the Σ isospin one system. The $\Sigma^{\pm}$ mass is 1189.37 MeV and the Σ^0 mass is 1192.47 MeV. Finally, the (K^-, K^0) doublet is mirrored by the Ξ doublet, with the mass of the Ξ^- equal to 1321.29 MeV and the mass of the Ξ^0 1314.9 MeV. The masses of the isosinglet Λ^0 and η^0 are 1115.60 and 548.8 MeV, respectively. The spin of each of the particles in Fig. 4.1*a* is zero, while the spin of the particles in Fig. 4.1*b* is $\frac{1}{2}$. The particles in Fig. 4.1*a* are said to form the pseudoscalar octet, while those in Fig. 4.1*b* form the baryon spin-$\frac{1}{2}$ octet. This classification based on SU(3) symmetry is a generalization of the SU(2) isospin symmetry of the nucleon system. If SU(2) symmetry were exact, the neutron and proton would have the same mass and each would be an example of the nucleon. If SU(3) symmetry were exact, the masses of all the particles in Fig. 4.1*a* would be identical and one would refer to them as states of one particle, the pseudoscalar boson. Similarly, Fig. 4.1*b* represents a spin-$\frac{1}{2}$ baryon. As the masses are not the same, SU(3) symmetry is broken.

It will be useful for us to give the quark description of these particles. We shall need only the *u* (up), *d* (down), and *s* (strange) quarks and their antiparticles. These quarks are spin-$\frac{1}{2}$ fermions. The properties of these quarks are given in Table 4.1. In Table 4.2 we list the combinations for the various particles shown in Fig. 4.1. Note that the antiparticles of a quark *q* is written $\bar{q}$.

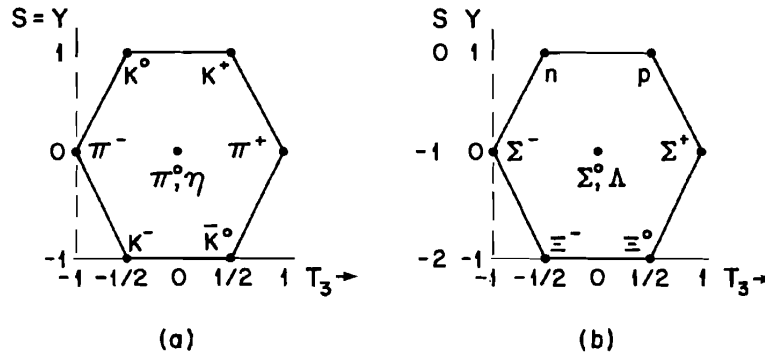

FIG. 4.1.

TABLE 4.1 Properties of the *u*, *d*, and *s* Quarks

Flavor	Charge	Strangeness	T_3	Baryon Number, B	Y
u	$\frac{2}{3}e$	0	$\frac{1}{2}$	$\frac{1}{3}$	$\frac{1}{3}$
d	$-\frac{1}{3}e$	0	$-\frac{1}{2}$	$\frac{1}{3}$	$\frac{1}{3}$
s	$-\frac{1}{3}e$	-1	0	$\frac{1}{3}$	$-\frac{2}{3}$
$\bar{u}$	$-\frac{2}{3}e$	0	$-\frac{1}{2}$	$-\frac{1}{3}$	$-\frac{1}{3}$
$\bar{d}$	$\frac{1}{3}e$	0	$\frac{1}{2}$	$-\frac{1}{3}$	$-\frac{1}{3}$
$\bar{s}$	$\frac{1}{3}e$	1	0	$-\frac{1}{3}$	$\frac{2}{3}$

TABLE 4.2 Quark Composition of Hadrons

Baryons		Bosons[a]	
p	(uud)	K^+	$(u\bar{s})$
n	(udd)	K^0	$(d\bar{s})$
$\Sigma\Lambda$	(uds), (uus), (dds)	π, η	$(\bar{u}d)(\bar{u}u)(\bar{d}d)(u\bar{d})$
		$\bar{K}^0$	$(\bar{d}s)$
Ξ	(uss), (dss)	K^-	$(\bar{u}s)$

[a]This list omits the $(\bar{s}s)$ combination, leading to the existence of another particle, the η'. In fact, both the η and η' contain the $\bar{s}s$ combinations: $\eta = 1/\sqrt{6}(u\bar{u} + d\bar{d} - 2s\bar{s})$ and $\eta' = 1/\sqrt{3}(u\bar{u} + d\bar{d} + s\bar{s})$. Within the SU(3) framework we are using, the η is included in Fig. 4.1*a* octet, while the η' is regarded as a singlet.

This quark description must be used with some care. The *constituent quarks*, as they are sometimes called, are quasi-particles, as their environment is rich with quark–antiquark pairs as well as gluons. Moreover, we have not assigned spin and still another internal degree of freedom, called *color*. All this is presumably a consequence of *Quantum Chromodynamics* (QCD). We shall not describe that theory here, as we shall be concerned only with qualitative considerations. The interested reader will find the details in a number of references [Gottfried and Weisskopf (84, 86); Close (79); Gasiorowicz (66), Lee (81)]. The reader should confirm that the isospin of the baryons and bosons can be deduced from the isospin of the constituent quarks.

The conservation of isospin in the strong interactions is expanded by the additional requirement of the conservation of strangeness. The latter condition is illustrated by the fact (for example) that $\pi^- + p \rightarrow K^+ + \Sigma^-$ is allowed but $\pi^- + p \rightarrow K^- + \Sigma^+$ is forbidden. More compactly, the strong interactions are SU(3) symmetric [i.e., the strong interactions commute with the generators of the SU(3) group]. From the quark point of view, for sufficiently low-energy phenomena one need consider only the *u*, *d*, and *s* quarks. The other known quarks, the *c* (charm) and *b* (bottom), are much more massive than the *u*, *d*,

and s. The c mass is 1.5 GeV and the b mass 5 GeV greater than the mass of the u and d.

SU(3) symmetry is broken. The masses of the members of the spin-$\frac{1}{2}$ octet and of the pseudoscalar boson octet differ substantially. In terms of the constituent quarks, the mass of the strange quark, s, is about 150 MeV greaer than the mass of the up and down quarks, whose masses are equal. This heavier mass for the strange quark provides much of the observed mass differences. In addition, the spin- and color-dependent forces between quarks generated by the exchange of colored gluons provide additions to the mass of the composites. This interaction also breaks symmetry since these exchange forces are mass dependent. These, together with the larger mass of the s quark, suffice to explain the mass spectrum of both the spin-$\frac{1}{2}$ baryons and the pseudoscalar bosons. [See Close (78) for the details.]

At large distances the baryon–baryon interaction is generated by the exchange of bosons [the singlet η', the pseudoscalar, and the vector (ρ, ω, etc.)]. Because of the difference in the boson masses, there will be strong symmetry breaking. For example, the one-boson exchange ΛN nucleon interaction, because of isospin conservation, involves the exchange of a kaon, while the pion mediates ΣN interaction (see Fig. 4.2). Since the mass of the kaon is larger than that of the pion, the ΛN interaction will have a range much shorter than that of the ΣN interaction. At small interparticle distances, the six-quark system must be considered. One would speculate that symmetry breaking would be weaker in this case. It has also been speculated that the $\Sigma N \to \Lambda N$ transition matrix element breaks SU(3) symmetry weakly [Dover and Feshbach (87, 90)].

The antiparticle of the K^0, $\bar{K}^0$ is not identical with K^0, differing in this respect from the π^0 or the photon γ for which the particle–antiparticle equality does prevail. This unique property of the K^0 system has important consequences. It surfaces in the pionic decays of the kaons. These violate conservation of strangeness and are therefore governed by the weak interactions. These (as well as the strong interactions) conserve CP, although neither C nor P is separately conserved. We recall the C is the operator that converts a particle into an antiparticle, while P is the parity operator that gives the effect of reflecting all the spatial coordinates ($\mathbf{r} \to -\mathbf{r}$) in a state. Since $C^2 = P^2 = 1$,

$$CPK^0 = e^{i\phi}\bar{K}^0$$

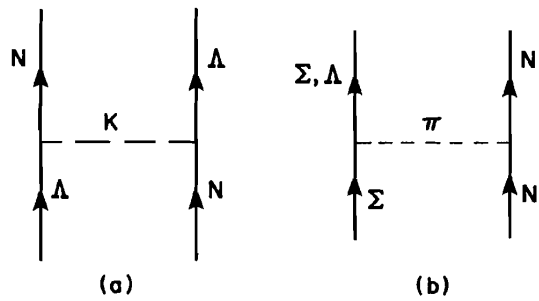

FIG. 4.2.

and

$$CP\bar{K}^0 = e^{-i\phi}K^0$$

We use the customary convention, $\phi = 0$, so that

$$\begin{aligned} CPK &= \bar{K}^0 \\ CP\bar{K}^0 &= K^0 \end{aligned} \tag{4.2}$$

Photons are odd under C. Since π^0 decays into two photons

$$C\pi^0 = \pi^0$$

so that the π^0 is an eigenstate of C. But the π^0 is a pseudoscalar, so that

$$CP\pi^0 = -\pi^0$$

We now consider the weak decay of the kaons into $\pi\pi$ and $\pi\pi\pi$. Since the spin of the kaon is zero, the two pions are in an $l = 0$ orbital state. The intrinsic parity of the two pions is $+1$ and the orbital state is even under parity. Thus the parity of the two-pion final state is even. If the two pions are π^0's, the operator C will not affect them. If they are a π^+ and π^-, C will interchange them. However, they are in a relative $l = 0$ orbit and their state is thus unchanged by C. Hence the two pion state formed by the decay of the kaon has even CP.

Consider next the three-pion system $\pi^0\pi^0\pi^0$. Our conclusion will be valid for kaon decays involving charged pions. Since they are bosons and their total spin is zero, they are in a spatially symmetric state (i.e., the exchange of any two will not affect the three-pion wave function. Under these circumstances the spatial parity of the three-pion system is even but the intrinsic parity of each is odd, so that finally the parity is odd. Since C = 1 for each of the pions, CP for the three-pion decay is odd.

Since the weak interaction is CP invariant, K^0 and $\bar{K}^0$ are not eigenstates of H, the total Hamiltonian, $H_{\text{strong}} + H_{\text{weak}}$. The eigenstates of H are

$$\begin{aligned} K_1 &= \frac{1}{\sqrt{2}}(K^0 + \bar{K}^0) \\ K_2 &= \frac{1}{\sqrt{2}}(K^0 - \bar{K}^0) \\ K^0 &= \frac{1}{\sqrt{2}}(K_1 + K_2) \\ \bar{K}^0 &= \frac{1}{\sqrt{2}}(K_1 - K_2) \end{aligned} \tag{4.3}$$

The state K_1 is even under CP, while K_2 is odd. The K_1 will therefore decay into two pions and the K_2 will decay into three pions. Thus if K^0 is produced in a reaction, its composition will change with time. If

$$\begin{aligned} HK_1 &= \left(m_1 - \frac{i\Gamma_1}{2}\right)K_1 \\ HK_2 &= \left(m_2 - \frac{i\Gamma_2}{2}\right)K_2 \end{aligned} \tag{4.4}$$

then

$$K^0(t) = \frac{1}{\sqrt{2}}(e^{-im_1t-\Gamma_1t/2}K_1 + e^{-im_2t-\Gamma_2t/2}K_2) \tag{4.5}$$

Note that (4.4) holds only in the rest frame of K_1 and K_2. The short lifetime $\hbar/\Gamma_1$ is 0.89×10^{-10} s, while the long lifetime $\hbar/\Gamma_2$ is 0.52×10^{-7} s. We see from (4.5) that the mixture of $S = 1$ and $S = -1$ changes with time. Eventually, $K_0 \to K_2$ with equal amplitudes for K_0 and $\bar{K}_0$. Moreover, the amplitudes of the K_1 and K_2 components can be obtained by measuring the ratio of 2π to 3π decays. From this result, using (4.5), the mass difference between K_1 and K_2 can be determined. It equals 3.52×10^{-6} eV.

Suppose that a beam of neutral kaons are incident on a nucleus. These kaons will all be in the K_2 state if a sufficient time has elapsed from the time of production. But the K_0 and $\bar{K}_0$ components of K_2 will scatter differently with amplitudes f and $\bar{f}$, respectively. The kaon wave function will then become

$$\begin{aligned} K_2 &\to \frac{1}{\sqrt{2}}(fK^0 - \bar{f}\bar{K}^0) \\ &= \tfrac{1}{2}[(f - \bar{f})K_1 + (f + \bar{f})K_2] \end{aligned} \tag{4.6}$$

As a consequence of the scattering, some K_1 has been poduced. This phenomenon is referred to as *regeneration* [Pais and Piccioni (55)]. The incident beam particles could only decay into three pions. After the scattering, two-pion decay can also occur because of the presence of K_1 in (4.6). By measuring the two- and three-pion decays, one can determine the amplitudes f and $\bar{f}$.

The discussion above is not entirely correct, for it is found that the long-lived kaon, which is referred to as K_L, decays into *both* 3π and 2π final states (Christenson, Cronin, Fitch, and Turlay (64)]. Thus CP canot be conserved. K_L must be a linear combination of K_1 and K_2:

$$K_L = \frac{1}{\sqrt{1+\varepsilon^2}}(K_2 + \varepsilon K_1) \tag{4.7}$$

The particle K_S, which has a short lifetime, is given by

$$K_S = \frac{1}{\sqrt{1+\varepsilon^2}}(K_1 + \varepsilon K_2) \tag{4.8}$$

The measured value of ε is $(1.6)(1+i) \times 10^{-3}$. Up to this time, no other system has exhibited CP violation. Since ε is small, for most of the phenomena to be discussed we can disregard the differences between K_L and K_2 and K_S and K_1:

$$K_L \simeq K_2 \qquad K_S \simeq K_1$$

A. Kaon–Nucleon Scattering‡

The study of kaon–nucleon reactions is far from achieving the completeness that we have seen to exist in the pion case. The associated phenomenology is therefore less secure. But there are some broad features that are understood qualitatively and in some cases quantitatively, which are of importance for an understanding of kaon-induced nuclear reactions. *Many of the numerical values given in the discussion must be regarded as tentative.*

The reactions induces by K^- beams incident on the nucleon are qualitatively different from those induced by K^+ beam. This can be seen in Figs. 4.3 and 4.4. One observes the complex structure of the K^- total cross section. These are a consequence of a number of resonances that are tabulated in Tables 4.3 and 4.4 for the energy range considered in Fig. 4.3.

In these tables the column labeled $L_{T,2J}$ gives the possible spatial configuration for each of these composite particles. The column labeled "dominant channel" indicates the most probable decay modes and therefore the most likely

TABLE 4.3

$T=0$	$L_{T,2J}$	Γ(MeV)	Dominant Channel	Mass (MeV)
Λ (1405 MeV)	S_{01}	40 ± 1	$\bar{K}N$	1405 ± 5
Λ (1520)	D_{03}	15.6 ± 1	$\bar{K}N$, $\Sigma\pi$	1519.5 ± 1.0
Λ (1600)	P_{01}	50 – 250	$\Sigma\pi$, $\bar{K}N$	1560 – 1700
Λ (1670)	S_{01}	25 – 50	$\Sigma\pi$	1660 – 1680
Λ (1690)	D_{03}	50 – 70	$\Sigma\pi$, $\bar{K}N$	1685 – 1695
Λ (1800)	S_{01}	200 – 400	$\bar{K}N$	1720 – 1850
Λ (1810)	P_{01}	50 – 250	$\Sigma\pi$	1750 – 1850
Λ (1820)	F_{05}	70 – 90	$K^*(892)N$	1815 – 1825
Λ (1830)	D_{05}	60 – 110	$\Sigma\pi$	1810 – 1830

Source: "Review of Particle Properties," Particle Data Group, *Phys. Lett. B* 204 (1988).

‡Dover and Walker (82); Arndt and Roper (85); Dalitz, McGinlay, Belyca, and Anthony (82).

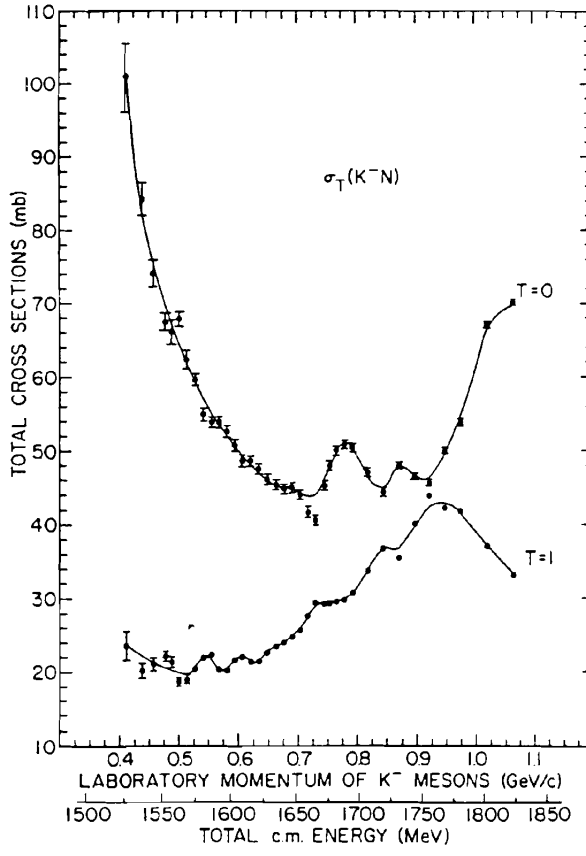

FIG. 4.3. Total K^--nucleon cross sections for isospin $T = 0$ and $T = 1$. [From Carroll, Chiang, et al. (76).]

TABLE 4.4

$T = 1$	$L_{T,2J}$	Γ(MeV)	Dominant Channel	Mass (MeV)
Σ^* (1385)	P_{13}	36 ± 1	$\Lambda\pi$	1382.8 ± 0.4
Σ^0 (1385)				1383.7 ± 1.0
Σ^- (1385)				1387.2 ± 0.6
Σ (1660)	P_{11}	40 – 200	$\bar{K}N$	1630 – 1690
Σ (1670)	D_{13}	40 – 80	$\Sigma\pi$	1665 – 1685
Σ (1750)	S_{11}	60 – 160	$\bar{K}N$, $\Sigma\eta$	1730 – 1800
Σ (1775)	D_{15}	105 – 135	$\bar{K}N$, $\Lambda\pi$	1770 – 1780

Source: "Review of Particle Properties," Particle Data Group, *Phys. Lett B* 204 (1988).

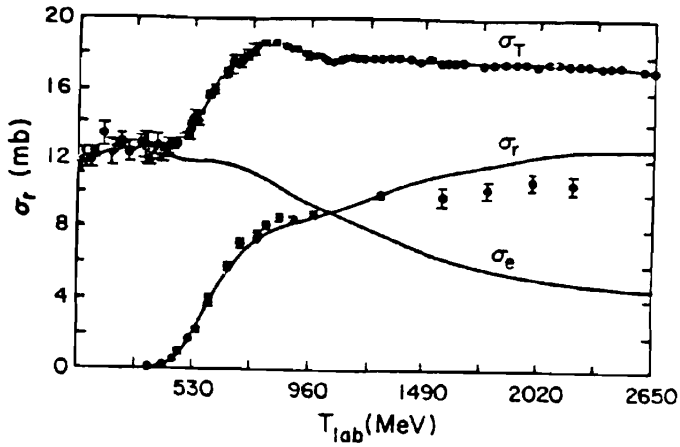

FIG. 4.4. Total (σ_T), inelastic (σ_r), and elastic (σ_e) K^+p cross sections. [From Arndt and Roper (85).]

production reactions. The $K^*(892)$ is a spin-1 particle with the same strangeness as the K. It is a member of the spin-1 octet that includes the ρ as a member. One can conclude from the rich spectrum seen in these tables that the $\bar{K}N$ system is strongly interactive.

The picture for the K^+N system is strikingly different, as we can see from Fig. 4.4. The total cross section for $K^+ + N$ is relatively constant up to a kaon laboratory kinetic energy of about 0.4 GeV ($p_L = 0.745$ MeV/c, $E_{cm} = 1.674$ GeV), after which there is a relatively steep rise up to about 0.8 GeV in the laboratory, after which it is relatively constant. Below 0.4 GeV, $\sigma_T \sim 1.2$ mb, while for energies greater than 0.8 GeV, $\sigma_T \sim 1.7$ mb. The last is the sum of a decreasing elastic cross section, σ_e, and a rising reaction cross section, σ_r. Three resonances are reported by Arndt and Roper (85), who find the evidence for $Z^*(1780)$ as strong; there are two other resonances listed as "highly probable" (see Table 4.5). In the "*Review of Particle Properties*," these resonances are considered to be uncertain. The difference between the NK and $\bar{K}N$ systems can be qualitatively understood by considering the quark structure in each case. The kaon, $\bar{K}$, is made up of $\bar{u}s$, while the nucleon, say the proton, contains two u's and one d. The $\bar{u}$ in the kaon and the u in the proton can annihilate, going off, for example,

TABLE 4.5

$T = 1$	$L_{T,2J}$	Γ (MeV)
$Z^*(1780)$	P_{13}	280
$Z^*(1725)$	P_{11}	180
$Z^*(2161)$	D_{15}	320

as a pion leaving behind *usd*, a Λ or Σ^0. When the incident kaon is K^+, which is a $u\bar{s}$ system, no such annihilation can occur and we are left with a five-quark system $uuud\bar{s}$. This system ($uuu = \Delta^{++}$, $d\bar{s} = K^0$) suggests the existence of an inelastic channel ΔK. Its threshold (for $K^+\Delta^+$) is 1725.67 MeV near to one of the Z^* resonances. One expects that the probability of forming a five-quark resonance in the low-energy domain is much less probable than that of forming a three-quark resonance.

B. The *KN* System[‡]

The reactions that are relevant are:

	$K + N \rightarrow K + N$
Elastic	$K^+ + n \rightarrow K^+ + p$
	$K_L^0 + p \rightarrow K_S^0 + p$
	$K + N \rightarrow K + N + \pi$
Inelastic	$K + N \rightarrow \Delta + K$
	$K + N \rightarrow K^* + N$
	0.305 GeV/c
Threshold (p_{cm})	0.466
	0.552

In these equations N can be either a neutron or a proton and K, K^+, or K^0. Let $f_2^{(1)}$ be the amplitude in the $T = 1$ channel and $f_2^{(0)}$ be the amplitude in the $T = 0$ channel for $Y = 2$. Then from isospin conservation, one obtains

$$f(K^+p \rightarrow K^+p) = f_2^{(1)} \tag{4.9a}$$

$$f(K^+n \rightarrow K^+n) = \tfrac{1}{2}(f_2^{(1)} + f_2^{(0)}) \tag{4.9b}$$

$$f(K^+n \rightarrow K^0p) = \tfrac{1}{2}(f_2^{(1)} - f_2^{(0)}) \tag{4.9c}$$

If $f_0^{(1)}$ and $f_0^{(0)}$ are the amplitudes for $Y = 0$, then

$$f(K_L^0p \rightarrow K_S^0p) = \tfrac{1}{4}(f_2^{(1)} + f_2^{(0)} - 2f_0^{(1)}) \tag{4.10}$$

Similarly,

$$\sigma(K^+ + n \rightarrow \Delta + K) = \tfrac{1}{5}\sigma(K^+ + p \rightarrow \Delta + K) \tag{4.11}$$

[‡]Corden, Cou, et al. (82); Arndt and Roper (85).

In this reaction

$$K^+ + p \rightarrow \Delta^{++} + K^0$$
$$\rightarrow \Delta^+ + K^+$$

and

$$K^+ + n \rightarrow \Delta^+ + K^0$$
$$\rightarrow \Delta^0 + K^+$$

From (4.11) we conclude that Δ production by K^+ in nuclei will be sensitive to the proton distribution. In the regeneration reaction amplitude, (4.10), $f_0^{(1)}$ is obtained from $K^- p$ elastic scattering data, while $f_2^{(1)}$ is given by elastic $K^+ p$ scattering. Thus from the measurement of $f(K_L^0 p \rightarrow K_S^0 p)$ together with $K^- p$ and $K^+ p$ elastic scattering data, one can obtain the $T = 0$, $Y = 2$ amplitude. Much of the same information can be obtained from elastic scattering of K^+ by neutrons [Eq. (4.9*b*)] and from charge exchange scattering [Eq. (4.9*c*)].

Since we are dealing with the scattering of a spin-zero particle (K) by a spin-$\frac{1}{2}$ particle (N), the partial wave analysis of the scattering and polarization is identical with that described earlier in this chapter from an analysis of pion-nucleon scattering. The scattering amplitude is (see 2.16)

$$\hat{f} = f + i\boldsymbol{\sigma}\cdot\mathbf{n}g \tag{4.12}$$

where f and g are functions of the center-of-mass energy and the spherical angles ϑ and φ, while $\mathbf{n}$ is a unit vector perpendicular to the scattering plane. The expressions for the scattering cross section, the polarization, and the spin rotation parameter in terms of f and g are given by 2.20 and 2.20′. We recall that two phase shifts are associated with each value of the angular momentum, $\delta_{l+1/2}$ and $\delta_{l-1/2}$. The relations given by (4.9) are satisfied by both f and g of (4.12).

The $T = 1$ total and inelastic cross section is given in Fig. 4.4. This is supplemented in Fig. 4.5 by the $T = 0$ total and inelastic cross sections, in Fig. 4.6 by the $K_L^0 p \rightarrow K_S^0 p$ cross section, in Fig. 4.7 by the $K^+ n \rightarrow K^0 p$ cross section, and by Fig. 4.8 giving the angular distribution for $K^+ p$ ($T = 1$) elastic scattering for a range in K^+ momentum.

The elastic cross section is isotropic up to K^+ laboratory momentum of 800 MeV/c, corresponding to the dominance of the partial wave $L_{T,2J} = S_{11}$. Above 800 MeV/c higher values of L must be added as the angular distribution becomes anisotropic. Coulomb interference at small angles indicate that the S_{11} amplitude is repulsive. We observe that the charge exchange scattering $K^+ n \rightarrow K^0 p$ is important only in the neighborhood of K^+ momentum equal to 800 MeV/c. Note that $K^+ n$ scattering and charge exchange scattering must be deduced from K^+ collisions with deuterons.

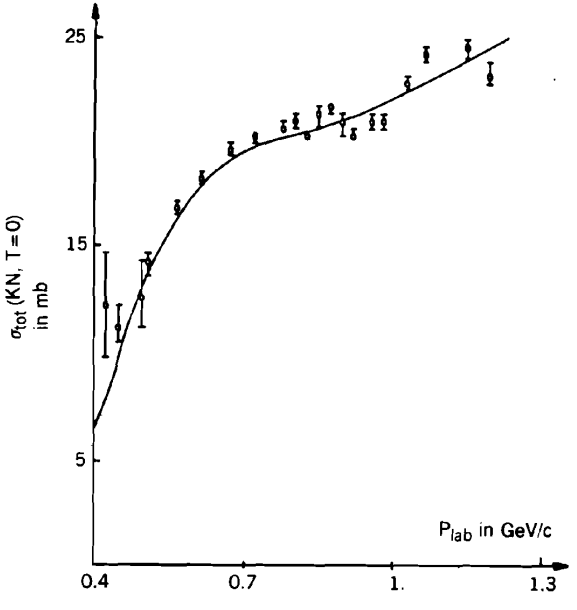

(*a*)

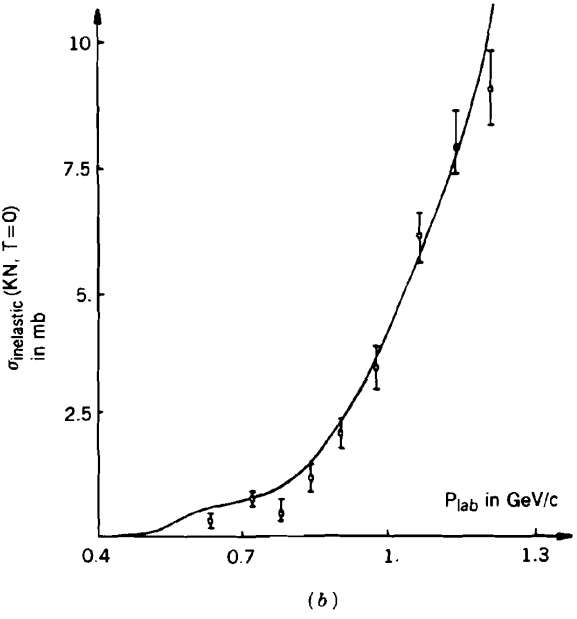

(*b*)

FIG. 4.5. Total (σ_{tot}) and inelastic ($\sigma_{inelastic}$) cross sections for KN scattering. [From Corden, Cox, et al. (82).]

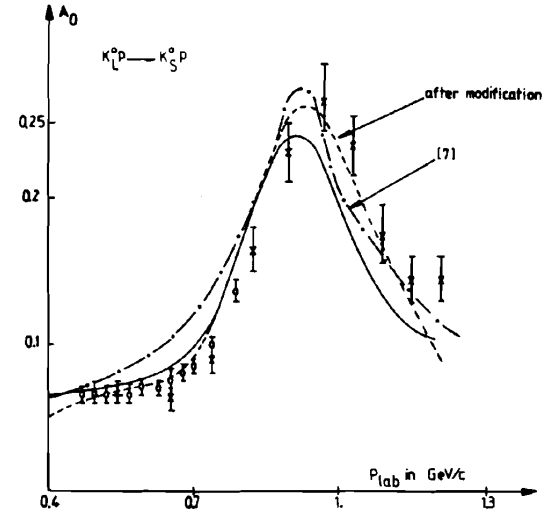

FIG. 4.6. Cross section for $K_L^0 \rightarrow K_s^0 p$. The preferred fit is given by the solid line. [From Corden, Cox, et al. (82).]

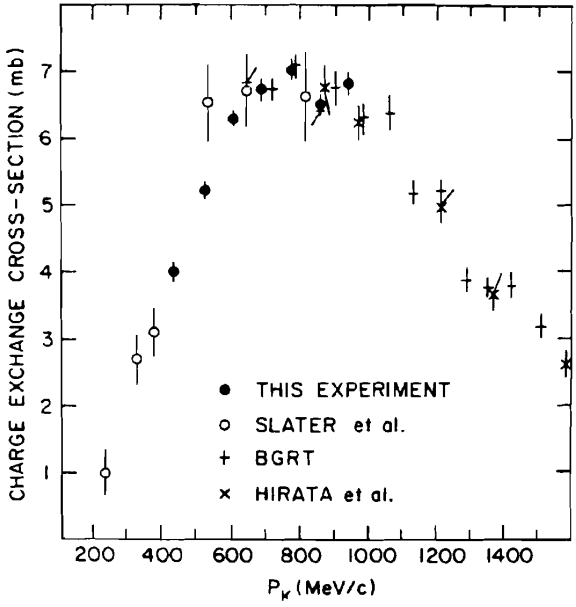

FIG. 4.7. Cross section for $K^+ n \rightarrow K^0 p$ charge exchange. [From Darnerell, Hotchkiss, et al. (85).]

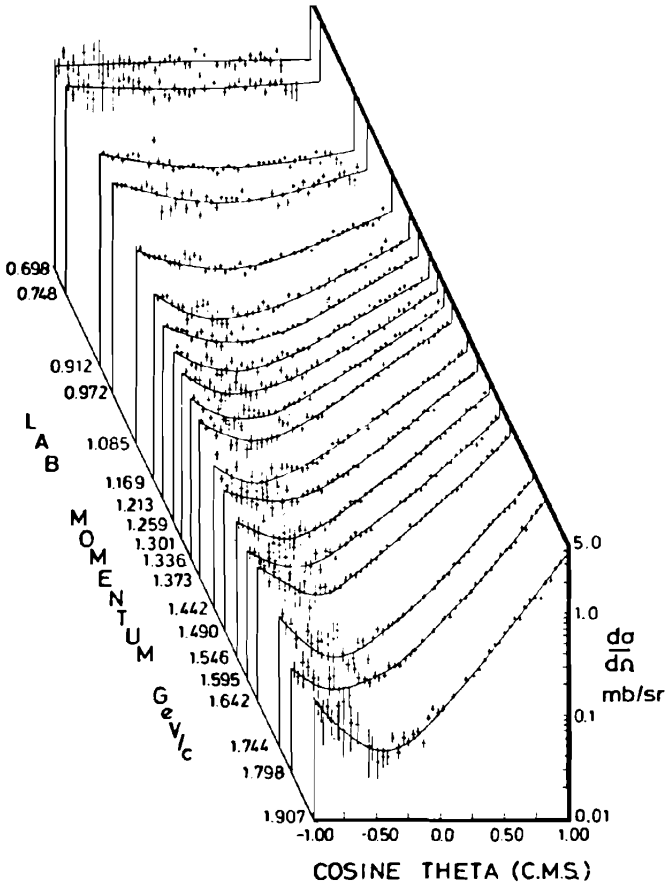

FIG. 4.8. Differential cross sections for K^+p elastic scattering. Below 700 MeV/c angular distribution is nearly isotropic. $S_{1/2}$, $T = 1$ channel dominates. [From Charles, Cowan, et al. (77); Charles, Cowan (72).]

The data at low energies can be summarized in terms of scattering length a, and effective range r, for S-wave scattering and scattering volume for the P-wave amplitudes. The effective range expansion is

$$k^{2l+1} \cot \delta = \frac{1}{a} + \tfrac{1}{2} r k^2 \tag{4.13}$$

For isospin $T = 1$ and S wave,

$$\begin{aligned} a_L(\mathrm{T}, 2J) &= a_S(1,1) \simeq -0.309 \pm 0.002\,\mathrm{fm} \\ r_L(T, 2J) &= r_S(1,1) \simeq 0.32 \pm 0.02\,\mathrm{fm} \end{aligned} \tag{4.14}$$

where we use the data of Cameron et al. (74). For the P-wave amplitudes

$$a_P(1,1) = -0.021\,\text{fm}$$
$$a_P(1,3) = 0.013\,\text{fm} \tag{4.15}$$

For $T = 0$,

$$a_S(0,1) \sim -0.035\,\text{fm}$$
$$a_P(0,1) \sim 0.086\,\text{fm} \tag{4.16}$$
$$a_P(0,3) \sim -0.019\,\text{fm}$$

where we have used the data of Martin (75). A summary of the data is given by Dover and Walker (82). From their summary we see that there is agreement among various experiments on the signs and magnitude of a (two significant figures) and r (one significant figure) for $T = 1$. For $T = 0$ there is no agreement on sign. As regards magnitude, there is agreement that the $T = 0$ scattering lengths and volumes are small and are considerably smaller than the comparable $T = 1$ quantities.

At higher energies a phase-shift analysis for $T = 1$ has been made by Arndt and Roper (85). Their analysis led to claims of the three resonances listed in Table 4.5. Their match with the data is shown in Figs. 4.4 and 4.9. Of special interest are the P_{13} amplitudes shown in Fig. 4.10 and the corresponding Argand diagram Fig. 4.11. We see that the P_{13} resonance is strongly inelastic, as it differs sharply from the bounding circle valid for elastic scattering.

Note on the Argand Diagram. We write the S matrix

$$S = e^{2i\delta}\frac{E - E_r - i\Gamma'/2}{E - E_r + i\Gamma/2} = e^{2i\delta}\frac{E - E_r - i\Gamma/2 + i\Delta/2}{E - E_r + i\Gamma/2}$$

where δ is the potential scattering phase shift, E_r the resonance energy, Γ the width, and $\Delta = \Gamma - \Gamma'$. When the scattering is elastic, $\Gamma' = \Gamma$ and $\Delta = 0$. The transition amplitude is taken to be

$$\mathcal{T} = \frac{(S-1)}{2i}$$

If $S = e^{2i\delta}$, $\mathcal{T} = \sin\delta e^{i\delta}$. Letting

$$\tan\phi = \frac{\Gamma}{2(E - E_r)}$$

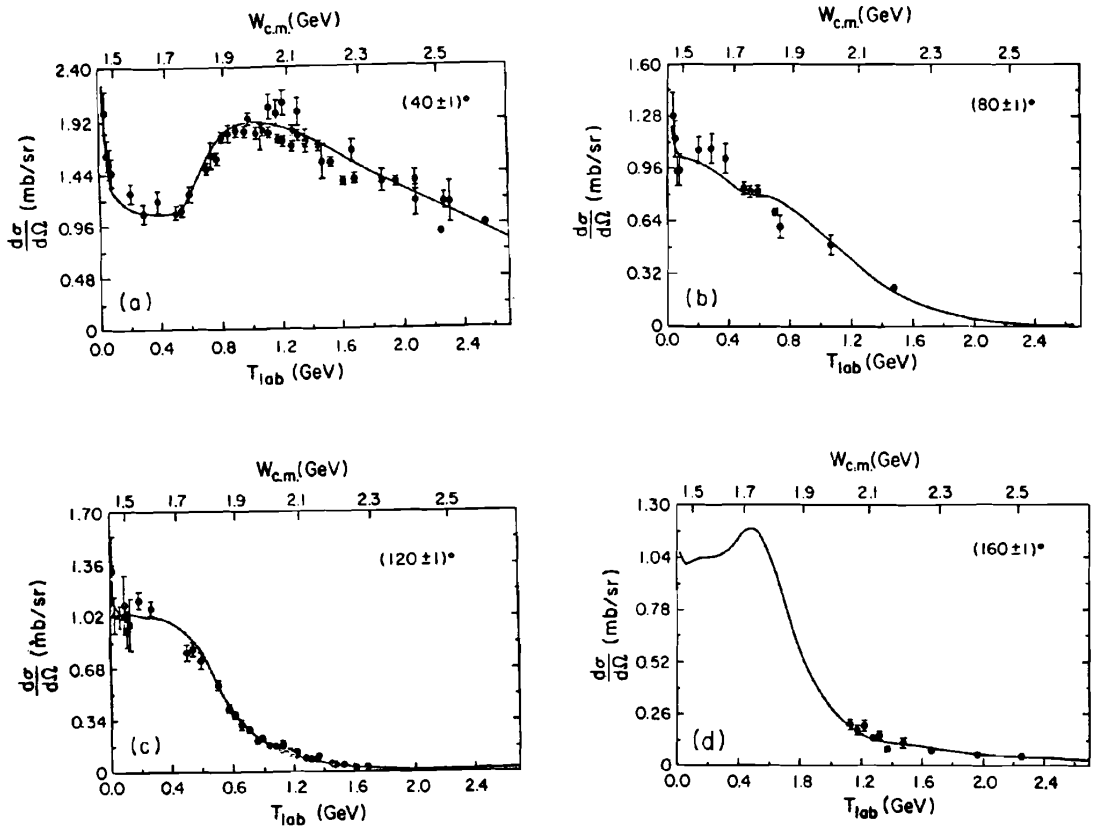

FIG. 4.9. Representative differential cross section data together with Arndt and Roper's predictions for K^+p scattering. [From Arndt and Roper (85).]

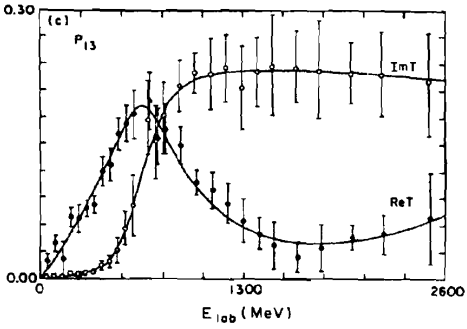

FIG. 4.10. P_{13} scattering amplitude. [From Arndt and Roper (85).]

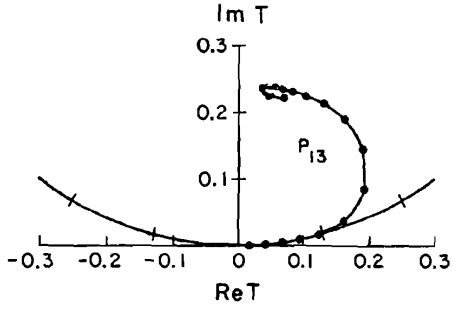

FIG. 4.11. Argand diagram for P_{13} amplitude. [From Arndt and Roper (85).]

one finds that

$$\mathrm{Re}\,\mathscr{T} = -\sin(\phi-\delta)\cos(\phi-\delta)+\frac{\Delta}{4H}\cos(\phi-2\delta) \tag{4.17a}$$

$$\mathrm{Im}\,\mathscr{T} = \sin^2(\phi-\delta)-\frac{\Delta}{4H}\sin(\phi-2\delta) \tag{4.17b}$$

$$|\mathscr{T}|^2 = \sin^2(\phi-\delta)-\frac{\Delta}{2H}\sin(\phi-\delta)\cos\delta+\frac{\Delta^2}{16H^2} \tag{4.17c}$$

where

$$H=\left[(E-E_r)^2+\frac{\Gamma^2}{4}\right]^{1/2}$$

Consider first the simplest case ($\delta=0$, $\Delta=0$), so that

$$\mathrm{Re}\,\mathscr{T} \to -\sin\phi\cos\phi = -\tfrac{1}{2}\sin 2\phi$$
$$\mathrm{Im}\,\mathscr{T} = \sin^2\phi = \tfrac{1}{2}(1-\cos 2\phi)$$

Therefore,

$$(\mathrm{Re}\,\mathscr{T})^2+(\mathrm{Im}\,\mathscr{T}-\tfrac{1}{2})^2 = \tfrac{1}{4}$$

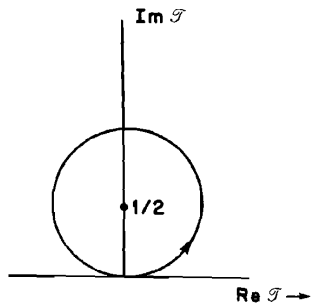

FIG. 4.12. Argand diagram.

A plot in which the horizontal axis is $\mathrm{Re}\,\mathcal{T}$ and the vertical axis is $\mathrm{Im}\,\mathcal{T}$ will be a circle of radius $\frac{1}{2}$ with the center on the vertical axis at $\frac{1}{2}$ (Fig. 4.12). For E negatively infinite, $\phi = 0$, and $\mathrm{Re}\,\mathcal{T} = 0$ and $\mathrm{Im}\,\mathcal{T} = 0$. As E increases, one travels counterclockwise, reaching the top of the circle at the resonance energy, $E = E_r$, where $\phi = \pi/2$, so that $\mathrm{Re}\,\mathcal{T} = 0$ and $\mathrm{Im}\,\mathcal{T} = 1$.

The second case is the most common, $\delta = 0$, Δ finite;

$$\mathrm{Re}\,\mathcal{T} = -\sin\phi\cos\phi + \frac{\Delta}{4H}\cos\phi$$

$$\mathrm{Im}\,\mathcal{T} = \sin^2\phi - \frac{\Delta}{4H}\sin\phi$$

$$|\mathcal{T}|^2 = \sin^2\phi - \frac{\Delta}{2H}\sin\phi + \frac{\Delta^2}{16H^2}$$

At resonance $\phi = \pi/2$,

$$|\mathcal{T}|^2 = \left(1 - \frac{\Delta}{4H}\right)^2 = \left(1 - \frac{\Delta}{2\Gamma}\right)^2 \tag{4.18}$$

so that the locus of $\mathrm{Re}\,\mathcal{T}$, $\mathrm{Im}\,\mathcal{T}$, will be in the interior of the circle. Moreover, at resonance

$$\mathrm{Re}\,\mathcal{T} = 0 \tag{4.19}$$

From Fig. 4.11 one sees that the amplitude for the P_{13} partial wave does approach the $\mathrm{Im}\,\mathcal{T}$ axis. The extrapolated value of $\mathrm{Im}\,\mathcal{T}$ at $\mathrm{Re}\,\mathcal{T} = 0$ is about 0.25 or $\Delta/\Gamma = 1$. The partial wave reaction cross section is

$$\sigma_r = \frac{\pi}{k^2}(1 - |S|^2)(2J + 1)$$

Inserting the expression for $|S|$, one finds that

$$1-|S|^2=\frac{\frac{1}{4}(2\Gamma\Delta+\Delta^2)}{(E-E_r)^2+\Gamma^2/4}$$

At $E=E_r$,

$$1-|S|^2\to\frac{2\Delta\Gamma+\Delta^2}{\Gamma^2}=2\frac{\Delta}{\Gamma}+\left(\frac{\Delta}{\Gamma}\right)^2$$

relating Δ/Γ to the inelasticity seen in (4.18).

C. The $\bar{K}N$ Reaction‡

Because of the existence of the Λ^0 at 1405 MeV and the Σ at 1385 MeV, this reaction is much more complex than the KN reaction. Note that the mass of the $\bar{K}p$ system is 1431.9 MeV, so that a conversion of the $\bar{K}p$ system to $\pi\Sigma$ or a $\pi^0\Lambda^0$ is energetically possible. Therefore, in addition to elastic scattering,

$$K^-+p\to K^-+p$$

we also have the open channels

$$K^-+p\to\pi^0\Lambda^0+180\,\text{MeV},\qquad T=1$$
$$K^-+p\to\pi\Sigma+100\,\text{MeV},\qquad T=1,0$$

as well as the charge exchange scattering channel,

$$K^-+p\to\bar{K}^0+n$$

Isospin invariance connects the cross sections for these reactions:

$$\sigma(K^-n\to\pi^-\Lambda)=2\sigma(K^-p\to\pi^0\Lambda) \tag{4.20}$$

and

$$\sigma(K^-n\to\pi^-\Sigma^0)=\sigma(K^-p\to\pi^+\Sigma^-)+\sigma(K^-p\to\pi^-\Sigma^+)-2\sigma(K^-p\to\pi^0\Sigma^0) \tag{4.21}$$

The analysis of this experimental data was pioneered by Dalitz and Tuan (60), who made use of the $\mathscr{K}$ matrix (see Chapter III, p. 169, and Appendix A). The

‡Note that $\bar{K}$ can refer to either K^- or $\bar{K}$.

$\mathscr{K}$ matrix is related to the $\mathscr{T}$ and S matrices are follows:

$$\mathscr{K} = \mathscr{T} + i\pi\mathscr{K}\delta(E_i - E_f)\mathscr{T} = \mathscr{T} + i\pi\mathscr{T}\delta(E_i - E_f)K \tag{4.21a}$$

$$S = 1 - 2\pi i\delta(E_i - E_f)\mathscr{T} \tag{4.21b}$$

$$S = \frac{1 - i\pi\delta(E_i - E_f)\mathscr{K}}{1 + i\pi\delta(E_i - E_f)\mathscr{K}} \tag{4.21c}$$

From (4.21c) we note that the unitarity of the S matrix implies that $\mathscr{K}$ is Hermitian. Second, because of time reversal invariance, $\mathscr{K}$ is real.

Equation (4.21a) is simplified greatly if it is restricted to a given partial wave. Then $\mathscr{K}$ and $\mathscr{T}$ become matrices involving the various channels. For $T = 0$,

$$\mathscr{K} = \begin{pmatrix} \kappa_{NN} & \kappa_{N\Sigma} \\ \kappa_{N\Sigma} & \kappa_{\Sigma\Sigma} \end{pmatrix} \qquad T = 0 \tag{4.22}$$

where

$$\kappa_{NN} \equiv \langle N\bar{K}|\mathscr{K}|N\bar{K}\rangle$$

and

$$\kappa_{N\Sigma} = \langle \Sigma\pi|\mathscr{K}|N\bar{K}\rangle \tag{4.23}$$

It is necessary to insert the diagonal matrix elements of $\delta(E_i - E_f)$ for the two channels. Those matrix elements will depend on the normalization convention for the states involves. For $l = 0$, a spatial wave, the diagonal matrix for $\delta(E_i - E_f)$ is taken to be‡

$$\hat{\rho} \equiv -\frac{1}{\pi}\begin{pmatrix} k_N & 0 \\ 0 & k_\Sigma \end{pmatrix} \tag{4.24}$$

Equation (4.21a) [and similarly for (4.21b) and (4.21c)] becomes

$$\mathscr{K} = \mathscr{T} + i\pi\mathscr{K}\hat{\rho}\mathscr{T}$$

or

$$\mathscr{T}^{-1} = \mathscr{K}^{-1} + i\pi\hat{\rho}$$

More generally for $l > 0$, k_i on the right-hand side of (4.23) is replaced by k_i^{2l}

‡The minus sign in (4.24) is chosen so as to come into agreement with the Dalitz–Tuan choice for $\mathscr{K}$ and $\mathscr{T}$, which are the negatives of the $\mathscr{K}$ and $\mathscr{T}$ used in this volume.

by Arndt, Roper, and Steinberg (78). For the S partial wave the cross section is

$$\sigma = \frac{2\pi}{k^2 |\mathscr{T}_{fi}|^2} \tag{4.25}$$

For the $T = 1$ case, the $\mathscr{K}$ matrix involves three channels, so that

$$\mathscr{K} = \begin{pmatrix} \kappa_{NN} & \kappa_{N\Sigma} & \kappa_{N\Lambda} \\ \kappa_{\Sigma N} & \kappa_{\Sigma\Sigma} & \kappa_{\Sigma\Lambda} \\ \kappa_{\Lambda N} & \kappa_{\Lambda\Sigma} & \kappa_{\Lambda\Lambda} \end{pmatrix} \tag{4.26}$$

and

$$\hat{\rho} = -\frac{1}{\pi} \begin{pmatrix} k_N & 0 & 0 \\ 0 & k_\Sigma & 0 \\ 0 & 0 & k_\Lambda \end{pmatrix} \tag{4.27}$$

Dalitz, McGinley, Belyca, and Anthony (82) parameterize $\mathscr{K}^{-1}$ by an effective range expansion [Ross and Shaw (60, 61)]:

$$\mathscr{K}_T^{-1} = M_T + R_T k^2 \tag{4.28}$$

where k is the center-of-mass momentum in the $K^- p$ channel. The results obtained by Dalitz, McGinley, Belyca, and Anthony (82) using the column labeled new data in their Table 1 are in units of fermis:

$$\begin{aligned} T = 0: \quad & \kappa_{NN} = -1.863, \quad \kappa_{N\Sigma} = -0.955, \quad \kappa_{\Sigma\Sigma} = -0.382 \\ T = 1: \quad & \kappa_{NN} = 0.26, \quad \kappa_{N\Sigma} = -0.99, \quad \kappa_{\Sigma\Sigma} = 0.81 \\ & \kappa_{N\Lambda} = 0.29, \quad \kappa_{\Sigma\Lambda} = 0.44, \quad \kappa_{\Lambda\Lambda} = -0.55 \end{aligned} \tag{4.29}$$

From the results for $\mathscr{K}$, one can obtain $\mathscr{T}$ and in the low-energy approximation the scattering length [see (4.13)]

$$k \cot \delta_0 \to \frac{1}{a + ib}$$

The values of a for isospin 1, a_1, and for isospin 0, a_0, and similarly for b are [Dalitz, McGinley, Belyca, and Anthony (82)]

$$\begin{aligned} a_0 &= -1.57\,\text{fm} \qquad a_1 = 0.1075\,\text{fm} \\ b_0 &= 0.70\,\text{fm} \qquad b_1 = 0.57\,\text{fm} \end{aligned} \tag{4.30}$$

Note that in contrast to the KN scattering length, the scattering length for the

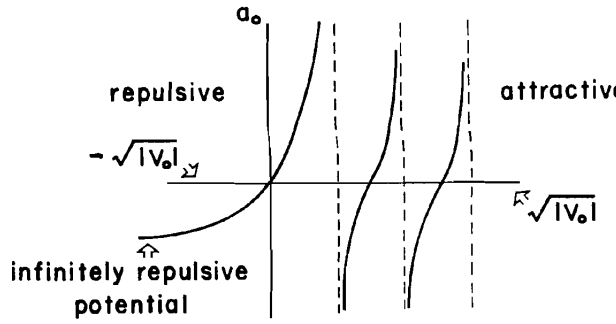

FIG. 4.13

$\bar{K}N$ is complex because absorption into other channels ($\Sigma\pi$ and $\Lambda\pi$) is possible even at threshold.

Note. For systems with bound states such as the $\bar{K}N$, the sign of the scattering length does not necessarily indicate the attractive or repulsive nature of the interaction. For a potential model, the dependence of the scattering length on the strength of the potential V_0 is illustrated in Fig. 4.13. From this figure we see that a positive S-wave scattering length does correspond to attraction. However, a negative scattering length can correspond to either an attractive or repulsive potential. For a weak interaction as is the case for the KN system, a negative a_0 does correspond to a repulsion. For the $\bar{K}N$ system, since there is a $T = 0$ (1405) bound state, a_0 must take on a value in the attractive half-plane.

The $T = 1$ scattering length is relatively small and positive. The interaction is therefore relatively weakly attractive. For both the $T = 0$ and $T = 1$ cases the absorption is strong.

The $\mathscr{K}$-matrix method can be carried out for each partial wave. This analysis was used by Arndt and Roper (85) in their analysis of K^+ reactions. Gopal et al. (77) employ a multichannel analysis. The total and elastic scattering $K^- p$ cross section are shown in Figs. 4.14 and 4.15. The charge and strangeness exchange cross sections are given in Figs. 4.16 to 4.18. The analysis of Gopal et al. (77) is used in constructing some of these cross sections. Included in these figure are the cross sections averaged over a Fermi-gas nucleon distribution. These are defined as follows. Let $\rho(k)$ be the Fermi-gas distribution normalized by

$$2\int_0^\infty dk k^2 \rho(k) = 1$$

Let

$$\left(\frac{d\sigma}{d\Omega_L}(p_k, k, 0)\right)_0$$

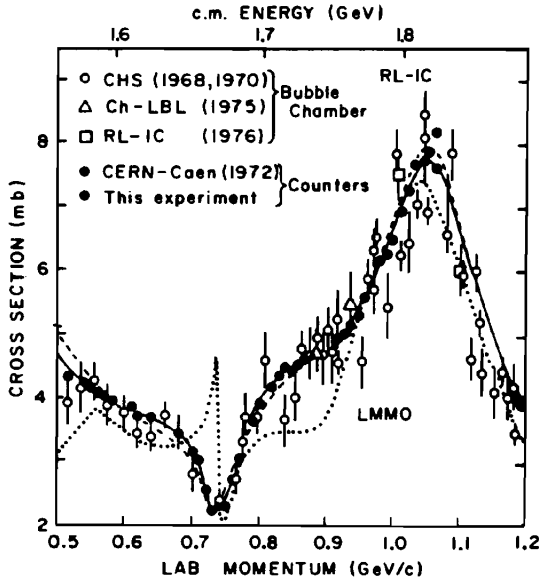

FIG. 4.14. Cross section for the charge exchange reaction $K^- p \to \bar{K}^0 n$. [From Alston-Garnjost et al. (77, 78, 80).]

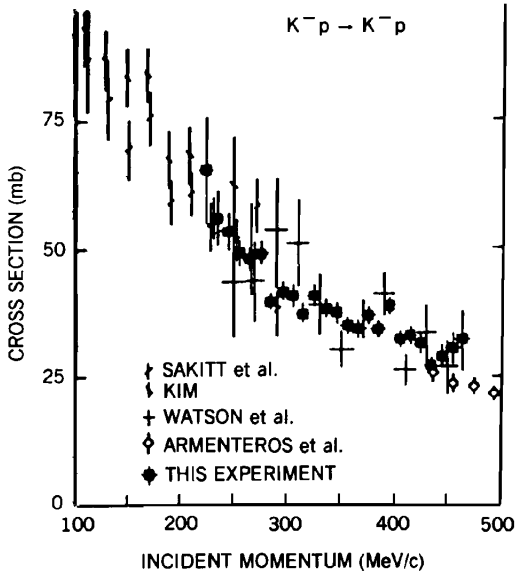

FIG. 4.15. Elastic cross section for $K^- p \to K^- p$. [From Mast, Alston-Garnjost, et al. (76).]

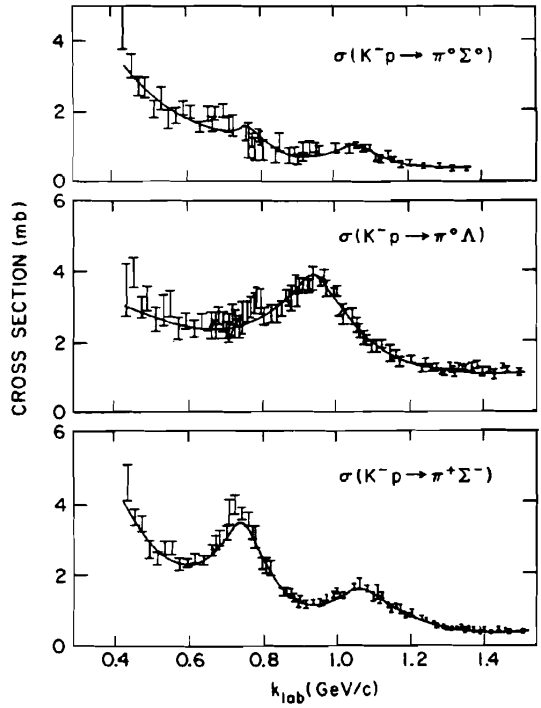

FIG. 4.16. Total cross sections for the reactions $K^- p \to \pi^0\Sigma^0$, $\pi^0\Lambda$ and $\pi^+\Sigma^-$. [From Dover and Walker (82).]

be the differential cross section for the scattering into the incident direction. This is a function of the kaon momentum p_k, the nucleon momentum k, and x the cosine of the angle between $\mathbf{p}_k$ and $\mathbf{k}$. Then

$$\left\langle \left(\frac{d\sigma}{d\Omega_L} \right)_{0^\circ} \right\rangle_{\text{av}} = \int_0^\infty dk k^2 \rho(k) \int_{-1}^{1} dx \left(\frac{d\sigma}{d\Omega_L}(p_k, k, x) \right)_{0^\circ} \tag{4.31}$$

and

$$\langle f_L(0) \rangle_{\text{av}} = \int_0^\infty dk k^2 \rho(k) \int_{-1}^{1} dx f_L(0) \tag{4.32}$$

where f_L is the reaction amplitude. Averaging smooths the strong fluctuations with energy of the free-space cross section and amplitude. The later is a consequence of the resonances in the $\bar{K}N$ system.

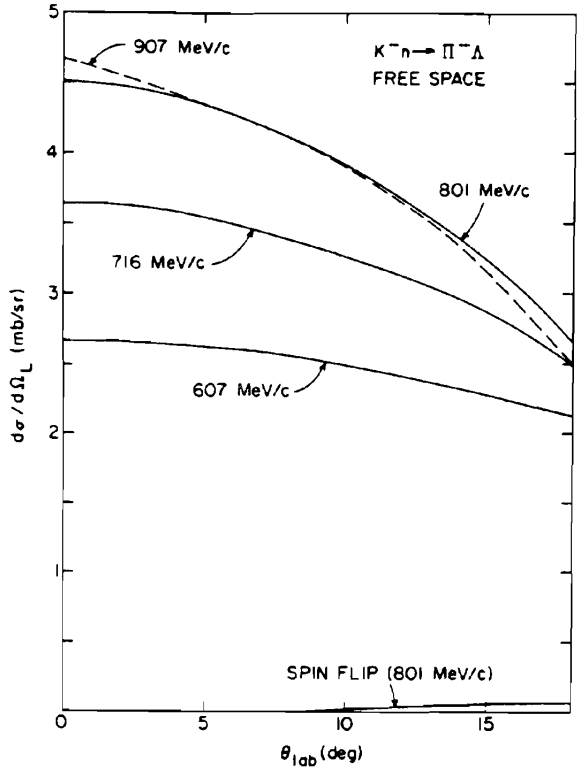

(a)

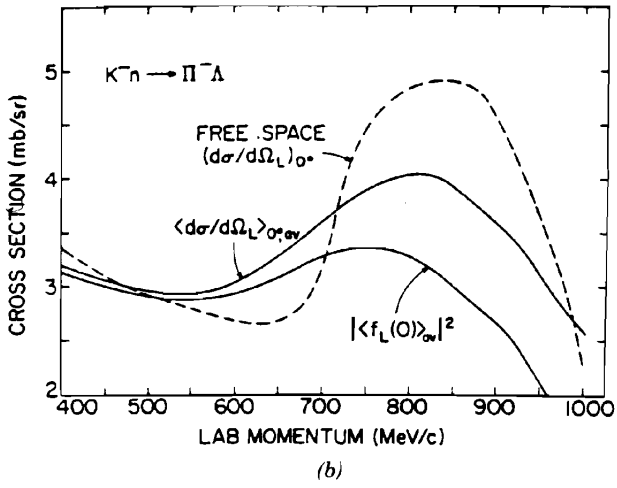

(b)

FIG. 4.17. (*a*) Laboratory differential cross sections for $K^- n \to \pi^- \Lambda$ [Gopal et al. (77)]; (*b*) Fermi-averaged forward $K^- n \to \pi^- \Lambda$ cross sections. [From Dover and Walker (82).]

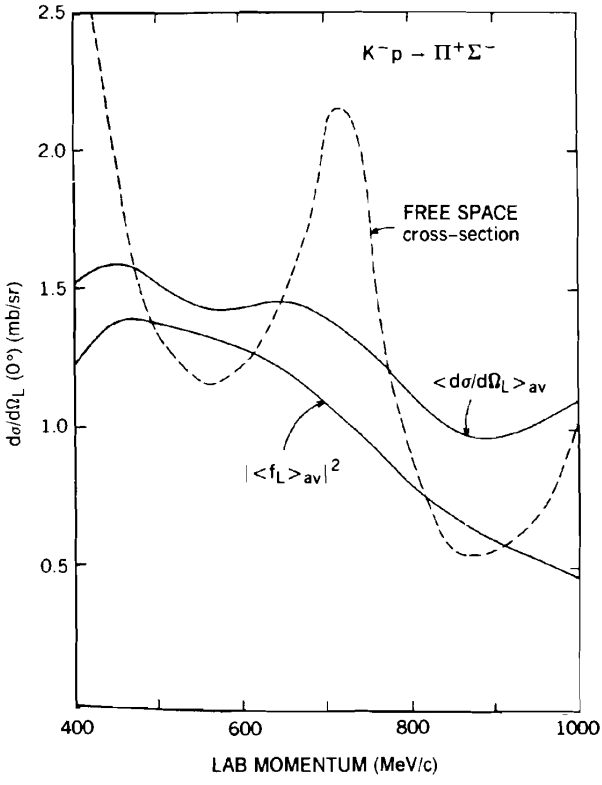

FIG. 4.18. Fermi-averaged $K^- p \to \pi^+ \Sigma^-$ laboratory cross section [Gopal et al. (77)]. [From Dover and Walker (82).]

Dover and Walker (82) use

$$\rho(k) = \frac{\rho_0}{1 + e^{(k - k_0)/\Delta(k)}}$$
$$k_0 = 100\ \text{MeV}/c \qquad \Delta(k) = 50\ \text{MeV}/c \tag{4.33}$$

as suggested by Allardyce et al. (73).

D. K^+–Nucleus Scattering[‡]

The K^+–nucleus scattering is of considerable interest because of the relative weak KN interaction. As a consequence, the K^+ can penetrate much farther into the nucleus than, for example, a nucleon. We have earlier commented on

[‡]Coker, Lumpe, and Ray (85); Siegel, Kaufmann, and Gibbs (84, 85).

the fact that because of the strong nucleon–nucleon interaction, high-energy nucleon–nucleus scattering reveals mostly surface properties of the density distribution of nucleons in the nucleus. K^+–nuclear scattering could be exploited to determine the properties of these distribution in the nuclear interior. Combined with the proton distributions obtained from elastic electron–nucleus scattering, one would have a complete picture of both nucleon distributions.

There are additional simplifications. Because of the weak KN interaction, the first order, ρt, in the multiple scattering series should be sufficient. Second, because the K has a zero spin, the analysis of experiment should prove to be more easily performed.

Elastic scattering K^+–nucleus scattering have been performed with the ^{12}C and ^{40}Ca nuclei [Marlow, Barnes, et al. (82)]. The momentum of the K^+ beam is 800 MeV/c. The results are shown in Fig. 4.19. The solid lines are first-order optical model ρt calculations [Rosenthal and Tabakin (80); Marlow, Barnes, et al. (82)] based on the KN phase shifts given by Martin (75). It is, of course, necessary to transform these from the kaon–nucleon reference frame to the K–nucleus one. The agreement in the ^{40}Ca case is good. In the ^{12}C case the theoretical curve lies below the experimental one. The total cross sections reflects this difference. (see Fig. 4.20) The deviation from theory may be because of experimental artifacts (such as normalization of the cross section, errors in the measurement of angles, energy spread in the incident beam, etc.). There is after all just one experiment. These are analyzed by Siegel, Kaufmann, and Gibbs (84) with the conclusion that agreement with theory is possible. In addition, there may be errors in the KN phase shifts used, although the agreement with the K^+ ^{40}Ca results indicate these are not major. By comparing the K^+ ^{12}Ca results with the K^+ deuterium scattering, the effects of such errors are reduced. The suggestion has been made by Siegel, Kaufmann, and Gibbs (85) that within the nucleus there is an increase of the $S_{11}KN$ phase shift from that given by Martin. Two explanations have been offered. Siegel, Kaufmann, and Gibbs (85) suggest that the effect arises from an increase of nucleon size because of an increase in the confinement radius of the nucleon inside the nucleus. This is suggested by the EMC effect [Aubert et al. (83); Bodek et al. (83); see Close (88a) for a review of this effect.] Brown, Dover, Siegel, and Weise (88) ascribe this increase to the change in the mass of the ρ and ω which mediate the K^+ reaction in the nuclear medium. This leads to an optical potential that depends nonlinearly on the nucleon density giving rise to an increased repulsion (over the first-order ρt) and a decreased effective nuclear radius. The agreement with experiment is shown in Fig. 4.21. The parameter λ describes the change in mass of the ρ and ω in the nuclear medium,

$$\frac{m_V^2(\rho)}{m_V^2(0)} = 1 - \frac{\lambda\rho}{\rho_0}$$

In this equation V can be either ρ or ω, and ρ_0 is the equilibrium nucleon

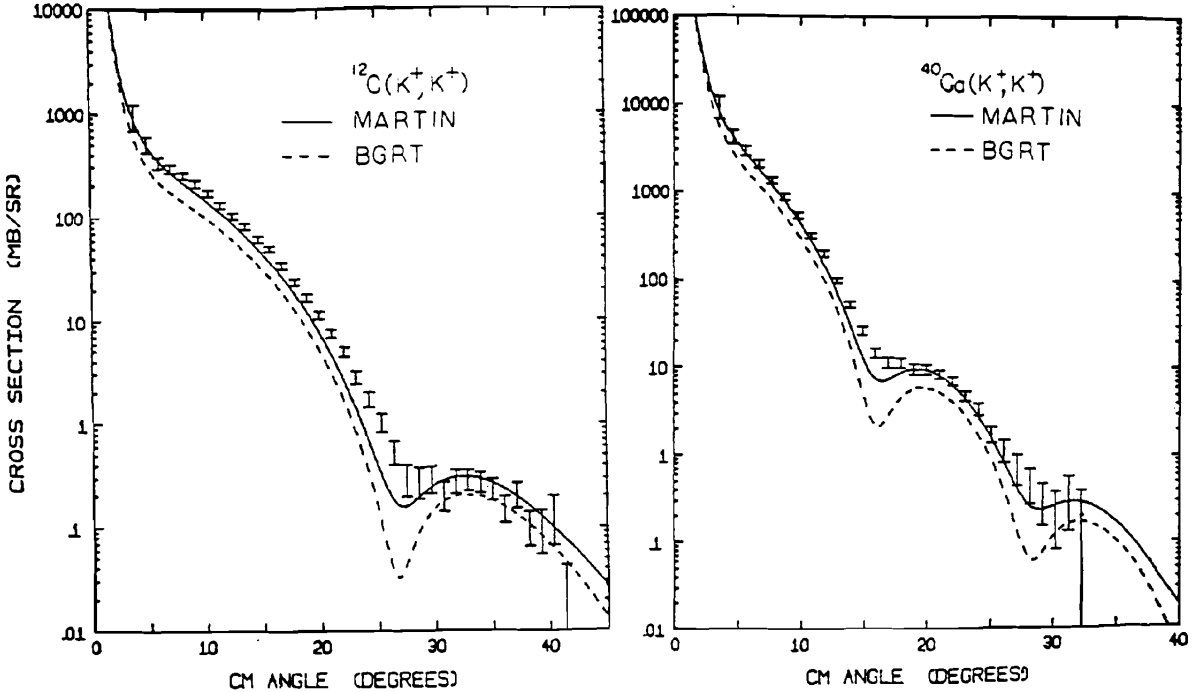

FIG. 4.19. Elastic scattering differential cross section for $K^+ + {}^{12}C$ and $K^+ + {}^{40}Ca$ at 800 MeV/c. [From Marlow, Barnes, et al. (82).]

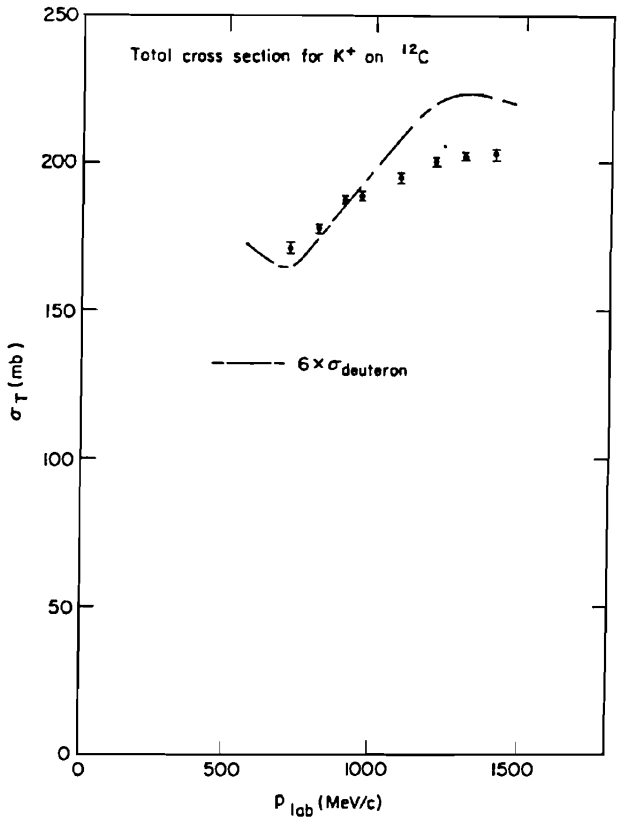

FIG. 4.20. Total cross section for K^+ scattering by ^{12}C. $\sigma_{deuteron}$ is the cross section for K^+ scattering by ^2H. [From Siegel, Kaufmann, and Gibbs (84).]

density. According to these authors there is little effect of this density dependence on the $K^+ + {}^{40}Ca$ elastic cross section.

Assuming that the ρt first-order term suffices for the heavier nuclei, one can ask for the sensitivity of the K^+ nucleus scattering to the nucleon density distribution [Coker, Lumpe, and Ray (85)]. These authors use the Martin phase shifts. This is illustrated by Figs. 4.22 and 4.23 for elastic scattering by Pb. The solid lines give the percentage change from a standard nucleon distribution induced by a Gaussian addition to the exterior surface or tail region of the neutron density. The dotted–dashed line gives the cross section for proton elastic scattering. We see that as predicted the K^+ projectile provides more information since the proton does not successfully penetrate into the nuclear interior.

Similar results are obtained for inelastic scattering using the DWIA. According to Dover and Walker (82), the dominant amplitude for a closed shell $J = 0$, $T = 0$ nucleus involves no spin, $\Delta S = 0$, or isospin $\Delta T = 0$, change.

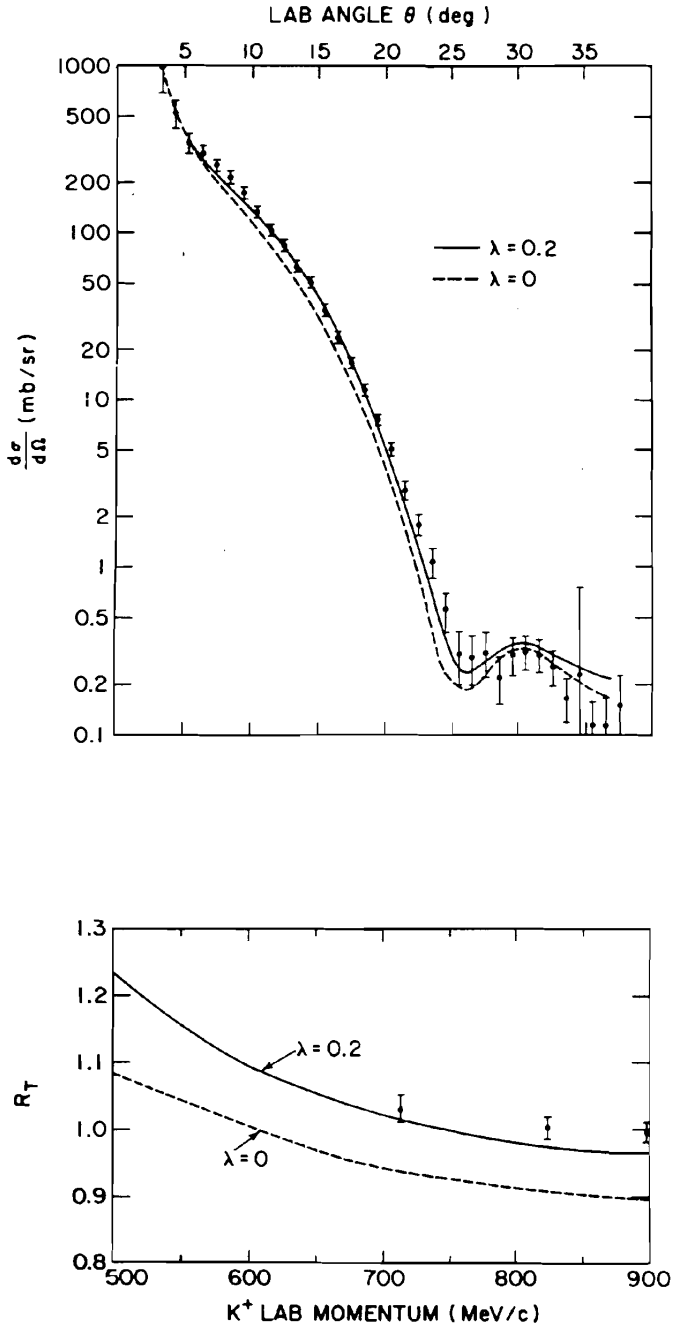

FIG. 4.21. Angular distribution for $K^+ + {}^{12}C$ elastic scattering at 800 MeV/c is shown at top; at the bottom, the total cross section ratio. [From Brown, Dover, Siegel, and Weise (88).]

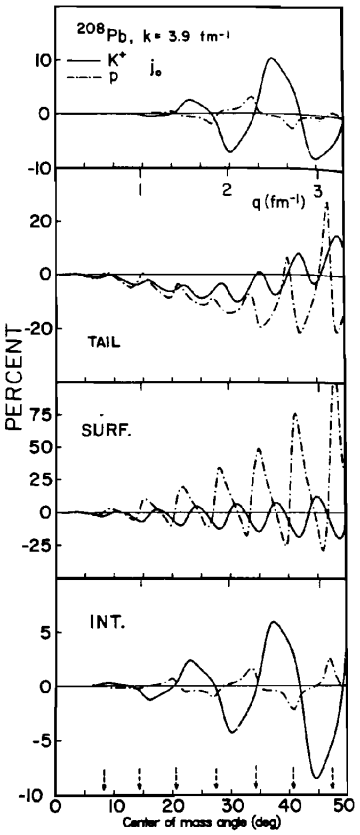

FIG. 4.22. Percent changes in the K^+ ^{208}Pb and p ^{208}Pb because of perturbations of the neutron density. Arrows indicate minima in the proton angular distribution. $E_k = 442$ MeV; $E_p = 297$ MeV. (j_0 = damped interior wiggle). [From Coker, Lumpe, and Ray (85).]

Coker, Lumpe, and Ray (85) use the DWIA formalism to compute the excitation of the collective 3^- level in Pb using the transition potential

$$U_{\text{trans}} = \frac{\beta}{\sqrt{2L+1}}\left[R\frac{d}{d\tau}U_{\text{opt}} + (V_H + iW)e^{-[r-(r_0)/a_0]^2}\right] \tag{4.34}$$

where β is the deformation parameter, U_{opt} is given by ρt, and the last term is an interior perturbation. The results are shown in Fig. 4.24, where again the solid line are K^+ induced and the dotted–dashed ones the proton induced. Again we see that the K^+ inelastic reaction is much more sensitive than the proton-induced reaction. More experiments are needed!

E. K^-–Nuclear Scattering

As in the case of K^+ scattering, the ρt first-order optical potential yields cross sections in substantial agreement with experiment when the kaon wavelength is

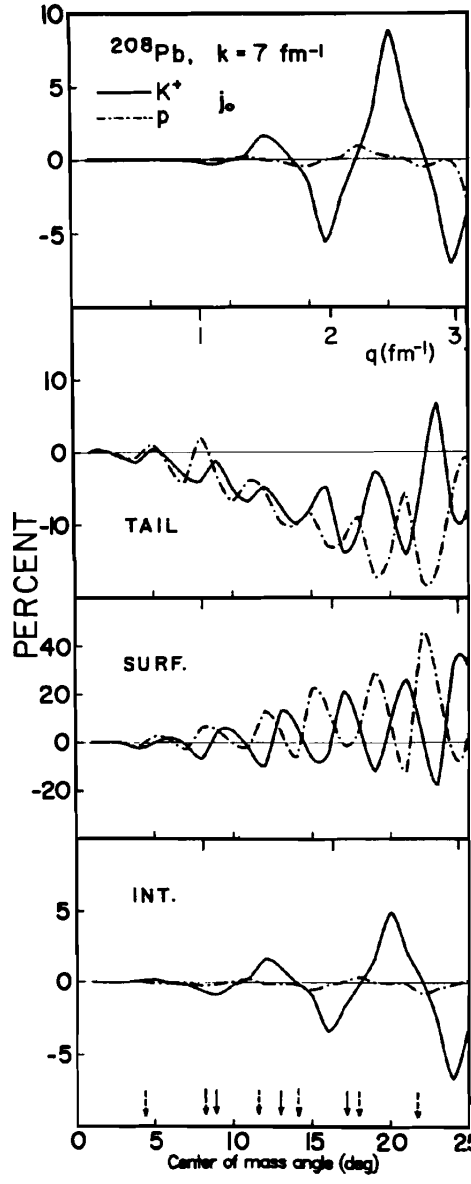

FIG. 4.23. Same as Fig. 4.22 except that $E_k = 991$ MeV and $E_p = 800$ MeV. [From Coker, Lumpe, and Ray (85).]

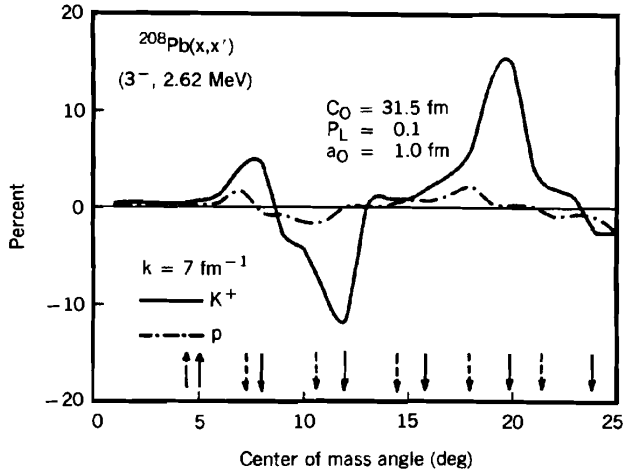

FIG. 4.24. Percent change in K^+- and p-induced inelastic differential cross section for ^{208}Pb resulting from an interior perturbation in transition potential. [From Coker, Lumpe, and Ray (85).]

sufficiently small. This is seen in Fig. 4.25, where $p_k = 800$ MeV/c and $\lambda = 1/4$ fm. The K^-N phase shifts used for t are those of Gopal et al. (77). Evidence for an anomaly in the $K^- + {}^{12}$C scattering is not as strong as in the analogous $K^+ + {}^{12}$C case.

At low energies, the $t\rho$ optical potential fails badly. If one were to use the $T = = 0$ K^-N scattering length [Eq. (4.30)], the $t\rho$ potential would be repulsive, whereas we know from the existence of bound $\bar{K}N$ states listed in Table 4.3 that the $K^- + N$ interaction, and therefore the K^- + nucleus interaction, is attractive. A much more sophisticated approach similar to that of Mahaux and his collaborators, who use a Bruckner–Hartree–Fock approach (see Chapter IV), is required.

Theoretical studies of the inelastic K^- scattering by nuclei are described by Dover and Walker (82). The results are similar to those obtained for K^+ inelastic scattering. Again the cross section is dominated by the $\Delta S = \Delta T = 0$ transition interaction. Hence one expects that the normal-parity, nonisospin flip states will be preferentially excited. Good agreement is obtained for the excitations of the 4.4- and 9.6-MeV levels on ^{12}C using nuclear density as determined by electron scattering. The agreement with a collective model [see (4.83)] is poor (see Fig. 4.26).

Dover and Walker (82) point to usefulness of the $(K^-, \bar{K}^0)$ reaction, since in that case we have $\Delta T = 1$. [Compare with (p, n) reaction] This reaction converts a proton into a neutron. For $T = 0$ nuclei only $T = 1$ states will be excited. For a $T \neq 0$ nucleus, the $T_>$ states would be easily identified.

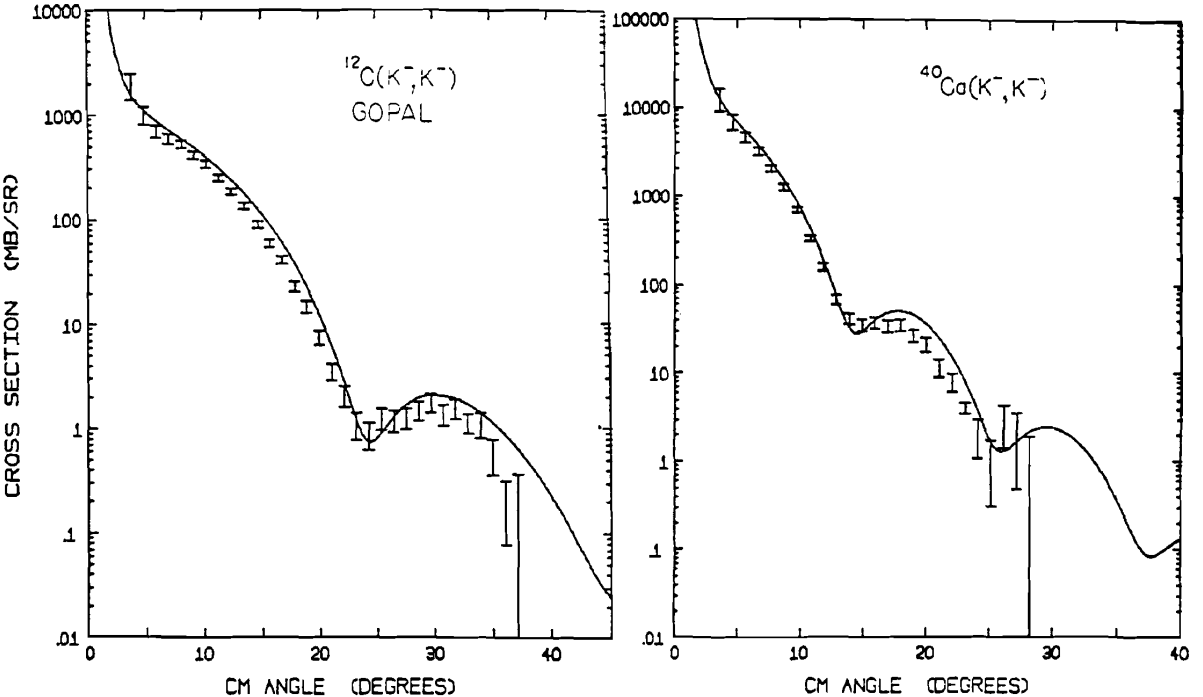

FIG. 4.25. Elastic scattering of K^- by ^{12}C ad ^{40}Ca. Curves are first-order optical model calculations using Gopal (77) free-space K^-N amplitudes. [From Dover and Walker (82).]

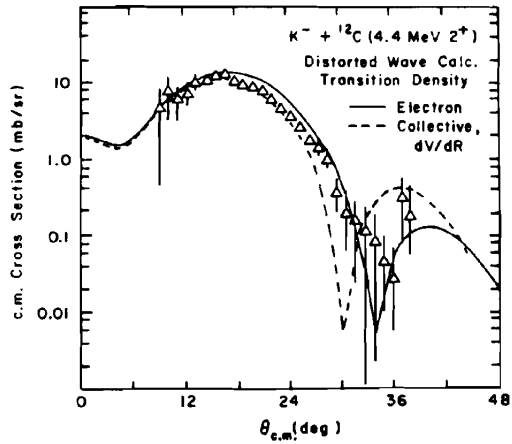

FIG. 4.26. Inelastic K^- scattering at 800 MeV/c to first 2^+ level in ^{12}C. [From Dover and Walker (82).]

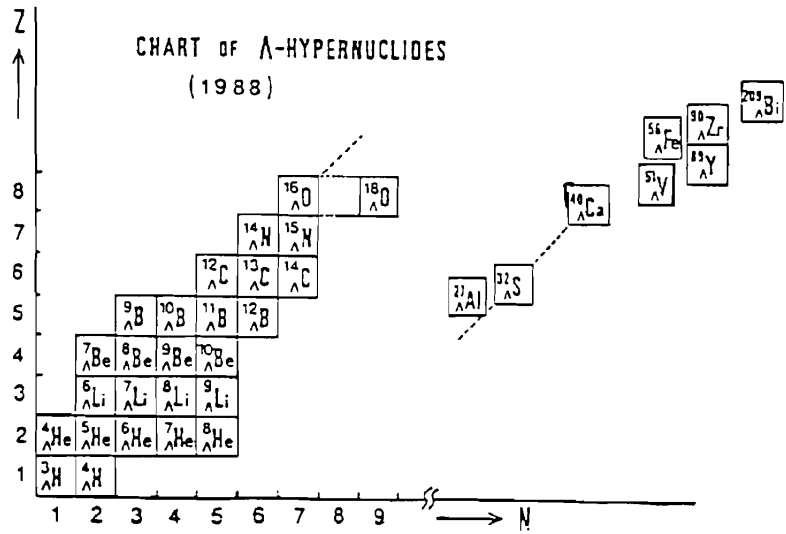

FIG. 4.27. Chart of observed Λ hypernuclei as of 1988. [From Bando (89).]

F. The Strangeness Exchange Reaction and Hypernuclei

By using the (K^-, π^-) or (π^+, K^+) reaction a nucleon in the nucleus is converted into a hyperon. Under appropriate conditions the hyperon is bound to the residual nucleus to form a hypernucleus. A (K^-, K^+) reaction could lead to the formation of a doubly strange ($S = -2$) hypernuclei. The Λ hypernuclei which have been observed are shown in Fig. 4.27. The existence of Σ hypernuclei

[Bertini et al. (84, 85); Walcher (88)] is controversial. These are very interesting systems since the Λ has approximately the same mass (Λ mass = 1115.6 MeV) as the nucleon, has the same spin, but has a zero isospin. The simplest assumption is that the Pauli exclusion principle does not limit the Λ, so that it can occupy orbits in the host nucleus which are forbidden to a nucleon.‡ As a consequence, new low-lying states that would not be present in the target nucleus will make their appearance.

Lambda hypernuclei were first observed in nuclear emulsions [Davis and Sacton (67)]. They have also been observed in the capture of K^- particles in Coulomb orbits about the carbon nucleus [C. Vandervelde-Wiquet, J. Sacton and J. H. Wickens (77)], forming a kaonic atom. Experimental opportunities were expanded substantially when it was shown that a small momentum transfer (K^-, π^-) reaction leading to the formation of a hypernucleus was possible. A review of the experiments using this reaction has been made by Povh (76, 78). Most recently, experiments at BNL have employed the (π^+, K^+) reaction, permitting the excitation of states in the large A hypernucleus, not as accessible with the (K^-, π^-) reaction.

The underlying physical processes using kaon beams of interest in the production of bypernuclei are

$$\begin{aligned} K^- + n &\rightarrow \Lambda + \pi^- \\ &\rightarrow \Sigma^0 + \pi^- \\ K^- + p &\rightarrow \Sigma^+ + \pi^- \\ &\rightarrow \Sigma^- + \pi^+ \end{aligned} \tag{4.35}$$

where we have limited the reactions to ones in which the final pion is charged. Another possible reaction is radiative capture:

$$K^- + p \rightarrow \Lambda + \gamma \tag{4.36}$$

Using π^+ beams, the pertinent reactions are

$$\begin{aligned} \pi^+ + n &\rightarrow \Lambda + K^+ \\ &\rightarrow \Sigma^0 + K^+ \\ &\rightarrow \Sigma^+ + K^0 \\ \pi^+ + p &\rightarrow \Sigma^+ + K^+ \end{aligned} \tag{4.37}$$

‡This is not completely true since the u and d quarks in the Λ and the u and d quarks in the nucleon do satisfy the Pauli principle. One of the investigations that is of fundamental importance will be to determine the effect of the Pauli principle satisfied by the quarks on the spectra of hypernuclei. In particular, this would depend on the degree of deconfinement of the quark.

The small momentum strangeness exchange reaction $n(K^-,\pi^-)\Lambda$ is possible because the mass of the K^- plus nucleon is about 178 MeV greater than that of the mass of the $\pi+\Lambda$. Consider the case when a K^- strikes a neutron at rest. Then there is a "magic momentum" for which th Λ is at rest and π^- moves in the forward (0°) direction. The equation determining this momentum is

$$m_n+\sqrt{m_K^2+p^2}=m_\Lambda+\sqrt{m_\pi^2+p^2}$$

or

$$E_K=\sqrt{m_K^2+p^2}=\frac{m_K^2-m_\pi^2+(m_\Lambda-m_n)^2}{2(m_\Lambda-m_n)} \tag{4.38}$$

For values of the kaon momentum that differ from the value obtained from (4.38), about 531 MeV/c, the momentum transfer to the Λ when the pion is observed at 0° can be small. This is illustrated in Fig. 4.28, where we see that the momentum transfer, $q(0)$, is less than the Fermi momentum over the entire range in the momentum p_k of the incident kaon. Much the same can be said for the $K^-+n\rightarrow\Sigma^0+\pi^-$ reaction, for which the magic momentum is about 284 MeV/c:

$$m_n+\sqrt{m_K^2+p^2}=m_\Sigma+\sqrt{m_\pi^2+\pi^2}$$

or

$$E_K=\sqrt{m_K^2+p^2}=\frac{m_K^2-m_\pi^2+(m_\Sigma-m_n)^2}{2(m_\Sigma-m_n)}$$

Thus when the K^- with the momenta shown in Fig. 4.28 strikes a nucleus and one studies the case where the pion goes off in the forward direction, it is very likely that the Λ will "stick" to the residual nucleus so that a hypernucleus is formed. In the simplest example of this reaction, a neutron in the nucleus is replaced by the Λ and the wave function of the system is not changed. For this

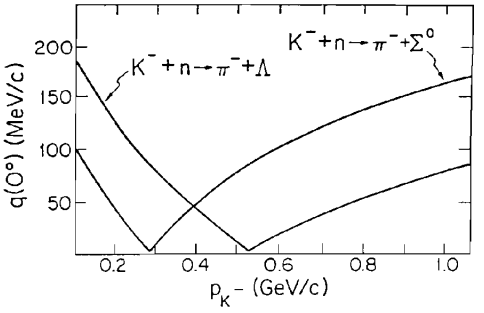

FIG. 4.28. Kinematics of the (K^-,π^-) reaction.

reason the reaction is referred to as a "substitutional" reaction. The angular momentum change is $\Delta l = 0$. When the emitted π^- is observed at angles greater than zero, $\Delta l = 1$ and $\Delta l = 2$ transitions become possible. Examples of the production of hypernuclei states by the (K^-, π^-) are shown in Fig. 4.29. The sharp peaks in the pion spectrum correspond to states in the hypernucleus.

The (K^-, π^-) reaction is not as useful for excitation of the low-lying Λ hypernuclear states for the heavier nuclei principally because the single-particle

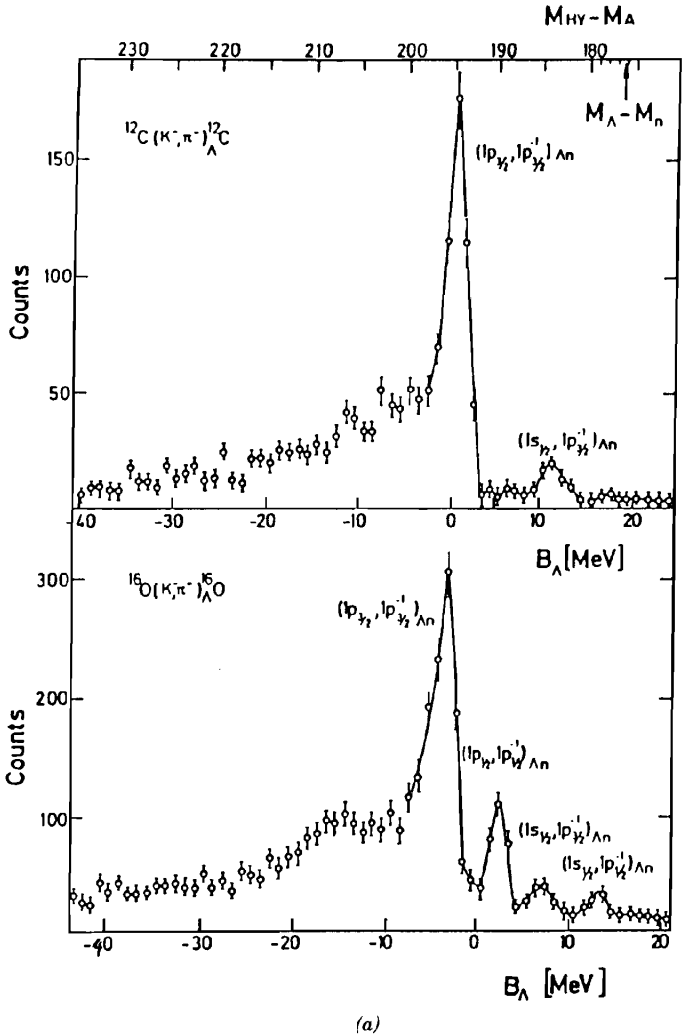

(a)

FIG. 4.29. (*a*) Production of hypernuclei ^{12}C, ^{16}O by the K^-, π^- reaction. [From Brückner, Granz, et al. (76).]; (*b*) Production of hypernuclei $^{12}_\Lambda C$, $^{27}_\Lambda Al$, $^{51}_\Lambda V$, $^{209}_\Lambda Bi$. [From Bertini, Bing, et al. (81).]

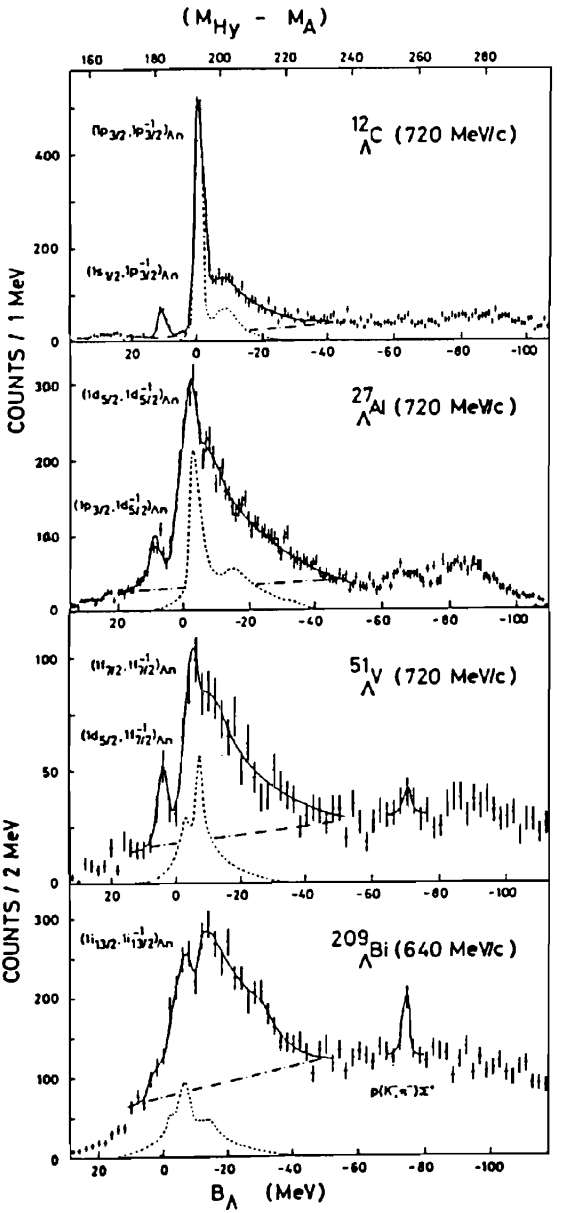

(b)

FIG. 4.29. (*Continued*)

neutron orbits have a large angular momentum, therefore requiring a large momentum change to generate a low-angular-momentum Λ orbit. This momentum change could, in principle, be obtained by examining the pion spectrum at large angles. But then the cross section is very much reduced.

The (K^-, π^-) has a number of innate difficulties. First, the incident K^- beam is accompanied by many more negative pions. Second, K^- decays and this compresses all the experimental dimensions. Moreover, the K^- decays into negative pions. The net resolution for the BNL experiments is a few MeV. Interpretation of the results is not easy since the K^- and π^- are strongly interacting. However, as we shall see, this difficulty is overcome by a careful DWA calculation.

Some of these restrictions are lifted in the (π^+, K^+) reaction. The momentum

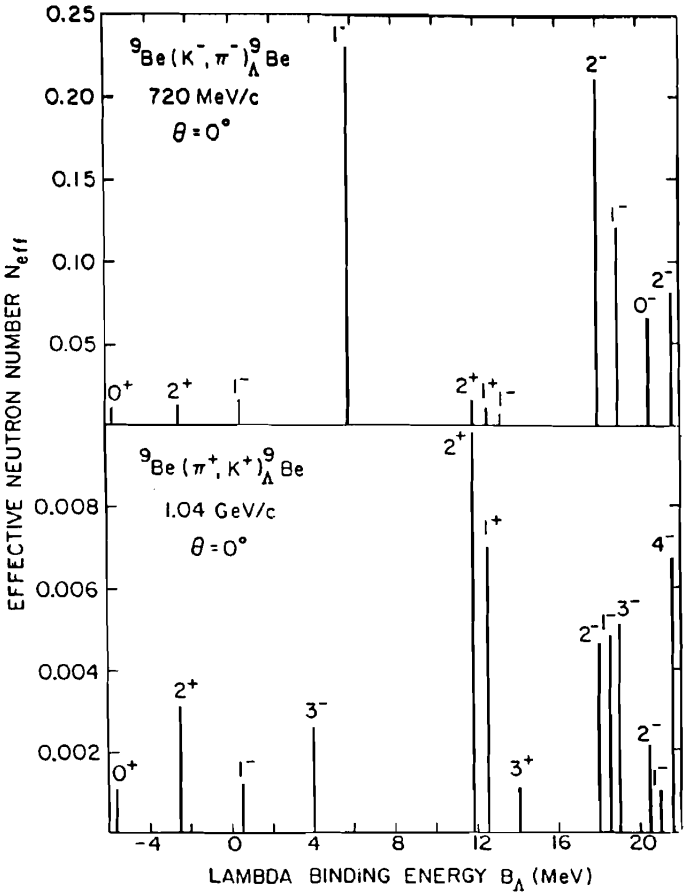

FIG. 4.30. Theoretical comparison of the production of $^9_\Lambda$Be hypernucleus using (K^-, π^-) and (π^+, K^+) reactions. [From Yamada, Ikeda, et al. (88).]

transfer is large. For $p_K = 1050\,\text{MeV}/c$, $q \geqslant 250\,\text{MeV}/c$. The cross sections for the formation of a hypernucleus are, of course, reduced, but this is compensated by the large pion intensity available in the incident beam. Interpretation is somewhat simpler since the K^+–nucleon interaction is relatively weak. Finally, the fact that the K^+ decays does not affect the experimental background. In fact, the decay is used to identify the K^+. The two reactions are complementary, as can be seen from Fig. 4.30, so that both experiments are needed to obtain a complete spectrum.

An example of the production of Λ hypernuclear states by the (π^+, K^+) reaction is shown in Fig. 4.31. In both examples, Figs. 4.29 and 4.31, the peaks are correlated with states in the hypernucleus. These are doorway states, which would fragment if experiments with sufficient resolution could be performed.

To determine the indicated configurations requires a calculation since there is much overlap in the experimental cross section. The DWA is used. That approximation has been discussed in Chapter V. Since no new principles are involved, we shall not discuss the details of the calculation in this chapter. The reader is referred to Auerbach, Baltz, et al. (83) and Hüfner, Lee, and Weidenmüller (74a, 74b, 79) for the detailed discussion.

The input into the DWA calculation for the (K^-, π^-) reaction requires (1) a wave function for the K^- nucleus system, (2) a wave function for the π^- nucleus system, (3) a wave function for the target neutron, (4) the Λ-host nucleus wave function, and (5) the transition matrix element converting K^- + neutron into

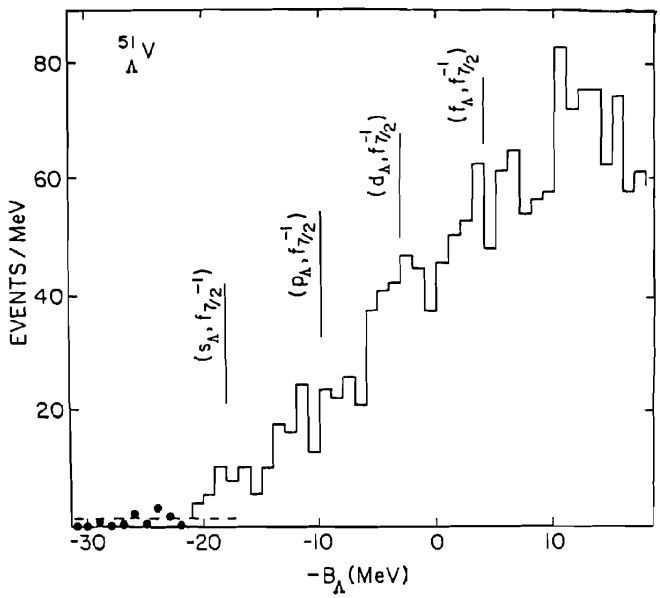

FIG. 4.31. Production of Λ hypernuclear states in $^{51}_{\Lambda}$V using the (π^+, K^+) reaction. [From Chrien (88).]

TABLE 4.6 Potentials for π^-, K^- Elastic Scattering at $p_K = 800$ MeV/c

Reaction	V_0(MeV)	W_0(MeV)	r_0(fm)	a_0(fm)	rms radius (fm)
$K^+ - {}^{12}C$	24.4	41.4	1.075	0.375	2.36
$\pi^- + {}^{12}C$	0.9	50.9	0.926	0.44	2.32
$K^- + {}^{40}Ca$	23.57	18.69	1.182	0.49	3.63

$\pi^- + \Lambda$. The first two of these is obtained by first adjusting the parameters in a simple Woods–Saxon potential so as to give the K^-–nucleus and π^-–nucleus elastic scattering. (The last should be the π^-–hypernucleus scattering.) The wave function is obtained from a solution of the Klein–Gordon equation assuming that potential to be the fourth component of a four-vector potential, neglecting the square of the potential in the Klein–Gordon equation. (See Chapter II for a discussion.) The resulting parameters are given in Table 4.6. The Woods–Saxon form is

$$U(r) = -(V_0 + iW_0)/f(r)$$

$$f(r) = 1 + \exp\left(\frac{r - r_0 A^{1/3}}{a_0}\right)$$

These potentials were used throughout the p-shell. The neutron and Λ wave functions were obtained by again using the Woods–Saxon form but adjusting so as to obtain the correct binding energy for the orbit in question. The parameters, r_0 and a_0 were taken to be 1.15 fm and 0.63, respectively. Parenthetically, we note that according to Auerbach, Baltz, et al. (83), the eikonal approximation for these wave functions does not suffice quantitatively, especially for $\Delta l = 0$ reactions.

The transition matrix element for the reaction $K^- + n \to \pi^- + \Lambda$ is taken to be

$$\langle \mathbf{r}_\pi, \mathbf{r}_\Lambda | v | \mathbf{r}_k, \mathbf{r}_n \rangle = V_T \delta(\mathbf{R}_{\pi\Lambda} - \mathbf{R}_{Kn}) \delta(\mathbf{r}_{\pi\Lambda} - \mathbf{r}_{Kn}) \delta(\mathbf{r}_{Kn}) \tag{4.39}$$

where V_T depends on isospin. The vectors $\mathbf{R}_{\pi\Lambda}$ and $\mathbf{R}_{Kn}$ give the positions of the center of mass of the $\pi\Lambda$ and Kn, respectively. The first δ function in (4.39) assures conservation of momentum in the $Kn \to \pi\Lambda$ reaction. The second term assumes that the interaction is local, while the last δ function is the zero-range approximation often used in the DWA. The strength V_T is given by the t matrix for $\bar{K}N \to \pi\Lambda$ at 0°. This must be transformed to the laboratory and averaged over a Fermi gas [see (4.31) and (4.32)]. The wave functions for the p shell core and the p-shell initial state were taken from Cohen and Kurath (65) using the POT interaction [see Fig. IX.4.1 in deShalit and Feshbach (74)]. The basis wave functions used to describe the hypernucleus is simply the core wave function Ψ_c times the Λ orbital ψ_Λ combined to yield the total angular

momentum J and isospin T. The wave function Ψ_c can refer to the ground state or excited states of the core. This representation for the hypernucleus wave function is called the *weak coupling approximation.* To obtain agreement with experiment it is necessary to introduce some residual Λ–N interaction [see Millener, Gal, Dover, and Dalitz (85)].

Qualitatively [and this is shown in the detailed analysis of Auerbach, Baltz, et al. (83)], one expects that the cross section will be proportional to the cross section for the pickup process [e.g., (p,d)], in which the picked-up particle is the neutron that is to be replaced by a Λ to produce a neutron hole. This is very useful since in some cases this pickup cross section has been measured.

We illustrate with the calculations for $^{13}C(K^-,\pi^-)^{13}_{\Lambda}C$. The energy-level diagram for the core nucleus, ^{12}C, and the resultant spectrum for $^{13}_{\Lambda}C$ are indicated by the dashed line shown in Fig. 4.32. If we combine the 0^+ ground state of ^{12}C with an $l=1\Lambda$ orbital, we obtain in the weak coupling basis a $\frac{1}{2}$, $\frac{3}{2}$ hypernuclear state that can be split by a spin-orbit coupling. Similarly, the 2^+ state of ^{12}C when combined with the Λ yields the upper three levels, which can be further split into six levels. The brackets [441], [54] give the number of

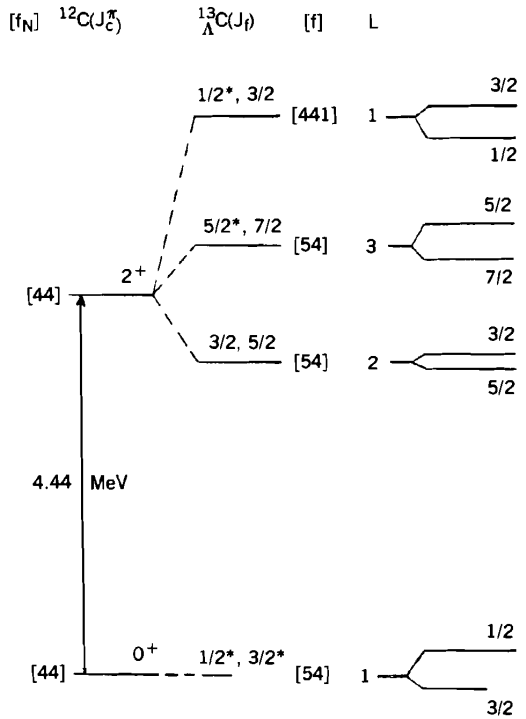

FIG. 4.32. $^{12}C(O^+, 2^+)\otimes p_\Lambda$ spectrum. States that dominate in the 10- and 16-MeV peaks are marked with an asterisk. $\mathscr{L} = J_c + l_\Lambda$, where J_c is the core spin and l_Λ is the Λ angular momentum. [From Auerbach, Baltz, et al. (83).]

particles in each orbit. In ^{12}C we have four neutrons and four protons in $p_{3/2}$ orbits. Thus the spatial symmetry [54] is forbidden for nucleons by the Pauli principle. The substitutional reaction can thus lead only to the [441] states.

The DWA results for the various possible transitions $p_n \rightarrow s_\Lambda$, $\Delta l = 0, 2$, $p_n \rightarrow p_\Lambda$, $\Delta l = 1$, and so on, are shown in Fig. 4.33 and in Table 4.7. As is clear from Fig. 4.33, it should be relatively easy to pick out the $\Delta l = 0$ $p_n \rightarrow p_\Lambda$ transition. However, before the $p_n \rightarrow s_\Lambda \Delta l = 1$ transition can be extracted, it is necessary to unfold the $\Delta l = 0$ cross section. The $\Delta l = 2$ transition requires unfolding both the $\Delta l = 0$ and $\Delta l = 1$ cross sections before it will be visible quantitatively.

The experimental results for $^{13}C(K^-, \pi^-)^{13}_{\Lambda}C$ are compared to theory in Fig. 4.34. Theory and experiment agree quite well. As expected, the $\Delta l = 0$ and $\Delta l = 1$ transitions dominate at small angles ($\vartheta_{lab} = 4°$). At high excitation energies the $\Delta l = 1$ transitions to (sd) Λ orbitals become visible. The $\Delta l = 2$ transition is appreciable only at $\vartheta_{lab} = 15°$. The dominant transition is the $\Delta l = 1$,

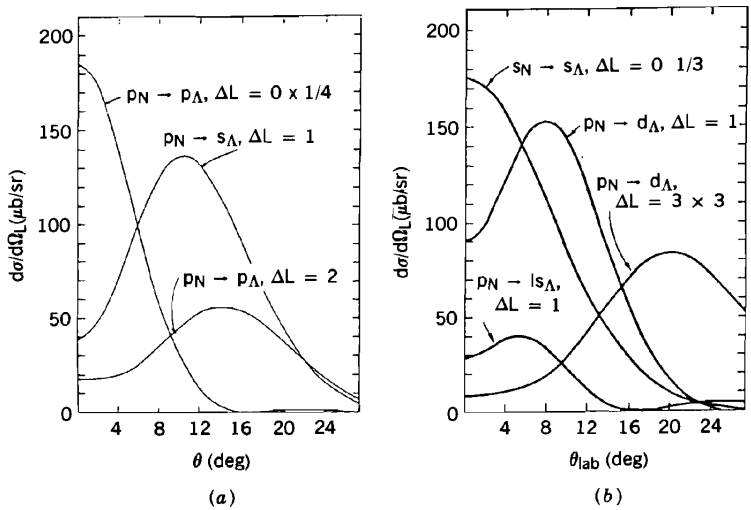

FIG. 4.33. Laboratory cross section for the (K^-, π^-) reaction on a ^{13}C target. In (*a*) $p_n \rightarrow p_\Lambda$ and $p_n \rightarrow s_\Lambda$. In (*b*) $s_n \rightarrow s_\Lambda$ and $p_n \rightarrow s_\Lambda$ and d_Λ. The K^- momentum is 800 MeV/*c*. [From Auerbach, Baltz, et al. (83).]

TABLE 4.7 Differential Cross Sections in $\mu b/st$, $p_k = 530$ MeV/c, $^{13}C(K^-, \pi^-)^{12}_{\Lambda}C$

	θ_{cm}	4°	10°	15°
$p_n \rightarrow p_\Lambda$	$\Delta l = 0$	708	375	109
$p_n \rightarrow p_\Lambda$	$\Delta l = 2$	9.1	12.6	32.8
$p_n \rightarrow s_\Lambda$	$\Delta l = 1$	19.8	78.8	113

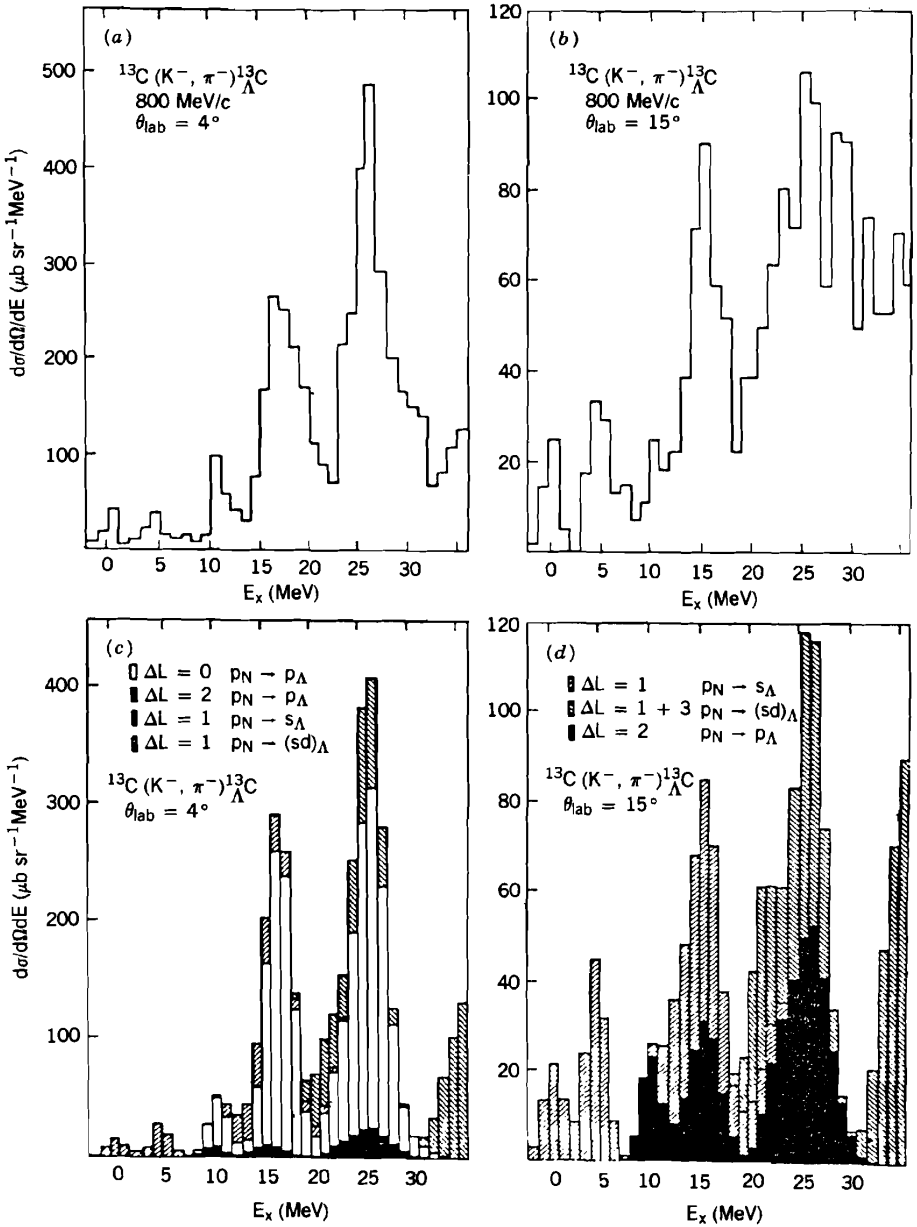

FIG. 4.34. Comparison of experiment and theory for the reaction $^{13}C(K^-,\pi^-)^{13}_{\Lambda}C$. [From Auerbach, Baltz, et al. (88); May et al. (81).]

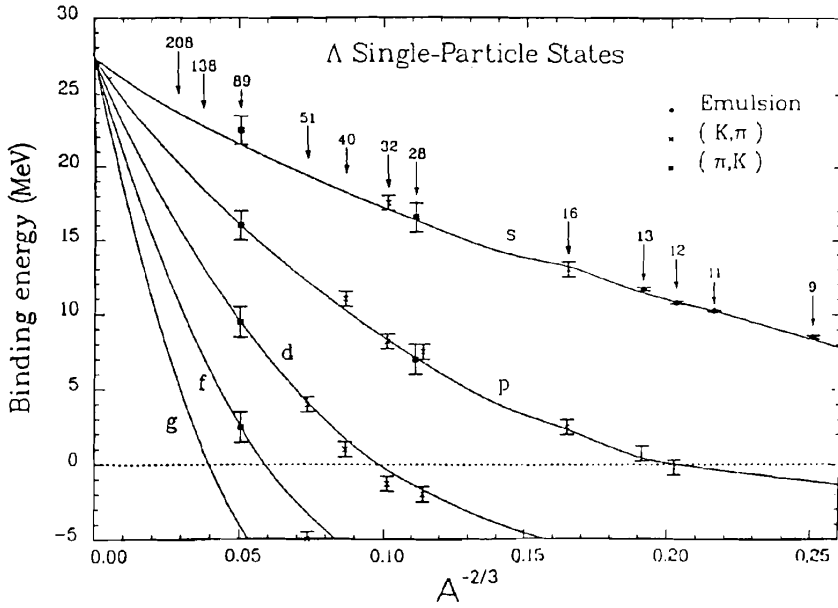

FIG. 4.35. Λ single-particle states. The solid lines are theoretical. [From Millener, Dover and Gal (88).]

$p_n \rightarrow s_\Lambda$. Coupling the s_Λ to the ^{12}C core (ground and excited states) yields the states populating the peaks at 0, 5, and 12 to 16 MeV. Coupling the p_Λ to the ^{12}C core yields the starred states shown in Fig. 4.32. These states will occur at excitation energies about 10 MeV (the energy difference between s_Λ and p_Λ) greater than the values for s_Λ hypernuclei.

A similar analysis has been performed for other target nuclei by Auerbach, Baltz, et al. (83) and for the states seen in the (π^+, K^+) reaction (Fig. 4.31) by Millener, Dover, and Gal (80). The conclusions that can be drawn include: (1) the ΛN spin-orbit potential is small; and (2) the effective mean field potential is nonlocal and density dependent. The single-particle states that have been determined are shown in Fig. 4.35. Because the Λ interacts relatively weakly with the host nucleus, one obtains a very clearly observed set of single-particle states. They are doorway states, which would fragment if the energy resolution were to be improved. These Λ shell-model states provide a direct justification of the mean-field concept.

G. Σ Hypernuclei[‡]

Candidates for Σ hypernuclear states have been seen for $A = 4$ [Hayano et al. (89)], $A = 6$ [Piekarz et al. (82); Kneis (83)], $A = 7$ [Bertini (79)], $A = 9$ [Bertini

[‡] Millener, Dover, and Gal (89).

(80); Mayer (80)], and $A = 12$ [Yamazaki et al. (85); Bertini et al. (84); Peng (82)]. On the other hand, contradictory experiments have seen no evidence for narrow Σ peaks in $A = 7$ [Hungerford (86); Tang et al. (88)], $A = 12$ [Iwasaki (87)], and $A = 16$ [Piekarz et al. (82)].

The existence of long-lived Σ hypernuclei with widths of the order of 5 to 10 MeV was not expected because of the strong ΣN–ΛN conversion. Dover and Gal (80), using the optical model with $\mathrm{Im}\, V = -\langle v\sigma\rangle_{\mathrm{av}}\rho(r)/2$, obtain the following values for the width of single-particle Σ states:

$$^{13}_{\Sigma}\mathrm{C}: \quad \Gamma_{1s} \approx 23\ \mathrm{MeV}, \quad \Gamma_{1p} \approx 13\ \mathrm{MeV}$$

$$^{41}_{\Sigma}\mathrm{Ca}: \quad \Gamma_{1s} \approx 28\ \mathrm{MeV}, \quad \Gamma_{1p} \approx 23\ \mathrm{MeV}, \quad \Gamma_{1d} \approx 18\ \mathrm{MeV}$$

The width decreases with increasing orbital angular momentum because of the angular momentum barrier, which reduces the overlap of the Σ with the nucleons of the core. Several mechanisms have been proposed. Stepien-Rudzka and Wycech (81), Johnstone and Thomas (83), and Dabrowski and Rosynek (81, 82, 85, 86) have studied the effects of Pauli blocking and nuclear binding. Auerbach (87) has considered many-body effects Gal and Dover (82) point out that the transition $\Sigma N \to \Lambda N$ is dominated at low energies by $T = \frac{1}{2}$, $^3S_1 \to {}^3D_1$ transitions. If one neglects the $^1S_0$ contribution, the transition operator for the Σ + nucleus $\to \Lambda$ + nucleus transition is

$$\mathscr{T} = \sum_i v(\mathbf{r}_i - \mathbf{r}_\Sigma)(\tfrac{3}{4} + \tfrac{1}{4}\boldsymbol{\sigma}_i\cdot\boldsymbol{\sigma}_\Sigma)(\tfrac{1}{3} - \tfrac{1}{3}\mathbf{t}_\Sigma\cdot\boldsymbol{\tau}_i)$$

where $\mathbf{t}_\Sigma$ is the isospin operator for the Σ where $t_\Sigma^2 = 2$. This does lead to a reduction in width for some levels for light nuclei.

Finally, we mention the mechanism proposed by Dover and Feshbach (87, 90), who suggest that SU(3) symmetry breaking of the baryon–baryon interaction occurs only in the diagonal components. For the nondiagonal components responsible for the $\Sigma \to \Lambda$ transition, SU(3) symmetry is conserved. In analogy with the SU(2) isobar analog states, where the Coulomb symmetry-breaking interaction has small non diagonal components and relatively large diagonal matrix elements, these authors propose that the Σ hypernuclear states are SU(3) analog states.

There are several other suggestions, which are discussed by Millener, Dover, and Gal (89) in their review article, to which the reader is referred. Needless to say, more experiments are needed!